PALAEOENVIRONMENTAL INTERPRETATIONS OF THE A4 STROMATOLITES FROM THE KOOBI FORA FORMATION IN LAKE TURKANA, KENYA

By

JONATHON M. LACARRUBBA

A thesis submitted to the

School of Graduate Studies

Rutgers, The State University of New Jersey

In partial fulfillment of the requirements

For the degree of

Master of Science

Graduate Program in Geological Sciences

Written under the direction of

Dr. Craig S. Feibel

And approved by

_____

_____

_____

_____

New Brunswick, New Jersey

January 2018

ABSTRACT OF THE THESIS

PALAEOENVIRONMENTAL INTERPRETATIONS OF THE A4 STROMATOLITES FROM THE KOOBI FORA FORMATION IN LAKE TURKANA, KENYA

by JONATHON M. LACARRUBBA

Thesis Director:

Dr. Craig S. Feibel

The stromatolites of the A4 horizon in the Koobi Fora Formation in Lake Turkana, Kenya have predominantly been utilized as a marker bed horizon by researchers since the early 1980s to resolve questions about the sedimentary environments before and after layer precipitation around 1.616 MYA, but little is known about the actual environments in which the layer precipitated. This study interpreted the stable isotopes of two A4 stromatolites through the lens of Pleistocene stromatolite morphologies, extant stromatolitic environments, and recent developments into Lake Turkana $\delta^{18}O_{water}$ values to conduct a palaeoenvironmental reconstruction of the A4 stromatolite horizon.

The stromatolites studied here were collected from areas previously identified as the likely locations of the palaeo-Omo River delta and an outlet to the Indian Ocean called the Turkana River (Brown and Feibel, 1991). A negative correlation between the water temperatures calculated from the $\delta^{18}O_{calcite}$ of these stromatolites and the water column depth interpretted from the stromatolite morphologies confirms the previous conclusions about the locations of this basin inlet and outfall respectively. The A4 stromatolite horizon developed from a floodplain environment that was connected to the larger lake body with a shallow water column and low energy to a through-flowing water environment with a deeper water column and slightly more energy. The stromatolite producing organisms that precipitated the specimen studied here ultimately die during a period of local sedimentary infilling in an environment of shallow, low energy, higher-temperature water. While there is debate as to whether the Lake Turkana Basin has contained a lake consistently throughout

its history, this research demonstrates that a Pleistocene basin lake could not be the sole environment of precipitation and preservation of the A4 stromatolite horizon. This analysis of the A4 stromatolite morphology and stable isotopes underscores an environment of variable water column depth and water energy.

Changes in local evaporation, alkalinity shifting, and therefore $\delta^{18}O_{water}$, complicate temperature calculations from the $\delta^{18}O_{calcite}$ of stromatolites. Furthermore, stromatolite producing communities dissolve and recycle extracellular polymeric substance (EPS) in response to pH shifts, seasonal sediment cycles, temperature decreases, and photic zone changes, underscoring the complexity of temperature calculations using $\delta^{18}O_{calcite}$ derived from stromatolites. These kinetic or environmental effects are not well constrained; however, by deriving an ideal $\delta^{18}O_{water}$ for stromatolite producing temperatures, this study identifies that with a shift of about 1 to 2‰ it is possible to keep stromatolite precipitation within realistic ranges for stromatolitic growth. This study concludes that in the Koobi Fora collection areas of 107 and 123, the A4 stromatolites represent a period of variable environmental conditions that began as a floodplain and developed into a predominantly through-flowing water environment until local sedimentation infilled the horizon. This research also underscores the fact that stable isotopes derived from stromatolites are less than ideal for temperature calculations due to the biological and kinetic growth processes of stromatolite producing microbial communities.

ACKNOWLEDGEMENTS

The greatest of my thanks goes to my family. Mom, Dad, and Taylor, your support has been an unyielding source of strength for me. I love you and am grateful for you every day (FITMIT). To Hilary and Ginny, thank you for the last big push that helped me cross the line; I don't know what I did to deserve it, but I am very lucky to have your team on my side.

The support and effort from my committee has been immeasureable and is responsible for this research existing at all. Craig, what can I say? Thank you for all of this; you have been a far more patient and supportive advisor than most students are forunate enough to have and, for this, I am eternally grateful. Jim and Rick, thank you for entertaining the half-baked musings of a first year graduate student. I appreciate the back-and-forth, the countless crash-courses, and after-hours emails. I wouldn't have been able to take this research even half as seriously without your help. Dr. Schrire, thank you for steering a lost undergrad into something productive.

I am grateful for my mentors, academic, professional and extra-curricular, who have been so generous in sharing their knowledge and expertise. Thank you for entertaining my questions, reading my drafts, and sharing your encouragement. Cat and Emily, it may have been a while since we shared an office or a lab, but you helped to make this possible through the long days in Piscataway and New Brunswick. Jane, thank you for being a true friend and providing the reviews, comments, and words of encouragement to push me along these last few years. Doug and Tara, thank you for always being so supportive and never allowing me to doubt myself. Matt, thanks for bouncing these ideas around with me and for all the laughs over all of those beers.

Without all of my friends providing me some sort of outlet, I surely would have lost my mind by now. Thank you all for chucking dice, plucking strings, and hiking with dogs to keep me grounded.

I am fortunate in having had such a vast and supportive community with me on this journey. Thank you.

Contents

List of Figures

List of Tables

Chapter 1

Introduction

The Lake Turkana Basin is located in north-central Kenya in what is part of the East African Rift. The northeastern shore of Lake Turkana, the current body of water standing inside the basin, is known as the Koobi Fora region and has provided evidence for early hominid evolution and migration. Changing environmental conditions (both seasonal and climatic) influenced the migration and evolution of early hominids through the availability of food, water, and safety. Increasingly higher resolution palaeoenvironmental reconstructions of the landscapes inhabited by early hominids have allowed researchers to develop better explanations for the drivers of hominid evolution. Hominid fossils from the area can date to nearly 4 Ma and, of all the lakes in the East African Rift, Lake Turkana contains the greatest record of hominid expansion over the next approximately 2.6 Ma years ago (Leakey et al., 2001). Periods with stromatolites in Lake Turkana history span this period of hominid expansion. The A4 stromatolite layer is the most developed and geographically expansive of these. While the general environmental conditions needed for the formation of stromatolites is known, the conditions recorded in the stromatolites themselves has not been as thoroughly identified. This thesis focuses on the stromatolites of the Koobi Fora Formation's A4 layer in two areas of the Koobi Fora region and attempts to determine fluctuating environmental conditions recorded by them.

While research by others (e.g. Abel et al., 1982; Casanova, 1986; Lepre et al., 2007) has demonstrated that the stromatolite layers of the Koobi Fora Formation are useful

proxies for relative environmental conditions of the water in which they propagated (e.g. warm, saline, low energy). However, that research does not attempt to yield higher resolution (i.e. seasonal, yearly, or decadal) interpretations from these stromatolites as isotopic analyses were limtied to just a few point samples from inside the stromatolites with very little internal age control. Much like tree rings to dendrochronology, the laminae of A4 stromatolites identified in the Koobi Fora region of Lake Turkana may provide a valuable proxy for envronmental conditions including high resolution details concerning micro/macro-environmental changes and nearshore landscapes. Oxygen and carbon stable isotope ratios were analyzed for each millimeter through the transect of the stromatolites by the Rutgers University Stable Isotopes Laboratory at the Department of Earth and Planetary Sciences. Data for the δ^{18}O PDB and δ^{13}C PDB stable isotopes of each sample are recorded in tables A.1 and A.3. Hypotheses to explain the stable isotope values observed in the δ^{18}O and δ^{13}C values are listed below in Table 1.1.

TABLE 1.1: Hypotheses of A4 stromatolite δ^{18}O PDB and δ^{13}C PDB variability

$\mathbf{H}_{\#}$	**Description**
Null hypothesis	
H_0	A4 stromatolites do not record δ^{18}O and δ^{13}C values that are in equilibrium with the environment and are not good indicators of palaeoenvironments.
Large lake hypoteheses	
H_1	The δ^{18}O and δ^{13}C of the A4 stromatolites record contemporary environmental conditions at different locations of the basin lake (i.e. Lake Lorenyang).
H_2	The δ^{18}O and δ^{13}C of the A4 stromatolites record environmental conditions associated with different time periods of the basin lake (i.e. Lake Lorenyang).
Playa and solar pond hypotheses	
H_3	The δ^{18}O and δ^{13}C of the A4 stromatolites record the environmental conditions of a near shore sand bar on Lake Lorenyang.
H_4	The δ^{18}O and δ^{13}C of the A4 stromatolites record the environmental conditions of a playa or solar pond environment which is primarily spring or rainwater-fed (i.e. groundwater, rainwater).

Continued on next page

Table1.1 – continued from previous page

$H_{\#}$	**Description**
Through-flowing water hypothesis	
H_5	The $\delta^{18}O$ and $\delta^{13}C$ of the A4 stromatolites record the environmental conditions of an open river system dissociated from a lake or closed basin (i.e. rivers, streams).

This study is organized as follows. Geological setting and context is discussed in Chapter 2 which also goes into detail about the specimen collection sites. Due to the generally enigmatic and highly debated explanations for stromatolite formation, Chapter 3 summarizes research by others that examines the formation of stromatolites from the microbial factors that affect laminae character to the environmental factors that affect stromatolite morphology. The methodology used for the collection and analysis of samples from the stromatolite specimen are explained in Chapter 4. Results of the stable isotope analyses and the statistical analysis of said results are detailed in Chapter 5. A discussion of these results and how they pertain to the hypotheses in Table 1.1 is found in Chapter 6 and conclusions are summarized in Chapter 7. Appendix A contains tables of raw data colleted in this study.

Chapter 2

Geological and Climatic Setting

The eastern branch of the East African Rift System (EARS) in southern Ethiopia and northern Kenya contains the Turkana Basin (Ebinger et al., 2000) and within which there has been a major alternating fluvial-lacustrine system from approximately 4.2 Ma to the present (Brown and Feibel, 1991). Lake Turkana is the present day body of water in the basin and is one of the largest lakes in the EARS, occupying an area of 7,500 km^2 (Frostick, 1997). Lake Lorenyang was the major lake phase that had preceeded Lake Turkana between approximately 2.0 and 1.7 Ma (Joordens et al., 2011). Lake Lorenyang was fed by the palaeo Omo River and smaller rivers out of the southwest. At its largest extent it was approximately 9,000 km^2 (Quinn et al., 2007). Two notable outlets developed during this period: the Turkana River in the southeast created an outlet to the Indian Ocean, and an overflow created a link to the Nile River in the northwest. While the appearence of *Dasyatis africana* (an Indian Ocean stingray) is indicative of a southeasterly Turkana River outflow from the basin (Brown and Feibel, 1991; Feibel, 1994; Harris et al., 2003; Lepre et al. 2007), the appearance of *Crocodylus niloticus* (Nile crocodile) in the Plio-Pleistocene record is evidence of a link to the Nile. Around 1.9 Ma the size of this lake started reducing and, by the end of this phase, the lake basin was predominantly infilled (Feibel, 1997). Lake level records dating from 1.9 Ma to 1.5 Ma show highly variablity, but demonstrate a predominantly open hydrologic system.

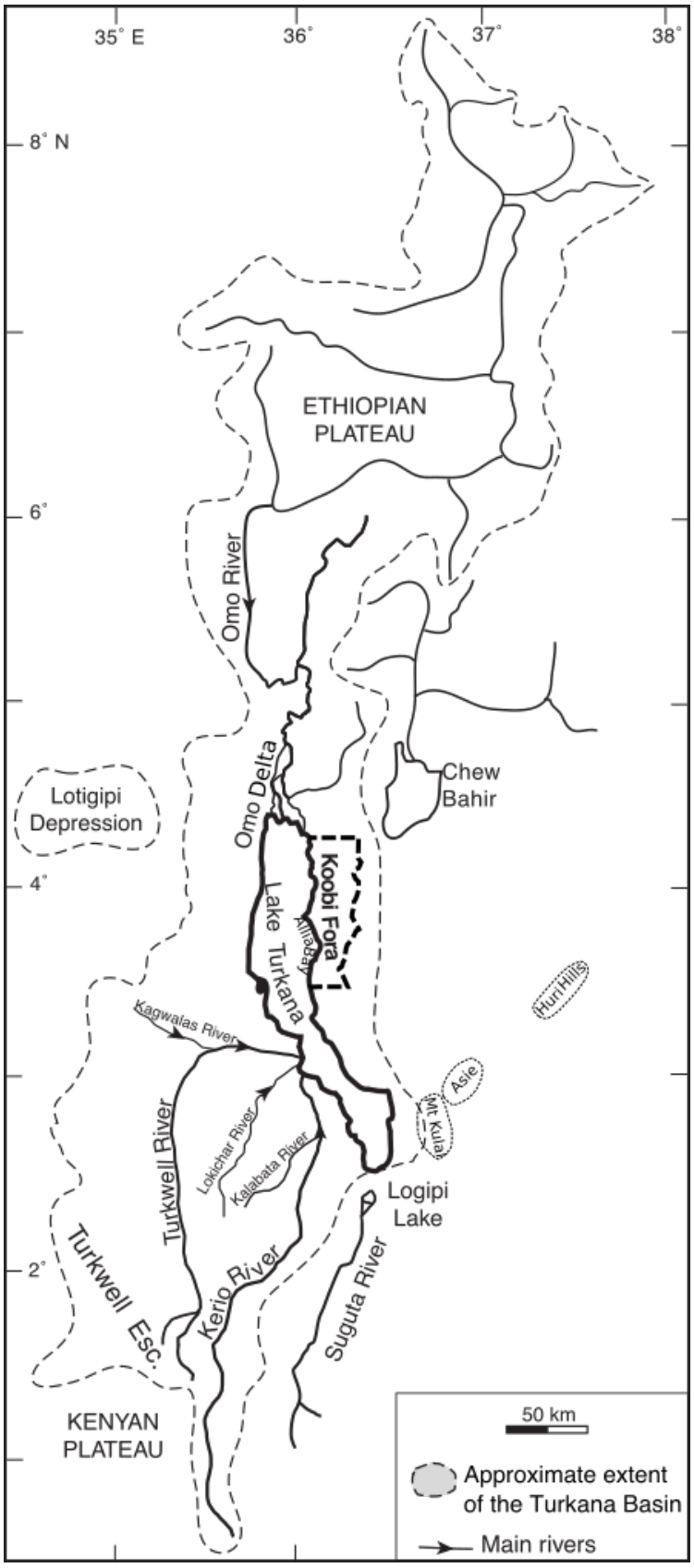

FIGURE 2.1: Lake Turkana Kenya and the modern Omo River. Modified from Vetel et al., 2004.

After the ≥100 kyr highstand of Lake Lorenyang, deltaic sediments show that the the Omo River began prograding into the Koobi Fora Region (Feibel, 1988; Brown and Feibel, 1991). Around 1.8 to 1.7 Ma the expansion of channel and floodplain sediments is evidence of an ancestral Omo River and channel system originating from the north (Feibel et al., 1989; Feibel et al., 1991; Brown and Feibel, 1991; McDougall et al., 1992). Transgressive and regressive cycles of lake margins (albeit shallow lakes or a series of lakes) were frequent at this time, but after this period lake related environments are limited (Brown and Feibel, 1991; Feibel et al., 1991; Feibel, 1994). Ancestral Omo channels were virtually inactive from 1.7 to 1.4 with the record of fluvial input limited to small distributary channels which deposited the Okote, Koobi Fora, and Ileret Tuff complexes at about 1.6–1.5 Ma. Channels during this period derived from either the main trunk of the ancestral Omo River or the northeastern margin of the basin (Feibel et al., 1991; Brown and Feibel, 1991). Periods of lower water input, where the system would fall below its outlet(s) and reduce in aerial extent while increasing its salinity-alkalinity, are highlighted by the limited lacustrine biota and (at times) expansive algal communities (e.g. stromatolites) recorded in the geologic record (Feibel, 1994; Feibel et al. 1991; Lepre et al. 2007). By 1.4 Ma, large river channels of the ancestral Omo returned to the region.

The geologic formation representing the Plio-Pleistocene is referred to as the Koobi Fora Formation. Brown and Feibel (1991) interpreted the Koobi Fora Formation as deposits originating from a large perennial river that flowed (generally) from north to south and was slightly elevated, with crevasse splays, floodplains, and flood basins lateral to the river that would transition to alluvial fans toward the margins of the basin. Through time the river would wander east and west across the basin until it periodically transitioned to a delta as it fed a basin lake. The shallows of the lake would at times be rich in cryptalgal biolithite and molluscan beds (Brown and Feibel, 1991).

Due to the optimal preservation of the lacustrine sediments, palaeolake environments are overrepresented in the sedimentary record and in actuality only account for approximately 15% of the basin history. For the better part of 5 million years, the Omo River has flowed from the Ethiopian Highlands into the Turkana Basin (Wolde-Gabriel and Aronson 1987). At times during the first half of the basin's history, the river exited the basin to the southeast based on the presence of the Tulu Bor Tuff (3.3 Ma) in the Loiyengalani

region and a *Dasyatis africana* stringray entering the basin from the Indian Ocean (1.9 Ma; Feibel 1994). The outlet (and the Turkana River) closed after 1.9 Ma when the volume of water in the basin began to decrease. At 1.7 Ma the periodic decreases in flow are attributed the diversion of the Omo River into the Nile headwaters. After this time, the stratigraphical record for the Middle and Late Pleistocene is notably complex due to opening and subsequent choking of channels with sediment by flooding (Brown and Feibel, 1991).

This research focuses on the time of the KBS Member - a time period between 1.87 and 1.6 Ma - and specifically the environments recorded by the stromatolite layers precipitated by the algal communities during a period of heightened aridity (Lepre et al., 2007). The deposition of the KBS Member is focused on an area centered on the Koobi Fora Ridge and Bura Hasuma. Distally from this area (north and east), the member thins and represents shallower water and a fluvial regime of less energy. In the above narrative, this period represents an interval of lake level variability in the stratigraphic record (Brown and Feibel, 1991; Lepre et al., 2007).

2.1 Tectonic Environment

The Turkana Basin is a tectonically active region. Many geomorphic features were formed contemporaneous with or after the deposition of the KBS Member: east of the current southern basin Mt Kulal formed between 2.5–2 Ma, Asie formed between 2.7–0.5 Ma, and the Huri Hills formed between 3–0.5 Ma. The Plio-Pleistocene basin was flat from Allia Bay (in the southeast of the Koobi Fora region) to the Omo Valley and rimmed by uplifted area at the basin margins (Brown and Feibel, 1991). The tectonics of the area mediated the origin of the lake $\geq$2.0 Ma and fostered the preservation of its stratigraphy.

2.2 Regional Plio-Pleistocene Sedimentology

Plio-Pleistocene strata are discontinuously exposed over approximately 1200 km^2 along the eastern side of present day Lake Turkana in a region referred to as Koobi Fora. This region

has been sub-divided into three broad areas (Ileret, Koobi Fora, and Allia Bay), which can be subdivided into eight subregions: Il Dura, Ileret, Karari Ridge, Il Naibar Lowlands, Koobi Fora Ridge, Bura Hasuma, Sibilot, and Southern Allia Bay Plains (Brown and feibel, 1991). To further organize the fossil collection areas, the Koobi Fora Region has also been split into more than 6 dozen fossil collection localities that have been prescribed numeric identifiers (Brown and Feibel, 1986). The Omo Group consists of five formations for the Pliocene and Pleistocene sedimentary units: the Koobi Fora, Nachukui, Shungura, Usno, and Mursi. At Koobi Fora, the Koobi Fora Formation includes the entire Plio-Pleistocene sequence excluding the latest portion of the Pleistocene (Brown and Feibel 1986). The Koobi Fora Formation pertains to strata that are unconformably atop Miocene and Pliocene volcanics and unconformably overlain by the late Pleistocene and Holocene Galana Boi Formation (Owen and Renaut 1986). It is further divided into eight members (from oldest to latest): Lonyumun, Moiti, Lokochot, Tulu Bor, Burgi, KBS, Okote, and Chari Members. Each member begins with the volcanic tuff from which it gets its name and includes the overlying strata up to the next overlying tuff (ie the KBS member starts at the KBS Tuff and ends before the start of the Okote Tuff)(Brown and Feibel, 1986). See figure Figure 2.2 from Feibel et al. (2009) included here for reference. This research focuses on the 136 m thick KBS Member that represents a period of time between 1.89 Ma – 1.53 Ma (Brown and Feibel 1991, Lepre et. al. 2007; Feibel et al. 2009). Earlier terminology referred to the strata included in this member as the KFIIA, KFIIB, and KFIII stratgraphical terminology (Behrensmeyer 1970, Vondra et. al. 1971). It is exposed at Bura Hasuma (which includes areas 107, 110, 119, 120, 121, 123, and 124; Brown and Feibel 1991, Feibel et al 2009) and the Koobi Fora Ridge (containing areas 100, 101, 102, 103, 104, and 115). Area 102 and 103 contain the type section of the KBS Member (Brown and Feibel, 1991).

Sediments of the Koobi Fora Formation represent five depositional palaeoenvironments: fluvial channels, fluvial floodplains, deltas, lake margins, and lake basins. The palaeogeography of the depositional environment of the KBS Member was likely one of a lake margin. These facies are low-energy accumulations (especially compared to the higher energy lake margin facies on the western side of the lake). Arenaceous bioclastic carbonates (ABC) like cryptalgal biolithites (stromatolites), molluscan packstones, and calcareous sandstones are

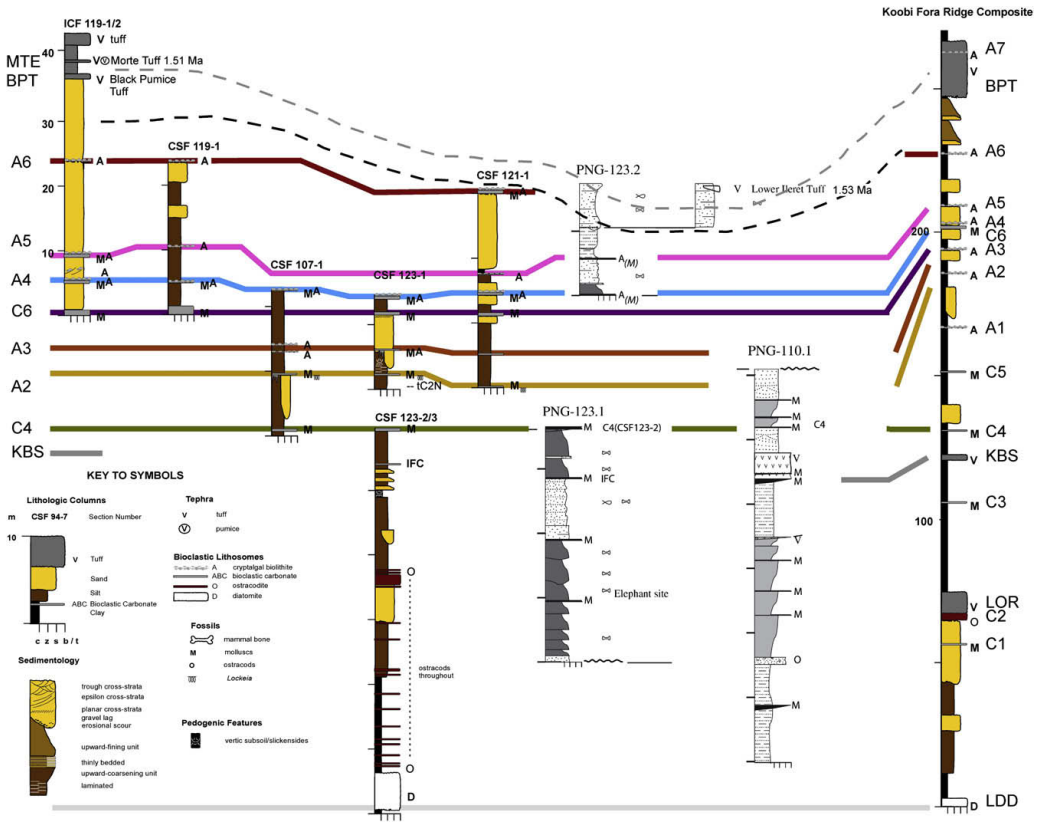

FIGURE 2.2: Stratigraphic sections from the Bura Hasuma region correlated by lithostratigraphic and tephrostratigraphic markers, compared to composite type section for this portion of the Koobi Fora Formation along the Koobi Fora Ridge (redrawn after Brown and Feibel [1986])... Section ICF 119-1/2 redrawn from Findlater (1976). Individual sections are shown to a common scale, but note scale change for composite type section. Dashed lines in upper part of diagram indicate possible erosion surfaces (from Feibel et al., 2009).

the most prominent deposits in this palaeoenvironment. The beaches of the lake margin provide valuable sources of vertebrate fossils (including the KMN-ER-1813 skull) (Brown and Feibel, 1991; Lepre et al., 2007; Feibel et al, 2009).

As will be discussed, the local variability in sedimentation between areas that starts with the KBS Member is common in the later members of the Koobi Fora Formation (named above). The member exhibits a range of interbedded upward-fining detrital clastic and bioclastic units implying lacustrine or lake margin environments to more homogeneous but coarser detrital clastics with pedogenic modification interpretted as fluvial and floodplain settings (Brown and Feibel, 1991; Feibel et al., 2009).

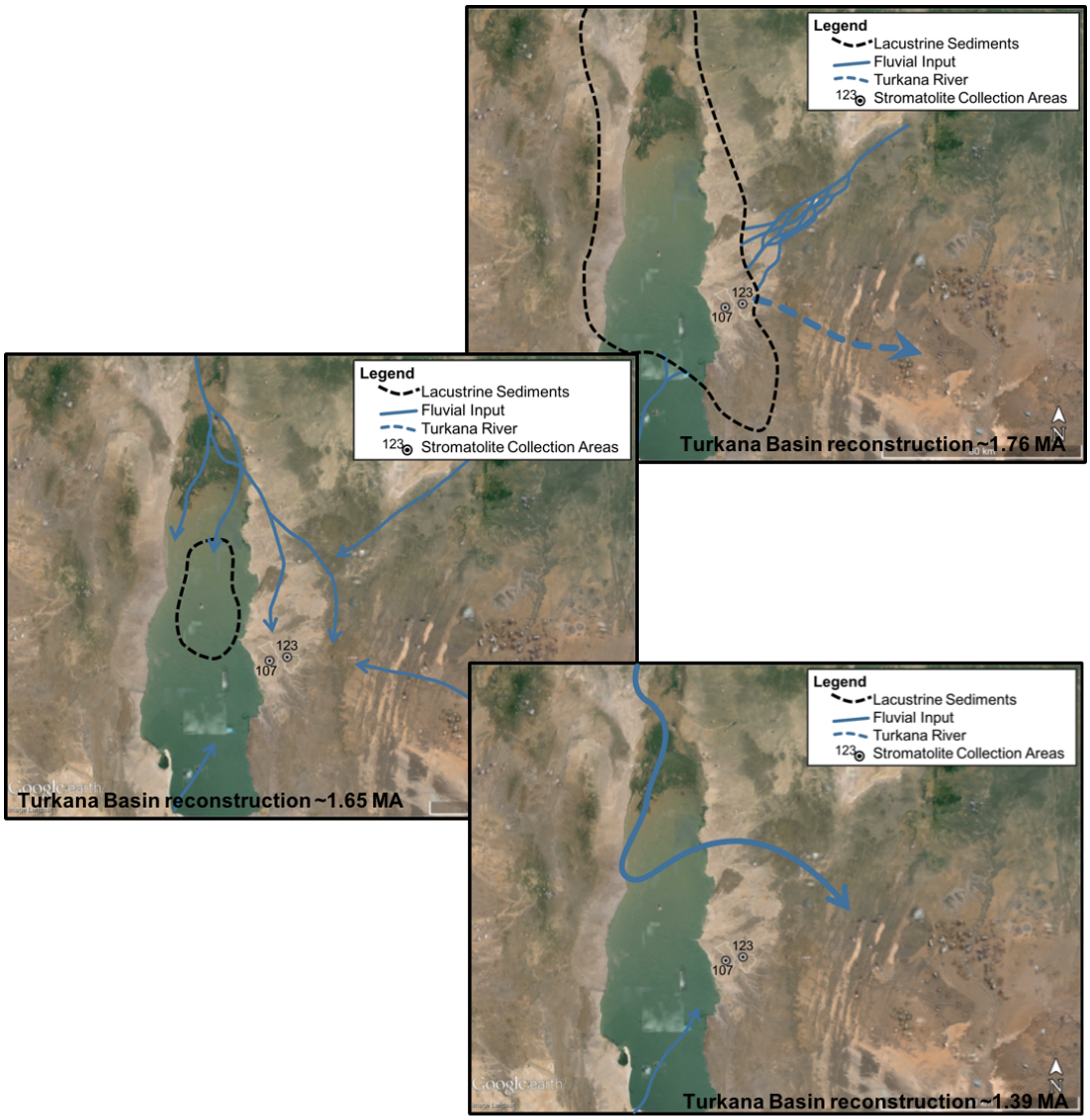

FIGURE 2.3: Stromatolite collection areas from palaeogeographic reconstruction of Turkana Basin at 1.76 Ma, 1.65 Ma, and 1.39 Ma. Modified from Brown and Feibel, 1991.

2.3 KBS Member Exposure Across the Koobi Fora Region

In Bura Hasuma the strata of the KBS Member are flat lying with minor faulting common. It includes several marker beds of cryptalgal biolithites (stromatolites) and bioclastic sandstones that correlate to the Koobi Fora Ridge (Feibel 1983). While these beds are found east of the Bura Hasuma subregion, they thin and disappear before the edge of the basin.

Generally, tuffs found in Bura Hasuma are poorly preserved, but the KBS Tuff and the Malbe Tuff are closely related to the marker bed horizons, making these horizons more useful in correlating between areas. Between stromatolite marker beds A4 and A5, relatively complete skeletons of vertebrate fossils have been found (including the in situ Elephas skeleton exhibited in the "Elephant House" by the National Museums of Kenya in Area 123) (Feibel et al., 2009).

The Koobi Fora Ridge contains the type section for the KBS Member is in Area 102 and Area 103 northwest of Bura Hasuma (Brown and Feibel, 1986). In Area 102 the upper Burgi and KBS Members are thicker and more complete than in any other part of the Koobi Fora region. Here, the upper Burgi represents a deeper lake and deltaic lobe infilling system. These deltaic palaeoenvironments contain nearly all of the mammalian fossils from the upper Burgi Member. Transitioning into the KBS Member, approximately 20 cycles of shallow lacustrine intervals (1-2 m) are punctuated by fluvial sequences in Area 102. The KBS Member in Area 104, representing fluvial channels, notably contains more mammalian fossils than other nearby areas adding to and aiding its palaeoenvironmental interpretation (Brown and Feibel, 1991).

The northeastern extension of the Koobi Fora Ridge is referred to as the Karari Ridge. The KBS Member is represented by fluvial sands and a distinctive gravel component on the Karari ridge. Here, the upper Burgi Member transitions to the KBS Member as fossiliferous fluvial channel deposits. Within the KBS Member, intraformational conglomerates (including basalt pebble conglomerates) are common. Basalt pebble conglomerates imply deposition of streams originating in the volcanic highlands at the eastern margin of the basin (Brown and Feibel, 1991).

Ileret, northeast of the Karari Ridge and north of the Koobi Fora Ridge, exhibits the KBS Member far down in dissecting drainages as several cycles of upward-fining sediment with the lower part of the member including mollusc bearing sandstones in the cycles (Brown and Feibel, 1991).

Il Dura is the northernmost subregion of the Koobi Fora region. It includes includes sparse outcroppings of the upper Burgi and KBS Members which have been unconformably deposited on an eroded basalt terrain. The upper Burgi Member at Il Dura includes

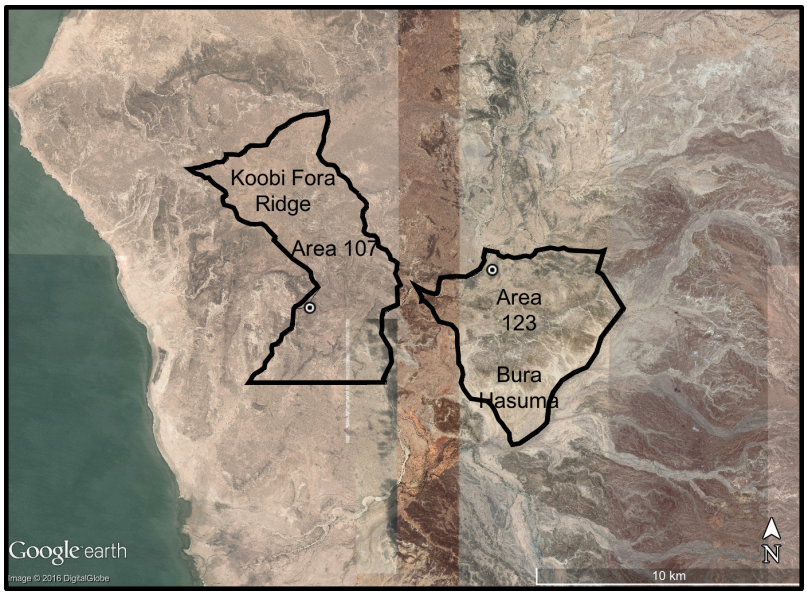

FIGURE 2.4: Areas 107 and 123 in Koobi Fora, Koobi Fora Ridge and Bura Hasuma respectively. Circle icon designate sample collection areas.

laminated siltstones and molluscan sandstones which are covered by the KBS Tuff (starting the KBS Member). The tuff is comprised of thin upward-fining cycles (Brown and Feibel, 1991).

The highly resistant and mappable bioclasic carbonates and sandstone marker beds of the KBS Member are arguably the most useful stratigraphic markers available when dateable or correlatable tephra are inaccessible. Stromatolites for this research were collected from the A4 layer of Areas 107 and 123 in Bura Hasuma. It is therefore important to describe this area in further detail and provide context for an accurate interpretation of its depositional environments. The Koobi Fora Ridge provides a valuable proxy for such an exercise.

The western Koobi Fora Ridge with its high accumulation rates has an exceptionally complete stratigraphic record (Feibel, 1988; Lepre et al., 2007) where the sequence and terminology of these ABC marker beds was first developed (Feibel, 1983). To illustrate the differences in accumulation rates and place in them in their broader context mentioned earlier, the Bura Hasuma region has seven of these transgressive-lacustrine-regressive cycles over approximately 40-50 m of section while the Koobi Fora Ridge to the northwest (lakeward) expresses this pattern 10 times over a stratigraphic interval of 130 m. The consistency of the thinning of sedimentary packages as they are identified and correlated east

of the lake serves to strengthen the confidence and utility of the marker beds (in context with their sequences) for the interpretation of depositional environment and correlation of the geology of the region.

Interpreting the stable isotope record of the A4 stromatolites requires an understanding of their depositional environment. The sedimentology at Bura Hasuma represent a slightly different depositional environment than that of the Koobi Fora Ridge (e.g. clastic input, wave energy). Examining these differences and recognizing the effects they have on the isotopic record, will aid in removing (or acknowledging) any locational bias and bolster the A4 interpretation presented here.

2.4 Bura Hasuma

The Bura Hasuma Hill in southern Area 110, as the most prominent local landmark, has lent its name to the Bura Hasuma subregion of Koobi Fora. Area 123, where this study's samples were collected, is significant as it is the location where KNM-ER 1813 (a remarkably complete *Homo hablis* skull; Klein 1999) and many other fossils were found. The area is located in the southern section of the subregion, nearly 2 km from the landmark for which the subregion is named. The KBS Tuff, found at the base of Bura Hasuma Hill is the only tephra with which to correlate the bottom of the section; however faunal assemblages and similar sedimentary packages are recognized in Area 123 that correlate to the KBS Member (Feibel et al. 2009).

2.4.1 Complications of Correlation in Area 123

North-south trending faults (with diplacements of meters to tens of meters) exist in the area, complicating geological mapping of the subregion. Without exposed tephra to unambiguously correlate over wide discontinuities, correlation is limited to marker beds and their associated lithologic sequences whose continuity is broken by the aforementioned faulting (Feibel et al., 2009). Over the course of a decade, characteristic lithologic sequences (of which stromatolitic marker beds are associated) were mapped from the Karari Ridge to

the Koobi Fora Ridge (Bainbridge, 1976; Frank, 1976; White, 1976; Burggraf et al., 1981; White et al., 1981; Feibel , 1983; Tindall, 1985) and have proven to be vital for identifying the geology across correlation gaps for an area of over 200 km^2 (Feibel et al., 2009). Internal characteristics, associated sequences, regional context, and an understanding of process all contribute to the correlation of these marker beds and sequences. An improved understanding of these correlative characteristics can greatly enhance the ability of researchers to tease more value from these correlations.

2.4.2 Stratigraphy of Bura Hasuma

Upper Burgi, KBS, and lowermost Okote Members are well represented in the Bura Hasuma region when compared to their type sections (Brown and Feibel, 1986) with two significant differences: the Upper Burgi member exhibits delta front depositional dips, and the KBS Member thins to the south and east (as noted above). The Bura Hasuma stratigraphy can be organized into three separate packages which in turn are interpreted as three distinct depositional environments.

Representing a lacustrine environment and the movement of deltaic lobes (with up to 14 m of relief on the subaqueous front), the first/lowest package is made up of the upper Burgi Member strata and exhibits claystones, siltstones, and fine sandstones with a significant biogenic component of molluscs, ostracods, and fish (Brown and Feibel, 1986). The palaeotopography of this package limits its continuity and original horizontality — two caveats making correlation of units over large distances complex (Feibel et al., 2009). Prominent bioclastic units (molluscan coquinas etc.) provide marker beds for correlation, but are only useful locally and cannot be traced over distances much greater than a few hundred meters.

The middle/second package is a series of repetitive cycles of transgressing lake margin and lacustrine phases from the KBS Member. The strata of this member are identified by prominent and extensive marker beds of bioclasic carbonates or Arenaceous Bioclastic Carbonate (ABC, Vondra, 1974; White et al., 1981; e.g. stromatolites), or sandstone followed/overlain by clays or laminated siltstones. When found with channel-form sandstones, the clays/siltstones commonly grade upwards to mudstones with a pedogenic overprinting.

This mudstone/sandstone associated strata is indicative of the fluvial channel and adjacent floodplain soils and represents a regressive portion of the cycle. Marker beds from the Bura Hasuma subregion have been mapped and correlated to the more complete sequences at the western Koobi Fora Ridge.

The ABC marker beds identified in the Bura Hasuma region are C4, A2, A3, C6, A4, A5, and A6 (Feibel, 1983, 1988; Brown and Feibel, 1986, 1991). Of these, the sequence from A2 through A4 is the most characteristic stratigraphic progression of the interval while the underlying C4 through sub A2 is poorly preserved and exposed (Feibel et al., 2009).

The third and final depositional environment/phase continues from the regressive cycle of the second, representing a fluvial system with channel-form sandstones, upward-fining cycles, and tuffaceous silts. Again, the differences between the Koobi Fora Ridge (Area 103 specifically) and Bura Hasuma (Area 119) are striking. Area 103 along the present day lake margin contains a couplet of fluvial cycles above stromatolitic marker bed A6 while the comparable section in Area 119 to the east is approximately 20 m in thickness and has a large sand body and a complex of tuffs and tuffaceous silts. Following the broader context of poor expression in this area, the third depositional phase is not well expressed due to weakly indurated lithologies; however the package does contain the Black Pumice Tuff, Lower Ileret Tuff, and Morte Tuff (1.51 Ma) capping the sequence which allow the stratigraphic sequence to be scaled (Brown et al. 2006; Feibel et al. 2009)

2.5 Koobi Fora Ridge

The Koobi Fora Ridge provides context for the stratigraphy of the KBS Member found at Bura Hasuma. As stated above, the Koobi Fora Ridge is known for its high accumulation rates and notably complete stratigraphic record (Feibel, 1988; Lepre, et al. 2007). Through examination of the more complete lakeward stratigraphy available at the Koobi Fora Ridge, the depositional environment of Bura Hasuma is better understood. While the stratigraphy of the KBS Member at Bura Hasuma has thinner transgressive-regressive cycles, the Koobi Fora Ridge provides the type section for this member. Examining not only what is present

at Bura Hasuma, but what it lacks through comparison aids in resolving the geospatial distribution of the palaeoenvironment in which the KBS Member was deposited.

2.5.1 Stratigraphy of the Koobi Fora Ridge

Along the Koobi Fora Ridge, basal and capping units of the KBS Member are the KBS Tuff and the Koobi Fora Tuff Complex (Brown and Feibel, 1986, 1991). Between these two units, the stratigraphy records a lake margin depositional setting that is far more expansive than that of the Bura Hasuma region.

Offshore facies/deltaic environments in the Koobi Fora Ridge are equivalent to the first package at Bura Hasuma. The offshore sediments are implied by a suite of characteristics. Offshore mudstones can be differentiated from mudstones of the alluvial environments through their preservation of depositional features. The mudstones of the offshore are well sorted medium silts to clays and have 1 to 20 cm sandy lenses with ostracod and bivalve remains (Feibel, 1988; Lepre et al. 2007) suggesting fallout of grains in suspension. Dark-light color laminations are preserved implying limited erosion and subaqueous deposition below a wave base (Bowen 1974; Lepre et al. 2007); and distinctive gypsum and limonite nodules are found in outcrop.

The nearshore facies environment found at the Koobi Fora Ridge is equivalent to the second package of Bura Hasuma interpretation. These are dominated by cycles of sandstones and ABC marker beds much like in Bura Hasuma. ABC units range from 10 to 150 cm in thickness and can cover areas of more than 250 km^2 (Feibel, 1983; Tindall, 1986). Found among the ABC units (consisting of stromatolites and molluscs) are fossil fish nests (Feibel 1987, 1988). The matrix between the biolithites making up the ABC units is a moderately sorted and calcareous medium to coarse sand exhibiting ripple marks, planar crossbeds, and massive bedding. ABC units grade into 1-5 m thick sandstones and/or sand vertically and laterally. These deposits are distinguishable from channel deposits as they have a smaller thickness with flat basal surfaces and their proximity to the ABC units (Feibel, 1988; Lepre et al. 2007).

Bowen (1974) determined that trace and body fossils demonstrate that there was low clastic input to the waters where the ABC beds propagated, leaving the stromatolite beds to be interpreted as evaporative, photic zone conditions (Johnson, 1974; Abell et al., 1982; Casanova, 1986). Molluscan species variety suggests relatively fresh waters compared to the stromatolite beds (Williamson, 1982), while the sand deposits imply beachface/shoreface settings (Lepre et al. 2007).

Similar to the third package of Bura Hasuma, the Koobi Fora Ridge sediments display alluvial facies environments made up of channel and floodplain deposits. Channels are suggested by sandstones that are poorly to moderately sorted with concave-up bases that have incised underlying strata between 5 and 10 m. Sedimentary features such as scour-and-fill, crossbeds, and laminations are observed in these units. The sandstones vertically fine into fine grained massive mudstones with 10–100 thick slickensides horizons and dish-shaped fractures. This suggests suspension deposits of floodplains with palaeosols forming under drying-wetting conditions. Color mottles found in the mudstones also point towards local water table fluctuations (Feibel, 1988; Wynn, 2004; Lepre et al. 2007).

2.6 Age of Marker Bed A4

The Bura Hasuma region provides valuable magenetostratigraphic information for the period during KBS Member deposition. The ransition from the normal polarity to reversed polarity at the top of the Olduvai Subchron (tC2N, 1.778 Ma; Lepre and Kent, 2010) is not far above marker layer C4 and below A2 (both deposited earlier than layer A4). Likewise, the aforementioned Lower Ileret Tuff and Morte Tuff are dated to 1.53 and 1.51 Ma respectively (Lourens et al. 2004; Feibel et al. 2009). The capping unit of the KBS Member is the basal tuff in the Koobi Fora Tuff Complex, the Lower Koobi Fora Tuff, dated to 1.476 Ma $\pm$ 0.013 Age modeling for the Bura Hasuma region by Brown and Feibel (1986) places the KBS Member between the KBS Tuff dated to 1.869 $\pm$ 0.021 Ma (McDougall and Brown, 2006) and 1.50 Ma (with the lower Okote Member here dated to 1.53 Ma). The estimated age of 1.84 Ma for the C4 layer is consistent with age estimates in other areas, specifically Area 102 where the type section for the KBS Member is located. Shifting accumulation rates close to the upper Burgi/KBS Member boundary ($\pm$1.9 Ma) that provide potential

complication to age modeling are consistent with the estimated period for the opening of the Turkana River and/or flow piracy by a connection to the Nile river (Feibel, 1988; Feibel et al. 2009).

The age of Marker Bed A4 and the stomatolites discussed here was derived by using average sedimentation rates and chronostratographic/absolute dating techniques developed by others (i.e. McDougall and Brown, 2006; Lepre et al., 2007; Lepre and Kent, 2010). The A4 layer is located approximately 93 meters above the KBS Tuff (1.869 $\pm$ 0.021 Ma from McDougall and Brown, 2006), about 47 meters above the Olduvai-Matuyama tC2n transition (1.778 Ma), and 43 meters below the Lower Koobi Fora Tuff (1.476 Ma; Lepre et al., 2007). With an average sedimentation rate of approximately 29 cm/yr during the Matuyama (Lepre and Kent, 2010), A4 can be dated to approximately 1.62 Ma. Figure 2.5 provides a generalized section and time scale with sedimentation rates.

2.7 Stable Isotopes of the Lake Turkana Region

The source of the parent water is important when attempting to reconstruct the palaeoenvironment associated with carbonate formation.The source of $\delta^{18}O_{water}$ and $\delta^{13}C_{water}$ are useful when interpreting stable isotope data of calcites pecipitated. Generally speaking, but detailed below, the sources of $\delta^{18}O_{water}$ and $\delta^{13}C_{water}$ are understood to be local and headwater rainfall and decaying organic matter respectively.

2.7.1 Interpretation of $\delta^{18}O_{water}$ in the Turkana Basin

Previous work interpreting the stable isotope records of sedimentary carbonates, determined that freshwater conditions develop negative oxygen isotope values while evaporative and brackish conditions develop more positive values (Abell and McClory, 1986). It has been suggested that $\delta^{18}O$ values of -3 to -4 ‰ are representative of reshwater/rainfall conditions and that $\pm$ 1 or 2 ‰ about zero are likely representative of African equitorial parent water norm and imply conditions of brackish to freshwater (Abell and McClory, 1986). This has been interpreted as a system similar to the modern headwaters, however

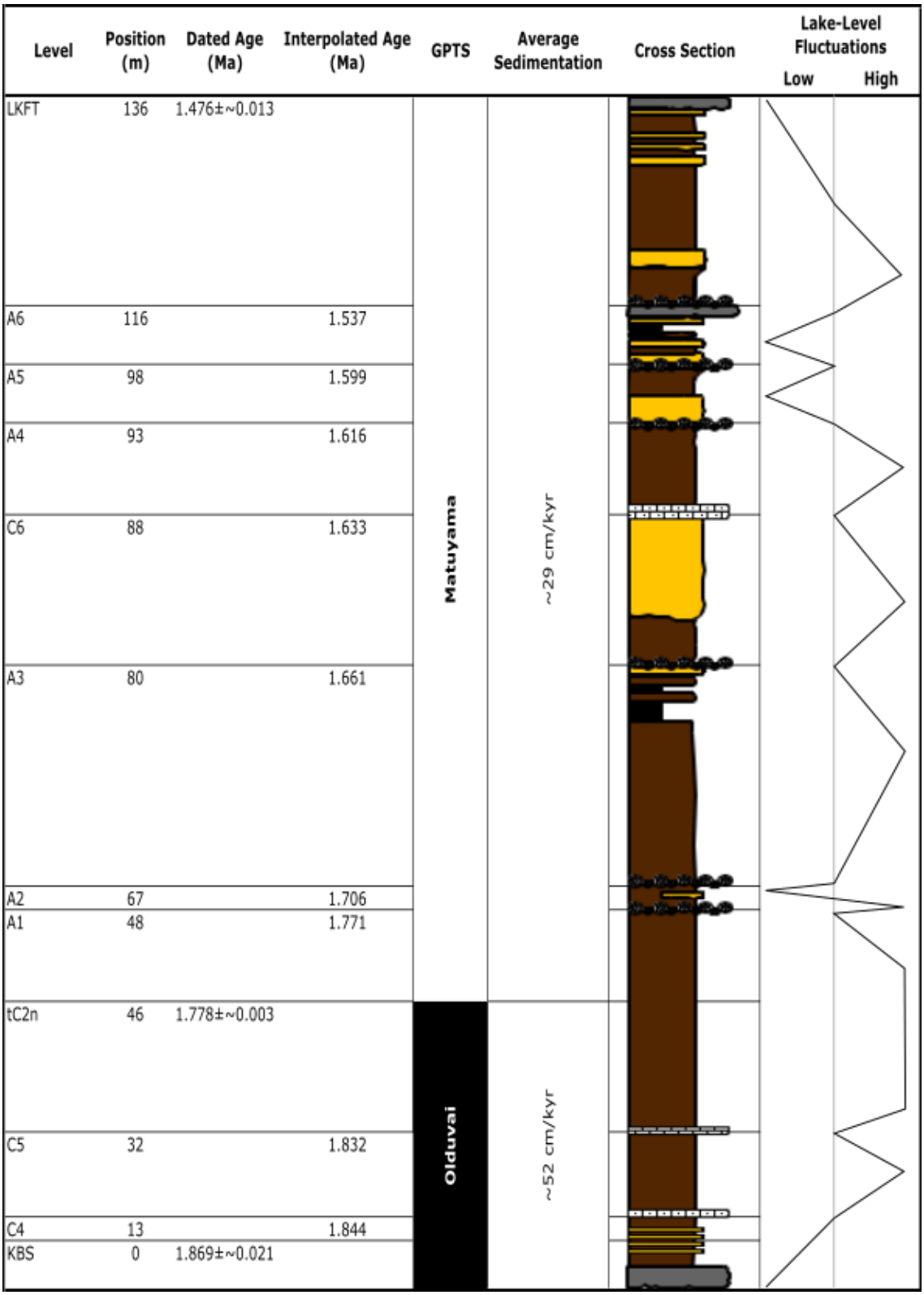

FIGURE 2.5: Time scale with generalized cross section. Average sedimentation rates from Lepre and Kent (2010), position from Lepre et al. (2007). Stratigraphic layer thickness scaled to time, not thickness.

more recent research has evaluated the difficulties in making such conclusions (Levin et al., 2009).

To evaluate the stable isotope values found in the Turkana Basin, the system for the parent water source must be appreciated. The system is refreshed in two ways; the Omo River (fed by Ethiopian rainfall) is the primary contributor of water with its headwaters in the Ethiopian Highlands to the north, and the rainy seasons twice a year are the secondary influence on the water budget of the region. The rainy seasons of the Turkana Basin contribute about 200 mm/year (Nicholson et al., 1988; Johnson and Malala, 2009), whereas the annual evaporation rate is about 2,300 mm/year (Ferguson and Harbott, 1982; Johnson and Malala, 2009). As the $\delta^{18}O$ and δD of meteoric water from Ethiopia is enigmatically high for high elevation settings (in Africa and worldwide), it has differing stable isotope values from those of meteoric water from Kenya (Levin et al., 2009), so qualtifying the rainfall and headwater contributions will lend itself to a more robust understanding of how best to approach the development of the palaeoenvironmental / palaeotemperature profiles from the stable isotopes recorded in the stromatolites of this study. It is believed low-level air streams, convergence zones between air streams, and the topography are the three main factors contributing to complex climate of equatorial eastern Africa (Levin et al., 2009).

There are three major air streams for eastern Africa. These air streams are (1) the mostly dry air of the northeast monsoon, (2) the southeast monsoon from the Indian Ocean, and (3) bringing humid air from Congo, the westerly southwesterly stream (Levin et al., 2009). Separating the northeast and southeast monsoons is the Intertropical Convergence Zone (ITCZ) while the westerly flow is separated from the low-level easterly flows by the Congo Air Boundary (Levin et al., 2009; Johnson and Malala, 2009). The two monsoon systems control the distribution of the two rainy seasons of Kenya and Ethiopia (Levin et al., 2009).

In Kenya the two rainy seasons brought on by the southeasterly winds from the Indian Ocean are the Masika (March through May) and Vuli (October through December, shorter and weaker than the former). In Ethiopia the two rainy season are Kiremt (June through September, and are the heavier rains) from the southwesterlies and westerlies and Belg (March through may) from the southeast (Gamachu 1977; Griffiths, 1972; Vizy and Cook, 2003; Levin et al., 2009). The Belg lose influence in northern Ethiopia where the one annual

peak of rainfall lasts from June to September. Southeastern Ethiopia, bordering Kenya, has rainfall evenly distributed between March through May and July through October. Like Kenya, it also lacks mesoscale convective systems (i.e. radar precipitation features greater than 2000 km^2) (Levin et al., 2009).

There are two definitions that need to be explained before proceeding. First θ_e is the equivalent potential temperature of meteoric water and is an indicator of stability in the lower atmosphere. For deep convection to occur, high θ_e is needed for a moist air parcel to be warm enough to initiate the release of latent heat condensation and make it potentially buoyant in its surroundings. Regions of high θ_e originate most of the rainfall in tropical Africa because the majority of rainfall there is convective. Deuterium-excess (d-excess) quantifies the how much evaporation has occurred at the source of the water and is indicative of the evaporative enrichment in ^{18}O after the water has condensed. D-excess it is derived by the best-fit line relating $\delta^{18}O$ and δD and defined by d-excess= δD-8 * $\delta^{18}O$ (Gat et al., 1994, Gat 1996, Levin et al., 2009).

Water formed from moisture recycling has $\delta^{18}O$ and δD values that are indicative of their source area (Levin et al., 2009). No fractionation occurs in terrestrial water returned to the atmosphere through transpiration. Conversely, terrestrial water does fractionate when it is returned to the atmosphere through evaporation. Rainfall from the latter source has high d-excess and is depleted in ^{18}O compared to its source water (Levin et al., 2009).

Confirming the Indian ocean as a source for Kenyan water, $\delta^{18}O$ values of first rains from the Indian Ocean are similar to those $\delta^{18}O$ values of water sampled in Kenya (Levin et al., 2009). The condensation of vapor derived from partially evaporated raindrops can lead to the high d-excess of some waters in Kenya. Conversely, southwesterlies and westerly winds of Ethiopia bring rain of a different $\delta^{18}O$ values than those of Kenya and the Indian Ocean (Levin et al., 2009).

The isotopic analysis of Ethiopian rainwater suggests that it has a large transpired component because the d-excess is low and the rain water is enriched in ^{18}O, i.e. not depleted as in the case of evaporative sources (Levin et al., 2009). The pattern of high θ_e (as a measure of transpiration) of the Sudd and Congo Basin in association with the continental outline of Africa in the lower troposphere points to the profound effect terrestrial water recycling

can have on moisture in tropical Africa (Brubaker et al., 1993, Gong and Eltahir 1996; Trenberth 1999). This transpiration model has been postulated by Taupin et al., 2000 where the absence of the continental effect in west Africa implies that moisture is recycled through transpiration as it is not fractionated. Typically evaporation and transpiration are combined (as evapotranspiration), however it is evident from this study that the two should be considered separately first as they can be distinctly identified and function separately (Levin et al., 2009).

Due to evaporation, Ethiopian and Northern Kenyan waters exhibit low d-excess values - as expected for river and shallow well waters in arid regions. Precipitation forming from water evaporated from near the land surface (e.g. rift valley lakes) may be the driver for the high d-excess value of Kenyan waters. Seasonal or annual precipitation is integrated at surface and near-surface water which may be useful in considering the altitude effect of Ethiopia. Kenyan and Ethiopian δ^{18}O altitude trends are less pronounced than those found elsewhere in the tropics (Gonfiantini et al., 2001; Lachniet and Patterson 2002). These researchers also suggest that the difference in isotopic values of δ^{18}O of Ethiopian waters and Kenyan waters is due to the differing moisture sources. The main moisture sources for eastern Africa being (1) marine vapor from the Indian Ocean and (2) terrestrial moisture (evapotransporation)from the Sudd and Congo Basin which are separated by the Congo Air Boundary (Levin et al., 2009).

Kenyan $\delta^{18}O_{water}$ values average -2.5 $\pm$ 2.4‰ (n=181) while Ethiopian $\delta^{18}O_{water}$ values average -0.2 $\pm$ 1.8permil (n=165). While Ethiopian δ^{18}O values are significantly higher than those of Kenya, the d-excess values of Kenya (averaging 11.2 $\pm$ 9.2‰; n=149) are higher than the Ethiopian d-excess (6.5 $\pm$ 5.7‰; n=164) (separate variance t test, p¡0.0001). Evaluated against elevation indicates that for every kilometer increase in elevation there is a 0.5‰ to 1.3‰ decrease in δ^{18}O (Levin et al. 2009). An explanation for the anomalous Ethiopian water is in the ^{18}O-enriched moisture source and in the processes that (typically at higher elevation, inland locations) minimize depletion of heavy isotopes (Levin et al., 2009).

Ultimately, if and when influxes of rainfall in the Ethiopian highlands greatly increased in the past, the isotopic signature of the rainfall could overwhelm evaporative alterations in

δ^{18}O in the lake waters (Abell and McClory, 1986). The variability between seasons could potentially be easily derived from stromatolites, fossil gastropods, and other carbonate sediments (Abell and McClory, 1986). Because of lake bathymetry, the range of isotopes throughout the formation of a carbonate could be relatively large. The northern end of the lake contains both the inflow and outflow of earlier lake systems (from when lake level was high enough), which means that to overwhelm the isotopic fractionation of the southern end of the lake (a positive signal) there would need to be a significant influx of headwaters (a negative signal) to obtain homogeneity. While the southern end would remain largely homogeneous, there would be rapid swings from potentially brackish to fresh water near Koobi Fora depending on how the $\delta^{18}O_{water}$ is interpreted. Relatively speaking, however it is possible to interpret macroenvironmental conditions of greater aridity to those of greater freshwater influx (Abell and McClory, 1986).

2.7.2 Interpretation of δ^{13}C of carbonates in the Turkana Basin

It has been demonstrated that the spread of C_4 grassess and floodplain environments in East African can be reconstructed using δ^{13}C record from pedogenic carbonates (Cerling et al., 2003; Quinn et al., 2007; Levin et al., 2011; Quinn et al., 2013). Photosynthetic pathways of C_4 (grassland, e.g. tropical grasses) and C_3 (woodland; e.g. trees, shrubs, temperate grasses) plants distinctly fractionate carbon isotopes (Ehleringer, 1989) with the former discriminating against δ^{13}C less than the latter (Quinn et al., 2007). The separation of δ^{13}C values between the pathways is stark with C_3 ranging -31.4‰ to -24.6‰ and C_4 ranging -14.1‰ to -11.5‰ (Cerling et al., 2003). The ratio between C_3 and C_4 decaying plant matter on the land surface can be incorporated into the δ^{13}C of pedogenic carbonates through CO_2 at depths greater than 30 cm if the soils have high respiration rates (Cerling 1984; Quade et al., 1989; Cerling and Quade, 1993; Quinn et al., 2007).

To derive environmental reconstructions of the floral community, Quinn et al. (2007) sampled the pedogenic carbonates of synchronous lateral horizons that developed in the paleosols of the Koobi Fora Formation. The established chronostratographic framework and scaled sedimentation rates were used for age control of the samples. Of import to this study was the sampling of those carbonates from the Koobi Fora Ridge subregion in

areas 101, 102, 103, and 104 - all located near the Koobi Fora Ridge area of 107 where TBS-107-A4-006 was collected. Quinn et al. (2007) interpreted floral communities (i.e. woodland versus tropical grassland) based on statistically significant shifts in δ^{13}C values. The population statistics were based on groups organized spatially and temporally. Spatially, samples were qualified based on the end members of basin margin to lake shore while temporally they were divided into five 100-kyr interval groups between 2.0 Ma and 1.5 Ma. The time period of import to the study of the A4 stromatolite layer presented here is generally from 1.778 to 1.6 Ma (the time period bracketed by the end of the Olduvai subchron, tC2n, and the Lower Koobi Fora Tuff) and is covered in the 1.8–1.7 Ma and 1.7–1.6 Ma intervals. Pedogenic carbonates of the Koobi Fora Formation recorded a δ^{13}C range of -10.4‰ to 0.4‰; forest to savanna grassland respectively. The mean δ^{13}C of -5.5 ‰ was interpreted as savanna mosaic (Quinn et al., 2007 after Wynn, 2000, 2001).

The high clastic content of the paleosol morphology in the Koobi Fora Ridge subregion has been interpreted as a result of the proximity to a fluctuating lake margin (Feibel, 1988). The sand filled surface cracks and thick calcic horizon of the Lorenyang pedotype, which appears in the record after 1.8 Ma, in interpreted as a soil that seasonnally supported sparse savanna grassland, but was quickly buried, inhibiting its time for development (Wynn, 2004; Quinn et al., 2007). Following 1.8 Ma, a more open savanna grassland environment develops until 1.65 Ma when the subregion is dominated by the low-tree shrub category.

Regional changes in aridity and local lake-level oscillaions in the Koobi Fora Ridge area created environments unsuitable for woodland floral communities and gave rise to the propensity of tropical grass environents (Quinn et al., 2007). Near channel and lake-margin settings with high water tables and sedimentation rates are ill-suited for paleosol and pedogenic carbonate development (Quinn et al., 2007; van Beemen and Buurman, 2002). Regions need to have negative water budgets and rainfall less than 100 cm/yr over hundreds to thousands of years to develop pedogenic carbonates (Quinn et al., 2007; Jenny, 1941, 1980; Birkeland, 1984; Srivastava, 2001). While the prevalence of paleovertisols in the Plio-Pleistocene Koobi Fora Formation are ideal for pedogenic carbonate growth based on an extended dry season and limited annual moisture (Feibel, 1988; Wynn, 2000, 2004; Quinn et al., 2007), reconstructions of floral communities are limited to these drier subaerial

landscapes potentially biasing results toward floodplain/grassed environments (Quinn et al., 2007).

δ^{18}O and δ^{13}C stable isotopes in both stromatolites sampled covariate well with Pearson correlations of 0.862 in TBS-A4-107-006 and .859 in TBS-A4-123-017. The implications of variability so close to 1 is that the carbon and oxygen captured by the stromatolites (i.e. microbial communities responsible for $CaCO_3$ production) are in equilibrium with the environment. Furthermore, Quinn et al. (2007) using pedogenic carbonate δ^{13}C values, demonstrates that between 2.0 and 1.5 Ma, the Turkana Basin lake system transitioned to a flow-through fluvial system. Those researchers found that the residence time of Omo River water in the basin experienced a through-time decrease, while subaerial landscapes expanded. This increase in basin water loss caused a decrease in wooded habitats and expanded subaerial floodplain habitats. The pedogenic carbonate δ^{13}C values exhibited in the Koobi Fora Ridge in that study (between approximately -6‰ and 1‰) is wider than the range of δ^{13}C found here in both TBS-107-A4-006 (the Koobi Fora Ridge specimen, range -3.34 to -0.18‰) and TBS-123-A4-017 (the Bura Hasuma specimen, range -4.16 to 0.68‰).

2.8 Temperature Interpretation of $\delta^{18}O_{calcite}$

Using the empirical relationship of $\delta^{18}O_{calcite}$ and temperature developed by Epstein et al. (1953) and the first palaeotemperature equation developed by Craig (1965), many palaeotemperature equations have been derived. To put this generally, the ratio of ^{18}O to ^{16}O in the atmosphere is known. Using the same ratio for water as starting point, deviations in carbonates can be indicative of temperature or changes in parent water ($\delta^{18}O_{water}$) fractionation. ^{16}O is more energetic than the heavier isotopes of oxygen and preferentially evaporates from water and in turn increases the concentration of available ^{18}O (which preferentially incorporates into a solid form). While many studies relate to molluscan carbonates, the premise is similar in stromatolites. When precipitated in isotopic equilibrium, unaltered biogenic carbonates record δ^{18}O ($\delta^{18}O_{calcite}$) as a function of the δ^{18}O of the water ($\delta^{18}O_{water}$) and water temperature at the time of formation (Sharp 2007; Craig

1965). With a stable $\delta^{18}O_{water}$, $\delta^{18}O_{calcite}$ of biogenic carbonate formation will vary with temperature at the time of formation.

$$T(\,^{\circ}\mathrm{C}) = 16.5 - 4.3 \times (\delta^{18}O_{calcite} - \delta^{18}O_{water}) + 0.1 \times (\delta^{18}O_{calcite} - \delta^{18}O_{water})^2 \quad (2.8.0.1)$$

Interpreting the water temperatures recorded by the stromatolites of the Turkana Basin requires that the variable values and contributions of $\delta^{18}O_{water}$ (e.g. rainwater sources for the headwaters, fractionation during water transportation along the Omo River, fractionation in the local environment) are appreciated to isolate the appropriate $\delta^{18}O_{water}$ for use in equation Equation 2.8.0.1. There are limited data for the local $\delta^{18}O_{water}$ of Lake Turkana marginal Pleistocene ponds, crevasse splays, and back bays; however, others have suggested that the modern Turkana climate may provide a useful proxy for that of the Pleistocene (Quinn, 2015). Data collected by others and compiled in Quinn (2015) is in Table 2.1. By substituting $\delta^{18}O_{water}$ in Equation 2.8.0.1 with values from Quinn et al. (2015), this study is able to narrow the potential palaeoenvironments which are conducive for stromatolite formation and end-of-life dissolution based on research completed by Wieland and Kühl (2000). Wieland and Kühl (2000) determined that mean water temperatures of 30°C are conducive for the formation of stromatolites and as temperatures approach or exceed 35°C stromatolites begin an "end-of-life" self-dissolution process (a process discussed later in chapter 3).

TABLE 2.1: Turkana Basin modern meteoric water $\delta^{18}O_{water}$ (SMOW) values.

Water Source (n)	Mean $\delta^{18}O_{water} \pm 1\sigma$(‰)	Range $\delta^{18}O_{water}$(‰)
Lake Turkana (12)	6.0 ± 0.7	4.4 to 7.2
Turkana Rainwater (6)	-0.3 ± 2.3	-3.7 to 1.9
Omo River at Turkana (5)	-0.8 ± 0.4	-1.2 to 0.1
Omo River (10)	-3.0 ± 1.0	Not reported
Rivers (7)	-1.4 ± 1.5	-2.5 to 2.3
Streams (3)	0.3 ± 1.7	-2.5 to 2.3
Springs (5)	-1.9 ± 2.3	-4.1 to 0.6
Wells (7)	-2.5 ± 1.6	-3.7 to 0.8
Waterholes (13)	-1.5 ± -2.1	5.5 to 2.1
Karsa waterhole (1)	8	-

From Quinn (2015); data from Cerling et al. (2003, 2008), Levin et al. (2009), and Vonhof et al. (2013)

Chapter 3

Stromatolites

The definition of stromatolites has been highly contested among researchers since it was first defined as a trace fossil that is implicitly biological by Kalkowsky in 1908. Kolkowsky's definition of "organogenic laminated, calcareous rock structures, the origins of which is clearly related to microscopic life, which itself must not be fossilised" (as translated in Krumbein, 1983) assumes and expects much from the geoloical record by way of preservation and interpretation. Conversely, Semikhatov et al., 1979 identifies stromatolites in terms of sedimentary structures as "an attached, laminated, lithified, sedimentary growth, accretionary away from a point or limited surface of initiation" (Mcloughlin et al., 2008). Most researchers can agree that the morphology of stromatolites can be mediated by both biological and physical (macro and micro environmental) factors. However, for ease of discussion, all carbonate stromatolite samples from the East African Rift display evidence for biological origin (Casanova, 1986) and will be discussed here as such. The importance of this to this study is that the implications of the stable isotopic analysis of stromatolites makes the most sense so long as stromatolites are of biological origin and the carbonate is precipitated at the same time as the structure which it forms. That being said, stromatolites have long been studied as valuable sources for palaeoecological and palaeohydrological reconstruction (Casanova, 1986).

The debate surrounding the definition of stromatolites in the geologic record underscores the limited understanding of living stromatolites in their modern environments. Through

an appreciation of the processes that can produce stromatolites in the modern environment, conclusions can be drawn about stromatolites in the palaeoenvironment. Laminated sedimentary structures (which includes stromatolites) can be produced through chemical, physical, and sometimes chemical biological processes - the contributions of which can be difficult to ascertain. Processes that create stromatolite growth are responsible for the records contained within them. It is of the utmost importance that there is an understanding of how stromatolites are produced in order to interpret the data contained within them. While morphologically distinct, due to the resemblance between microbial mats and ancient stromatolites, it is valuable to study microbial mats (or microbially induced sedimentary structures, MISS) as analogues for ancient stromatolites as extant examples are more wide spread (Dupraz and Visscher, 2005; Noffke and Awramik, 2013).

3.1 Biological process of stromatolite build-up

In most mats (and by extension stromatolites) the community of microbes can be understood generally as a cyanobacteria dominated layer at the near surface ($<$ 1-2 millimeter depth), followed by a layer of purple sulfur bacteria, underlain by green sulfur bacteria. The laminations tend to be more black with depth and can include gray bands (Riding et al., 2000, Dupraz et al., 2009). This coloring is indicative of iron sulfides with some pyrite and implies increased organic carbon composition with increased sulfide production in the case of black layers and decreased organic matter with an in crease in bound and trapped sediments in the case of the gray layers (Dupraz et al., 2009). Communities of cyanobacteria and heterotrophic bacteria comprising the mats that make up stromatolites form stromatolites through the processes of binding; biostabilization; baffling, trapping and extracellular polymeric substance (EPS) mineralization; and fossilization (Noffke and Awramik, 2013).

3.1.1 Binding, biostabilization, baffling and trapping, and EPS mineralization

Binding is the process by which microbes actively assemble to form the mat fabric. This is where the cyanobacteria proliferate to form a "sticky" substance (called extracellular polymeric substance, EPS, discussed later) with which to collect sediment grains. During erosional periods, mats biostabilize to reduce the influence of the hydrological energetics on the community (Noffke and Awramik, 2013).

Biostabilization refers to the fixation of sediment by microorganisms (Neumann et al., 1970; DeBoer, 1981; Grant and Gust, 1987; Dade et al., 1990; Gerdes et al. 2000b; Paterson and Daborn, 1981; Krumbein et al., 1994; and Paterson, 1997). This process serves to change the effects of external and internal forces (i.e., erosion and intradepositional gases, respectively) have on the mat (Noffke, 1997; Gerdes et al. 2000b). Sediments already present on/in the mat are stabilized by cyanobacteria three different ways that can be exclusive of one another: loose grains already present on the surface are fixed (and held to the outer layer), rough sediment surfaces are smoothed by the extracellular mucilages of the microbes (reducing friction on the surface), and finally sealing of the sediment by the mat itself (and incorporating the benefits of the first two)(Noffke et al., 2001). All three processes stave off erosion.

Grain fixation permits the mat to be flexible without fracturing. By keeping the community together, it increases the surface area of the mat allowing for more growth. During the process of sealing the sediment by the microbial mat, sediment is covered by the extracellular mucilages of the cyanobacteria which provides a dense layer prohibiting gas exchange from beneath the mat with the water and the atmosphere. Hollows formed beneath this outer layer can be observed in cross section of some stromatolites and microbial mats. According to Noffke 2001, these fenestrae structures are reflected by sponge pore fabrics and are well known in fossil carbonate environments (Black 1933; Dunham 1962; Tebutt et al., 1965; Noffke et al., 2001)

EPS production through photosynthesis is of paramount importance to the accretion cycle. This exopolymer traps sand grains as they settle out of suspension at low flow rates.

Filamentous cyanobacteria then binds the grains as they moves toward the surface. Likewise, during periods of sedimentation, filamentous cyanobacteria of the mat introduce baffling (turbulence) on the microenvironment of the hydrological system and trap sediment and grains in their matrix. These grains are then incorporated into the fabric of the mat through EPS secretion and mineralization. Heterotrophic bacteria bore through these trapped grains and secrete calcium carbonate ($CaCO_3$).

Precipitation of the EPS and the secretion of the heterotrophic bacteria are what contribute to a stromatolite's upward growth. Biomass, trapped and stabilized sediment, and precipitated minerals make up the starting substrate for a stromatolite. Through the lifecycle and fossilization of the stromatolite, the biomass is overlain, mineralized, degraded, or dissolved (Dupraz et al., 2009; Noffke and Awramik, 2013). However, as long as EPS production exceeds dissolution, evidence of the mat is preserved in the rock record. $CaCO_3$ precipitation is supported by two factors: the geochemical factor of the saturation index (SI), and the biological chemical factor of extracellular polymeric substances (EPS) (Dupraz and Visscher, 2005; Dupraz et al., 2009). While microbial and environmental factors are integral in the production and lithification of a microbial matrix, the saturation index (SI) and available nucleation sites of the microenvironment and community are the lynch pins to the processes. Organic EPS both promotes and prevents the formation of inorganic carbonate, and relies on its specific physiochemical microenvironment to do so. The EPS matrix is chemically reactive and functions as a barrier between the cell and the organic and inorganic metabolic substrates, predators, antimicrobial agents and other bacteria (Costerton et al., 1995; Dupraz et al., 2009). It is a high molecular weight polysaccharide matrix that can include protein, peptides, noncarbohydrate acidic moieties, inorganic compounds, and extracellular DNA (Sutherland 2001a, b, c, d).

3.1.2 Modification of the saturation index for favorable growth conditions

The saturation index (SI) relates the ion activity product (IAP) to the (thermodynamic) solubility product (K_{sp}) of the corresponding mineral. A solution is supersaturated when IAP $>$ K_{sp}. SI is defined as SI=log(IAP/K_{sp}). Simply, positive SI precipitate inorganic

carbonate, negative SI dissolve inorganic carbonate. To determine whether the SI of $CaCO_3$ is favorable for precipition or disolution (where conditions are at 25°C, 1 bar atmospheric pressure and 35 PSU salinity), IAP = $\{Ca^{2+}\}\times\{CO_3^{2-}\}$, K_{sp} is $10^{-6.19}$ and $10^{-6.37}$ for aragonite and calcite, respectively. The concentration of CO_3^{2-} in solution however is variable and tied to the carbonate equilibrium ($H_2CO_3 \leftrightarrow HCO_3^- \leftrightarrow CO_3^{2-}$ with a pKa of 5.9 and 8.9 respectively). As pH controls the balance of CO_3^{2-} produced, pH ultimately controls the precipitation or dissolution of $CaCO_3$ in this case. When the SI exceeds 0.8, $CaCO_3$ precipitates. The microbial communities, through the production of EPS, balance the microenvironmental conditions to favor the growth of the community and to control spontaneous inorganic precipitation of $CaCO_3$ (Dupraz et al., 2009).

3.1.3 Extracellular polymeric substance

The EPS matrix is an extension of the microbe and consists of polysaccharides and amino acids (Dupraz et al., 2009). Much like the stromatolites themselves, the component of EPS that makes up so much of their structure is difficult to define specifically due to the variety of polymers used to build its complex three dimensional matrix (Neu, 1994). Attempts to identify the integral parts of the EPS matrix have ultimately succeeded in only underscoring the complexity, not only within, but between the unique matricies. Each biofilm system has EPS of heterogeneous composition and microbial origin (Sutherland, 2001; Reid et al., 2003; Eckman et al., 2008). Different microorganisms that can produce EPS, create matrices of unique composition and structure that, much like the community, is a response to stressors and environmental conditions. Beyond EPS retaining nutrients and protecting the mat community against desiccation, ultraviolet radiation and other weathering mechanisms, it further bolsters the community by creating channels for water to transport metabolites, nutrients, and gene signaling compounds (in quorum sensing). These unique characteristics may be interpreted as regulators of physiological processes and microbial interactions within the community. Macromolecules of some EPS are responsible for inhibiting $CaCO_3$ precipitation and as such, the EPS is constantly modified through physiochemical and microbial degradation. Likewise, $CaCO_3$ precipitation is the result of EPS alteration in three ways: microbial decomposition of EPS (i.e. self-consumption

which releases HCO_3^- and Ca^{++}); organomineralization (which reorganizes acid binding sites allowing $CaCO_3$ to precipitate); and precipitation when negatively charged groups are saturated with Ca^{++} (Dupraz et al., 2009). The alkalinity engine is the interaction of processes that fuel the precipitation of calcium carbonate in microbial mats (Dupraz and Visscher, 2005; Dupraz et al., 2009). The environmental conditions must contain an available amount of minerals in solution for the microbial community to metabolize. Metabolic rate is determined by the availability of inorganic carbon (CO_2) for photosynthesis which in turn is converted to organic carbon and then respired by the microbial community. While this metabolic rate changes the microenvironment (and can provide a buffer for the community), the local environmental conditions ultimately throttle the type and rate of metabolism. As a result of the alkalinity engine, and as long as photosynthesis exceeds respiration, organic carbon is precipitated into the microenvironment as EPS in the microbialite and lithification of the microbial mat (Dupraz and Visscher, 2005; Dupraz et al., 2009).

3.1.4 Microbial guilds involved in EPS production

Microbial metabolism refers to the chemical reaction where reactants are removed from the environment and metabolic products replace them (Decho et al., 2005; Dupraz and Visscher, 2005; Dupraz et al., 2009). Thermodynamic yields from microbial metabolism typically decreases with depth in normal sedimentary systems. Aerobic metabolisms are understood as the highest yielding while anaerobic methanogenesis has the lowest energetic yield and is found at depth corresponding to the redox gradient. The mechanism allowing anaerobes to survive and thrive in the surficial layer of mats is unknown (Dupraz et al., 2009), but their presence nonetheless implies that the redox gradient typical to sedimentary systems is not followed in stromatolites and other Microbially Induced Sedimentary Structures (MISS, Dupraz et al., 2009). It is a sliding balance where the geochemical environment is continuously shifting between precipitation and dissolution reactions due to the lack or abundance of reactants and products. This can be most readily observed through the fluctuating oxygen-depth profile during the diel cycle. Layers with a supersaturation in excess of 600% oxygen during the peak of the diel cycle (solar midday) have been observed

to turn anoxic when the light period ends (Decho et al., 2005; Dupraz and Visscher, 2005; Dupraz et al., 2009).

MISS, microbial mats, and stromatolites are often viewed as semi-closed systems efficient in element cycling and requiring little more than light to function. The communities contained within have some of the highest metabolic rates per square surface area on the planet, rivaling those of rain forests (Dupraz and Visscher, 2005). Reduction-oxidation reactions are the core to the microbial metabolism. Changes in alkalinity, facilitating carbonate precipitation or dissolution, may be attributed to chemical alteration of the microenvironment by microorganisms. The bacteria and microalgae that produce EPS control its secretion with specific genes that are reglated by quorum sensing (or chemical signaling) from the bacterial/algal community (Miller and Bassler, 2001). Through quorum sensing, mat activities are coordinated and metabolisms are made more efficient (Dupraz and Visscher, 2005; Dupraz et al., 2009). The community of organisms whose communal metabolism can be attributed to mat production can be subdivided into separate guilds of microorganisms. These guilds are categorized based on their metabolisms and functions to cycle key elements - oxygen, nitrogen, sulfur, and carbon. The guilds (as defined by Dupraz et al., 2009) are:

1. Photolithoautotrophs (i.e. cyanobacteria, autotrophs)
2. Aerobic (chemoorgano-) heterotophs
3. Fermenters
4. Anaerobic heterotrophs (usually sulfate reducing bacteria, SRB)
5. Sulfide oxidizers
6. Anoxyphototrophs (i.e. purple and green (non)sulfur bacteria)
7. Methanogens

Microbial mat community composition is determined by light quantity and quality. Within 1-2 millimeters of the surface, the dominant phototrophs (cyanobacteria) are photoinhibited at normal daylight intensities. Photolithoautotrophs are responsible for converting inorganic carbon to organic carbon. This creates the energy source for (chemoorgano-)heterotrophs. Autotrophs use light to fix organic carbon (through photosynthesis) while

chemoliths oxidize sulfide, hydrogen, and ammonium to utilize redox reactions. Photosynthesis of the mat primarily fixes CO_2 at rates exceeding $5g/m^2$ per day (Dupraz et al., 2009). By fixing CO_2 through photosynthesis and depleting CO_2 in the environment, cyanobacteria can reestablish carbonate equilibrium in the microenvironment when the balance shifts unfavorably for the community. Furthermore, by increasing alkalinity (through removal of H^+) the microbes enables $CaCO_3$ precipitation. After the sun sets, the anaerobic communities start producing glucose and purple sulfur bacteria metabolisms thrive increasing the alkalinity of the micro-environment above the mat surface. The alkaline change creates a buffer for the cyanobacteria, whose metabolisms, which had been precipitating during the day, turn toward fermentation and nitrogen and ammonia fixation during the night (Dupraz et al., 2009). See figures 3.1 and 3.2 adapted from Dupraz et al. (2009).

Interestingly, experiments conducted by Wieland and Kühl (2000) on the Solar Lake, Egypt cyanobacteria mat, were able to couple the oxygen and sulfur cycling of the mat with temperature. O_2 consumption is most active in the aphotic zone at 30°C and saturation of sulfide oxidation and increased sulfide efflux occured at 35°C. Furthermore, a pH decrease due to aerobic respiration, sulfide oxidation, and fermentation was enhanced with temperature with incomplete sulfide oxidation occuring in the photic zone of the mat (Wieland and Kühl, 2000). At 25°, oxygen penetration into the mat was at its greatest, but the processes associated with respiration through the mat cross section (e.g. enhanced heterotrophic activity and sulfide oxidation) notably increased pH (Wieland and Kühl, 2000). Likewise, aphotic processes associated with the night-side of the diurnal cycles (e.g. fermentation) continued to increase mat pH (Wieland and Kühl, 2000). Although this research did not study the effects of temperatures lower than 25°C sustained increases in pH are not sustainable for precipitation and dissolution of $CaCO_3$ and growth of the stromatolite..

The heterotrophic guild requiring the organic carbon produced by the phototrophs through photosynthesis can be found in the same upper layer of the mat as the photoautotrophs. The surplus of organic carbon created by the autotrophs feeds aerobic heterotrophs that then depletes oxygen which allows anaerobes and other organisms vulnerable to O_2 to respire/metabolise in close proximity to the photolithoautotrophic cyanobacteria. Taking large organic molecules and breaking them down to low molecular weight matter, aerobic heterotrophs and fermenters provide fuel for methanogens and other respiratory processes

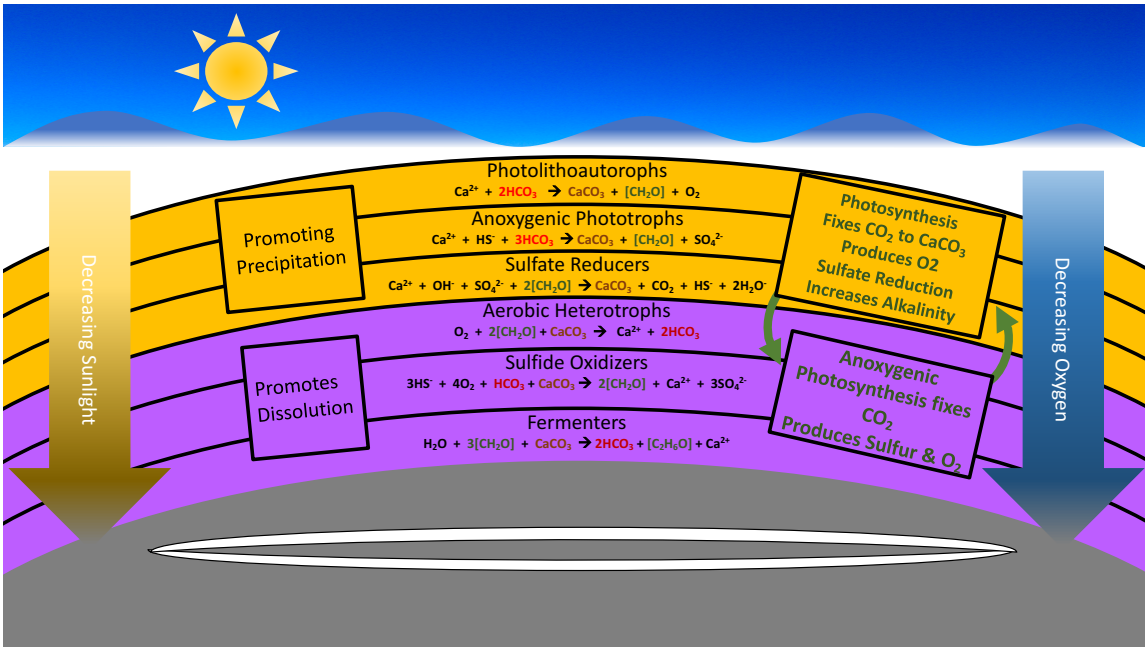

FIGURE 3.1: During the day, photosynthesis and sulfate reduction increase alkalinity and promote carbonate precipitation. Adapted from Dupraz et al., 2009.

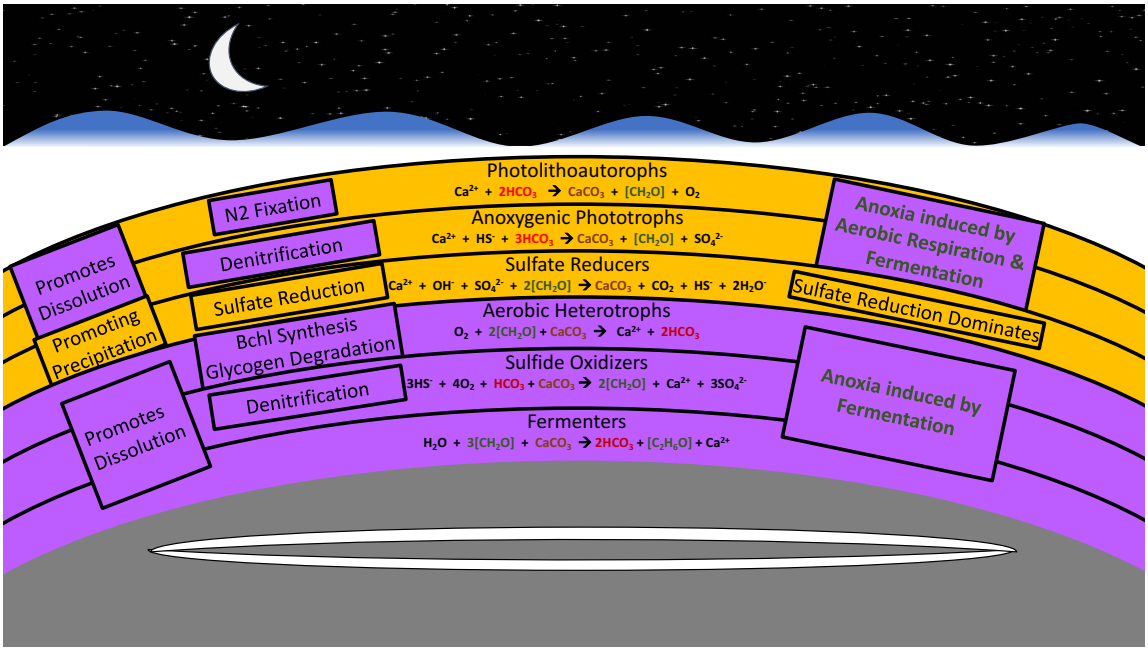

FIGURE 3.2: During the night, photosynthesis and oxygenic processes cease; anoxygenic processes (e.g. sulfate reduction) balance the dissolution induced by fermentation. Adapted from Dupraz et al., 2009).

at the process termination. Ironically, anaerobes, which are reliant on the heterotrophic community for sustinance (and vulnerable to oxygenated environments), are also found at the near surface area (Dupraz et al., 2009). EPS provides components that are consumed by the community and in particular anaerobes. This combined with the action of fermenting and SRB organisms may be responsible for the high HCO_3^- consumption rate of stromatolites. Rapid and extreme fluctuations in O_2 levels during light regime changes create anoxic environments attributed to fermentative microorganisms and SRB (Dupraz and Visscher, 2005).

Cyanobacteria (among other types of phototrophic microbes) are integral to the system due to this oxygen variability. Oxygenic photosynthesis results in the production of large amounts of organic carbon and oxygen. While photosynthesis fixes CO_2, it depletes the environment of CO_2 in excess of its replenishment forcing bicarbonate to dissolve into CO_2 and OH^-. The added OH^- in the system increases alkalinity (by definition) and encourages $CaCO_3$ precipitation i.e. $2HCO_3^- + Ca^{++} \rightarrow CaCO_3 + CH_2O + O_2$ (Dupraz et al., 2009)

Photosynthesis must exceed the rate of respiration. A 1:1 ratio results in no net precipitation or dissolution, so abiotic and biotic anoxygenic photosynthesis and sulfate reduction, which increase the SI, must do so in excess of the aerobic heterotrophy, sulfide oxidation, and fermentation that are decreasing it. Stromatolites in hypersaline environments (such as those found at the shores of the palaeo-Lake Turkana), rely heavily on sulfate reducers in shifting the alkalinity towards $CaCO_3$ precipitation (Lyons et al., 1984; Walter et al., 1993; Visscher et al., 2000; Dupraz et al., 2004; Baumgartner et al., 2006; Dupraz et al., 2009). The population of SRB through cross-section of the stromatolite mat layer demonstrate an increase in abundance and metabolic rate with depth in the carbonate precipitation horizon. Sulfate reduction (as evaluated by Visscher et al. 1998, and Dupraz and Visscher et al. 2005) is greater than the aerobic respiration in stromatolites. SRB are unique in that they rely solely on organic carbon and H_2, not O_2, allowing them to function not only outside of the diel cycle, but at beyond the photic zone. The increase of the SI by SRB allows for $CaCO_3$ precipitation and accumulation (Dupraz et al., 2009).

Production of EPS is not limited to one guild versus another. Both phototrophic and heterotrophic bacteria are capable of producing EPS. Although cyanobacteria are the primary

EPS producers in microbial mats (De Philippis et al., 1998; Stal, 2000; De Philippis et al., 2001; Stal, 2003; Richert et al., 2005; Dupraz et al., 2009), heterotrophic bacteria (like SRB) are also relevant contributors through the diurnal cycle. This leads to variable quality and character (e.g. composition, texture) throughout the mat transect. Coupled with variable relative metabolic contributions due to variable sediment and nutrient concentrations thoughout the year, evidence of the cooperative EPS production may be responsible for the differences between laminations observed in the mat transect (Dupraz et al., 2009).

3.1.5 The interaction of EPS, microbial communities and microenvironmental chemistry

Physically, EPS is highly variable ranging from gel-like to a dissolved solute state. Ultimately, the physical characterics are a function of the community's response to water activity on the molecular level. Functional groups within the molecular structure can be blocked inhibiting bond sites. This complicates the proportion of bonds created at a given pH level. Initially inhibition occurs on calcium carbonate formation, but these physiochemical properties can also promote degradation and alteration of the matrix (abiotic or biotic) thereby promoting calcium carbonate production. EPS removes free Ca^{++} ions from solution with negatively-charged acidic groups within the EPS matrix. This alters the local microenvironment depleting it of these ions restricting carbonate minerals from precipitating. As the pH increases, a negative charge builds in the EPS from the deprotonization of the functional groups. The pK values are generally unique to different chemical groups, so as separate functional groups are used in response to the changing microenvironment (i.e. pH), the metal binding properties (e.g. calcium, magnesium) of the EPS changes sequentially.

Between the various microbial guilds (which are each responsible for separate molecular functional groups), EPS can also function to network the community together. EPS has been observed to channel water in response to nutrient excesses and deficiencies as well as waste evacuation (Neu, 1994; Costerton et al., 1995; Decho, 2000). Extracellular DNA and its role in quorum sensing has been hypothesized to provide the backbone of the EPS that

directs formation and the exchange of genetic material (Dupraz et al., 2009; Whitchurch et al., 2002; Petersen et al., 2005; Vlassov et al., 2007).

Biologically-influenced mineralization can occur when binding capacity of the EPS is saturated. The combination of alkaline environmental conditions and free Ca^{++} ions can leads to the nucleation of $CaCO_3$ on the EPS matrix (Aeo et al., 1999a,b). As such, Ca^{2+} can preferentially bind with the EPS matrix and inhibit precipitation of calcium carbonate minerals within the microbial community. To overcome this, microbes have to modify the EPS through biologically-induced/influenced mineralization through super saturation of the binding sites, or alteration of the EPS (Trichet and Defarge, 1995). Biologically induced precipitation in stromatolites has been closely linked to using the EPS matrix as a metabolic substrate. Research (Decho et al., 2005) into the turnover of carbon in modern marine stromatolites demonstrated that initially 3-4% of the carbon fixed through photosynthesis was used in producing EPS. Within 24 hours 40-60% of this EPS was degraded to CO_2. Cyanobacteria consuming ^{14}C-HCO_3^- respire low molecular-weight organic carbon that is then consumed by aerobic and anaerobic heterotrophic bacteria predominantly in the $CaCO_3$ precipitating surficial layer (Decho et al., 2005). Oxidation is typically split evenly between aeobic and anaerobic pathways. Anaerobic pathways are highly important due to the fluctuation of oxygen concentrations with the variable light regimes (Visscher et al., 2002; Paerl et al., 2001; Troelsen and Jorgensen, 1982).

In closed basins, saturation of the binding sites is possible during seasonal upwelling of alkaline water and evaporation (Arp et al., 2003). Stagnant water with anoxic conditions can result in sulfate reduction and alkaline bottom waters where sinking organic carbon is oxidized, creating HCO_3^- and increasing alkalinity. Evaporation, upwelling, diffusion, or turnover of the water column can encourage $CaCO_3$ production/formation (Kempe, 1990; Kempe and Kazmierczak, 1994; Arp et al., 2003). This supersaturation pump can be mimicked within the EPS matrix of stromatolites and other mats in hydrated pockets (Dupraz et al., 2009).

3.2 Morphology and environment

3.2.1 Micromorphology and environment

The morphologies of stromatolites are representative of the physical and chemical microenvironment in which they formed (Reid et al. 2003, Eckman et al. 2008). Researchers studying modern marine stromatolites in have determined that growth stages are characterized on a spectrum of three mat types which represent variations in community structure in response to intermittent sedimentation (which has be interpreted a product of wind/wave energy). In open marine stromatolites laminae demonstrate three different types of mats that can be identified by their distinct mineral products. Type 1 are those dominated by trapping and binding cyanobacteria; Type 2 contain thin biofilms which are rapidly lithified by an abundance of heterotrophs (e.g. SRB) sealing underlying ooids with aragonitic micritic laminae; and Type 3 mats are colonized by coccoidal cyanobacteria which bore and fuse ooids together (MacIntyre et al., 2000; Reid and MacIntyre, 2000; Reid et al., 2003).

3.2.2 Three mat types and their implications for microbial communities

Type 1 stromatolites are made up of sparse populations filamentous cyanobacterium. These elongated cyanobacteria orient vertically, away from their underlying substrate, and entwine themselves around carbonate sand grains. They are most common in layers representing the binding and trapping of sediment grains (Eckman et al., 2008). Type 1 resemble pioneer communities (see Stal et al., 1985) which flourish during high sediment accretion intervals.

Mats which developed microcrystalline carbonate (micrite) on their surface are considered Type 2. These mats, similar to Type 1, have cyanobacterial filaments, but they are few. This type is dominated by amorphous, heterotrophic exopolymer, comprised of equally metabolically diverse microorganisms. Aragonite crystal needles are commonly found in the exopolymer matrix as spherical aggregates. Type 2 mats are indicative of more mature surface community and develop during quiescent intervals of no sedimentation. Mats begin

the lithification process at this time. In contrast to Type 1, carbonate silt (e.g., tunicate spicules) is entrapped in the surface film demonstrating the lower energetics of the water. A continuous film (conducive to heterotrophic activity of aerobic and anaerobic bacteria) can form in a matter of days. Sulphate reduction can account for 30-40% of the organic carbon consumption by the bacteria and promotes aragonite production and correlates with micritic crusts (Visscher et al., 2000). Bacteria and aragonite needles are found in association with each other and promote calcification of the biofilm when carbonate sands are accreted on to the stromatolite. This outer layer of film can extend below the cortex as a continuous layer of micritic cement (Reid et al., 2003; Eckman et al., 2008).

Type 3 mats are characterized as dominated by coccoid heterotrophic endolith cyanobacteria (Solentia sp.) and randomly oriented filamentous (Schizothrix) below a biofilm. Solentia bore into carbonate grains, fusing them together at contact points. This is indicative of a longer interval of no sedimentation and a more mature layer than Type 2 and represent the pinnacle of the stromatolite system. As cyanobacteria bore through the grains, their excretion encourages accelerated bacterial respiration while their boreholes are infilled by aragonite. Furthermore, this infilling between grains at contacts fuses grains together and develops the carbonate crusts. Similar to Type 2, this activity aids in the precipitation process - opposing the view that these microbores are fundamentally destructive to the community (Golubic and Brown, 1996; Perry, 1998; Reid et al., 2003). The crusts of the stromatolite extends below the cortex and enhances the structural strength for stromatolite growth and preservation. Fused grains were observed to have been formed in weeks to months under field and laboratory observations conducted by Reid et al., 2003. The development of this carbonate crust by Solentia has deeper implications when it is highlighted that Solentia is a photosynthetic microorganism and that its micrboring activities require that the community remains at or near the surface within the photic zone. Longer hiatal periods develop communities of eukaryotic algae incapable of forming laminated structures in vertical section as seen in stromatolites (Golubic and Brown, 1996; Steneck et al., 1998; Perry, 1998; Reid et al., 2003).

3.2.3 Stromatolite laminae

Lithified laminations observed in vertical section of the fossilized stromatolite correlate to former surface mats and occur approximately every 1-2 millimeter. Laminations correspond to 10-60um thick crusts of micrite and/or 1-2mm thick layers of fused microbored grains beneath the micritic crusts. While laminae can be observed in hand sample, they are subtle in petrographic thin section (Reid et al., 2003). Thin crusts are identical in thickness, composition, texture, observed under light microscopy and scanning electron microscopy to calcified biofilms. Marine cements are not observed during the early binding stages of growth, demonstrating that the laminated build up is developed by lithifying mat surfaces providing the structural support with topographic relief (Reid et al., 2003).

Stromatolites respond to the intermittent sedimentation of communities by lithifying during hiatal intervals (Reid et al., 2003). This response requires two microbial processes: photosynthetic production by cyanobacteria (light bands) and heterotrophic respiration by bacteria (darker bands). Laminations develop by precipitation of micrite in biofolms during periods of low to no sedimentation and below biofilms due to microboring and precipitation/infill (Reid et al., 2003). In the case of Lake Turkana, the pulsing of the Omo River and the typhoon seasons may be effective correllaries.

Light sparitic laminae are indicative of phases favorable to photoautorophic organisms (e.g. cyanobacteria) whereas dark laminae correspond to a slower metabolic rate of the same, but an increase in bacterial blooms (Casanova and Hillaire-Marcel, 1993). This is not correlative to the diel cycle, but rather variable photic intensities throughout the year during the rainy and dry seasons.

3.2.4 Macromorphology and environment

Much has been mentioned to this point concerning the effect of microenvironmental chemical and energetic conditions on microbial and laminae make up in stromatolites, while the larger-picture hydrologic settings affecting stromatolite morphologies has been underdiscussed. Therefore, the effects of the larger environment on morphology and microbial growth will be discussed here. Casanova (1986) examined several lakes and basins of the

East African Rift system (the Suguta valley and Lakes Abhe, Bogoria, Magadi, Natron, and Manyara) and derived palaeoenvironmental interpretations from morphological characterization and stable isotope analysis.

The calcium carbonate sinks of fluvial channel and spring environments are more similar to travertines, with relevant microbial communities resembling tufted mats or isolated colonies, than to stromatolites as defined earlier; however they represent an end member of the palaeoenvironmental spectrum that is necessary to include. The formation of travertines implies particular environments which where groundwater has concentrated a significant amount of dissolved calcium in the subsurface (Chafetz and Folk, 1984; Casanova, 1986).

Lakes Bogoria and Natron have several examples of these with the former interpreted as the terraces of former springs and the latter having extant examples forming a waterfall dam (Casanova 1986). While their gross morphology is responsive to their parent environments, the morphological features are mediated by the nature and shape of the substrate (Casanova, 1982). Cylindrical or planar encrustations are representative of spring environments while the encrustations of waterfall dams are massive, associated with bushes of non-vascular plants. Downstream carbonates precipitate as reef bed and gastropod encrustations representing a lower energy (calmer) environment, or as pebble encrustations and spheroidal oncolites representing higher energy (more agitated) hydrological conditions (Casanova, 1986). Diagenesis of these carbonates is common from frequent recrystallization. European travertines are exceptionally similar to those studied in Africa, maintaining the interpretation of the deposits (Casanova, 1986).

Floodplains are relatively rare in the present-day East African Rift system, but Lake Magadi provides a valid reference point for study (Eugster, 1980; Casanova, 1986). Floodplains are classified by a wide area which is inundated by a thin sheet of water, generally a few centimeters deep. They form during heavy rainy seasons and refreshed by only direct precipitation and runoff from the surrounding area (Casanova 1986). With no hydrodynamic potential, residence time of the water is limited predominantly by evaporation. While present, oncolites can form around a nucleus of detrital grains from trachytes or aggregates of carbonate mud (Casanova and Tiercelin, 1982). The form of these oncolites, as they

were collected from Lake Magadi, is typically discus with pinched centers a few centimeters in diameter (Eugster, 1980). It is important to note that both of these nuclei contain a degree of calcium that can be cannibalized by the overlying microbial community (Casanova, 1986).

These oncolites, in thin section, are generally made of light and dark laminae doublets with the light containing microbial filaments normal (i.e. perpendicular) to the nucleus; however fan shapes are possible as well. Biological structures are not observed in the dark layers (Casanova, 1986). Rhythmic laminations are difficult to discern as filaments commonly cut across laminae and the dark laminae of the doublets are often discontinuous. This is further complicated by the microenvironment also lending itself to major recrystallizations (Casanova, 1986).

The morphology of the oncolites (as with other stromatolites) is a clear indication of the microenvironment in which they formed. Due to the shallow depth and highly evaporative environment of the floodplain, the response of the microbial community was to focus the growth of the oncolite primarily to its zone of maximum wetness (i.e. the margins), creating the pinched disc morphology found in the record. Growth always occurs by successive planar laminae with no columnar forms in fluvial and floodplain environments (Casanova, 1986).

Hydrothermal environments are capable of producing stromatolitic formations in the East African Rift Basin as hot springs and geysers can be located where faults intersect the lake shorelines. The environment high alkalinity, pH (7.8 to 9.9), and temperature (40 to near 100 degrees Celsius) of the hot spring waters are conducive for stromatolite producing microbial communities (Casanova 1986). While biologically produced carbonates are not present in the extant lakes of the rift (namely Bogoria, Magadi, and Natron), aragonitic deposits have been found that are of abiotic origin (Casanova 1986).

The fossil record contains several examples of hydrothermal stromatolitic carbonates which form as pool-rim dams and chimneys (Fontes et al., 1975; Renaut, 1982; Casanova, 1986). Reaching tens of meters in height, they are associated with sub-lacustrine and shoreline settings. The size of the specimens and the coarseness of laminae are indicative of a stable environment throughout the lifetime of the microbial communities (Casanova, 1986).

The sodium carbonate-bicarbonate lakes of the East African Rift System do not currently form lacustrine or shoreline stromatolites, but fossil stromatolites have been employed to indicate former lake level highs and stratigraphic correlations (Casanova, 1986; Feibel et al., 2009). When found in the stratigraphic record, stromatolites are indicative of freshwater lakes during a period of significant dissolved $CaCO_3$ concentration and stable waters and can form as columnar growth (which is limited to lacustrine environments), although planar growth can be found (Casanova, 1986).Given periods of stability on the order of 10-100 years, stromatolites can encrust their substrates uniformly, maintaining the morphology of the substrate. These stromatolitic encrustations are evidenced in Holocene high stands in Lake Bogoria, Lake Abhe, Lake Turkana, and Natron-Magadi basin (Gasse and Rognon, 1973; Tiercelin, 1981; Renaut, 1982; Abell et al., 1982; Casanova, 1986). Longer lacustrine stability, between 10^3 to 10^4 years, can develop stromatolitic reefs that are indicative of water depth as well as lacustrine phase highstands. These reefs can be found in the stratigraphic record of the Suguta valley, Natron-Magadi Basin, Lake Manyara, and Lake Turkana (Casanova, 1986; Abellet al., 1986).

3.2.5 Stromatolites as depth indicators

The morphological forms of stromatolites indicate their depth at precipitation which in turn implies both hydrological energy regimes and ecological zones. The effects of energetic and depth zones of the palaeolake from the lake surface to a depth of 12 meters are discussed below(Casanova, 1986).

Floodplain oncolites have a highly distinctive morphology indicative of relatively arid environment with only periodic water refreshment (Casanova, 1986). The oncolites formed in fluvial and channelized flow display isotropic stromatolitic growth while the floodplain oncolitic forms resemble pinched disks (Casanova, 1986) like red blood cells.

Of all the environments in which stromatolites form, lacustrine stromatolites provide the most significant amount of information in the East African Rift. Lacustrine stromatolites resemble reef development in that as continental carbonate facies they provide geological and limnological information. These stromatolites indicate former shorelines and record

information for age, altitude, and hydrological and physiochemical characteristics of palaeolakes useful in palaeoenvironmental (and climatological) reconstruction (Casanova, 1986; Dupraz et al., 2006).

Between 0 and 2 meters below lake surface the water column contains the highest dissolved oxygen and highest light intensity which promotes biological competition as is evidenced by strong ornamentation from columnar growth of the stromatolite by the microbial communities (Casanova, 1986). Isolated bioherms, mammilated oncolites, and encrusted cobbles and vegetal remains are the morphologies most associated with this surficial zone (Casanova, 1986).

Between 2 and 7 meters the water column has stabilized substantially compared to the more surficial zone. Large flattened bioherms with low ornamentation form parallel the shorelines colonizing the entire substrate. These stromatolites are less influenced by the macroenvironmental conditions than those that are more shallow in the water column (Casanova, 1986).

Between 7 and 11 meters below lake surface the greatly diminished light intensity stresses the photoautotrophs of the microbial community and thereby diminishes the production of the dissolved oxygen. Sub-lacustrine currents in channels perpendicular to the shoreline are capable of promoting the development of spheroidal oncolitic to polyphased stromatolites (millimeter to centimeter scale) due to constant agitation and promoting isotropic stromatolitic growth (Casanova, 1986).

It is important to note that stromatolite significance in defining lake level highs and bathymetric information should be treated with care as these are both greatly tied to regional tectonics. Furthermore, stromatolites have been observed growing at depths exceeding 15 meters (and up to 60 meters in Lake Natron; Lake Suguta; and Lake Wondergat, South Africa; Gow, 1981; Casanova, 1986).

3.3 Interpretations of stromatolite laminae and the implications for stable isotopes

Researchers have found that stable isotope data elucidated from stromatolites does not always correlate with contemporaneous inorganic carbonates (Abell et al., 1982; Casanova and Hillaire-Marcel, 1993). One possible explanation is that stromatolites form in the uppermost waters where the palaeolake water exchanges O_2 and CO_2 with the atmosphere and the macroenvironmental photosynthetic metabolic system while inorganic carbonates are more likely to precipitate from underlying waters where total dissolved inorganic carbon (TDIC) is controlled primarily by the bicarbonate ions in solution and the ^{12}C of organic matter oxidation from decay (Abell, et al., 1982; Lee et al., 1987; Fontes and Gasse, 1991; Casanova and Hillaire-Marcel, 1993). There is no fractionation believed to occur between atmospheric CO_2 and dissolved CO_2 (Degens, 1969; Deins and Gold, 1972; Abell et al., 1982).

Casanova and Hillaire-Marcel (1993) developed a seasonality ratio for the interpretation of laminations. When light laminae are thicker than dark, the cyanobacterial filaments have passed through the EPS layer. These laminae exhibit higher detrital and organic matter with carbonates tend to be depleted in $\delta^{13}C$ (3.1 to 3.8 ‰ PDB) and $\delta^{18}O$ (2.4 to 3.7 ‰ PDB). In this case, it is interpreted that a period of high runoff and transport of clastic grains with increased dissolved phase nutrients promoted microbial growth and the extensive binding and trapping. These doublets are associated with a positive hydrologic budget and spreading vegetation where $\delta^{18}O$ is depleted due to the water being refreshed and $\delta^{13}C$ is depleted due to the shift towards C_3 (swamp) plants and input of light CO_2 from decaying organic matter (Casanova and Hillaire-Marcel, 1993).

Conversely, doublets with thicker dark laminae typically exhibit these laminae unconformably resting on the lighter ones suggesting cyanobacterial growth was interrupted and erosion followed before the darker laminae started to develop. These doublets have few detrital grains and little organic matter (when compared to the other end of the spectrum). Likewise, the carbonates tend to be richer in ^{13}C (4.0 to 5.4 ‰ PDB) and ^{18}O (3.5 to 5.4 ‰ PDB). Carbonates in equilibrium with atmosphere precipiate at approximately 1

to 2 ‰ PDB. In the semi-arid palaeoenvironment of the Turkana Basin, increased $\delta^{18}O$ (in mixed water) implies an extended residence time for the water (enrichment through evaporation; Hillaire-Marcel and Casanova, 1987). It is worth noting, however, that in an unmixed water column, this generality becomes far more complex. High $\delta^{13}C$ indicates an increase in the photosynthetic metabolisms of the photoautotrophs which preferentially metabolize $^{12}CO_2$ and $H^{12}CO_3^-$ (Rau, 1978; Herezeg and Fairbanks, 1987; Casanova and Hillaire-Marcel, 1993). This creates an enrichment of the heavier carbon (e.g. ^{13}C) in the water (dissolved phase) and carbonates they precipitate; a period of stronger evaporation (Hillaire-Marcel et al., 1986; Merz, 1992, Casanova and Hillaire-Marcel et al., 1993).

Increasing $\delta^{18}O$ and $\delta^{13}C$ values through the transect of a stromatolite suggest a change in meteoric water or increasing residence time of the waters of the macroenvironment (Casanova and Hillaire-Marcel et al., 1993). In addition to photosynthetic activity (when considered with the $\delta^{18}O$) the more enriched the $\delta^{13}C$ values are in a stromatolite the higher the C3:C4 plant ratio and/or the amount of organic matter in the soils from recharge zones (Hillaire-Marcel et al., 1989; Talbot, 1990; Aucour, 1992; Casanova and Hillaire-Marcel, 1993). A semi-covariablility between $\delta^{18}O$ and $\delta^{13}C$ implies that the carbon and oxygen used and precipitated by a specimen was in equilibrium with its environment (Abell et al., 1982). Departures from this covariability are most simply understood as departures from the pattern by the $\delta^{13}C$. Even while $\delta^{13}C$ in stromatolites is grossly parallel to $\delta^{18}O$, the $\delta^{13}C$ tends to be slightly more variable due to the changing TDIC in parent waters being closely linked to the local photosynthetic activity of the macroenvironment (e.g. the stromatolitic reef and metabolism or decay of other local plant life). The $\delta^{18}O$ reservoir is much more stable simply due to its size - the palaeolake water. Evaporation is the primary fractionating force of water.

3.4 The Abell et al., 1982 interpretation

The stable isotopes of the eastern Turkana Basin stromatolites were first analyzed by Abell et al. (1986). Reevaluation of their interpretation of isotopic data is complicated by the researchers' earlier stratigraphic terminology and understanding. Under the older stratigraphic interpretation, the seven stromatolite horizons were distributed between a period

prior to the KBS Tuff and after the Okote Tuff. The current understanding (established in Brown and Feibel, 1986) places the first six of the Turkana Basin stromatolitic marker beds (i.e. Marker Beds A1 – A6) between the KBS tuff and the Lower Koobi Fora Tuff (Brown and Feibel, 1986; Lepre et al., 2007; Feibel et al., 2009). These stratigraphic changes are discussed earlier in Chapter 2 of this study. Due to the discrepancy of this interpretation and the poor quality of the photographs published in Abell et al., 1982, direct correlation between the stromatolites from Marker Bed A4 studied here and those of that reference cannot be made. Attempts to acquire higher resolution copies of the photographs in that reference were to no avail as it is from the pre-digital age and higher resolution copies from the publisher do not exist (pers. comm.), so reinterpretation must be from a relative/holistic perspective.

With those qualifications, Abell et al., 1982 does make reference to stromatolite outcrops in Area 103 of Koobi Fora that would be difficult to miscorrelate. The researchers refer to a middle bed of two distinct layers where the lower centimeters of each bed are dominated by stromatolite coated mollusc fragments forming a loose molluscan pavement - each shell forming its own algally coated oncolite; a shape that would at the very least resemble a pinched disc. These oncolites have no evidence of turbulent water flow as they lack eroded, truncated or disrupted laminae; although the laminae are asymmetrical about the nucleus with the upper laminae thicker than those on the bottom (Logan et al., 1964; Abell et al., 1982). The oncolite beds form the substrate for bulbous stromatolites with the boundary between the two a sharp one. The bulbous forms tend to widen upwards with neighboring heads laterally limiting growth and expansion. The result is in polygonal shapes in the upper portion of the stromatolites that resemble desiccation cracks in appearance alone. All of this suggests in-situ reef formation of oncolites in a floodplain environment (Abell et al., 1982; Casanova, 1986). Desiccation cracks are not found in stromatolite beds. Sedimentological interpretation by Behrensmeyer (1975) of Area 103 defined it as a deltaic mud flat to a distributary channel complex. The consistency of the bed thickness and may represent growth in shallow, flat embayment of the ancient lake.

Chapter 4

Methodologies

δ^{18}O and δ^{13}C values were collected from discrete samples every millimeter through the cross-section of stromatolite specimen collected from the Koobi Fora Formation layer A4 to determine their viability as palaeoenvironmental and palaeoclimatological proxies.

4.1 Stromatolite Sample Collection

Stromatolites were collected from the target stratigraphic layer A4 of the Koobi Fora Formation in the Bura Hasuma and Koobi Fora Ridge regions. The collection levels were determined using stratigraphic sections CSF 107-1 and 123-1 from Feibel et al. 2009 (Figure 2.2). Locations were identified on Google Earth aerial with consultation from Dr. Craig Feibel (pers. comm.) and were navigated to by GPS (see Table 4.1 below and Figure 2.4).

Table 4.1: Stromatolite Collection GPS Locations

Stromatolite	**North**	**East**
TBS-A4-107-006	3°52.551'	36°17.287'
TBS-A4-123-017	3°53.320'	36°20.998'

Areas 107 and 123 were selected due to the prevalence of the A4 layer in those areas. As

FIGURE 4.1: Koobi Fora Formation A4 layer in Area 107. Field assistant Stephen Lokademo for scale (approximately 2 meters tall).

stated above, Bura Hasuma has a thinner representation of the KBS member than regions to the west (i.e. the Koobi Fora Ridge) making the ABC layers more easily identifiable (Brown and Feibel, 1991; Feibel et al. 2009 etc). At the locations selected, in-situ stromatolites are found abundant in "colonies" of similar physical character with size generally being the most variable characteristic through the stratigraphic layer. In the field, stromatolite samples were selected qualitatively for collection and analysis for this study when they met the following criteria:

1. The stromatolite was in-situ and preferably still locked in place by neighboring stromatolites;

2. The stromatolite was unbroken, with a consistent outer lamination;

3. The stromatolite had no obvious abnormalities or unique characteristics from those around it;

4. The stromatolite was of a size representative of the A4 stromatolites found in that layer and was not heavier than $\sim$25 kg.

FIGURE 4.2: Koobi Fora Formation A4 layer in Area 107. Field assistant Stephen Lokademo (left, approximately 2 meters tall) and driver Mwang'ombe Hezekiah (right) for scale. Not pictured, cook Samuel Baali.

All of the above characteristics aided in ensuring that the stromatolites selected for collection were representative of the A4 layer in that local area. Samples were bagged in the field and labeled with the identifier format as follows:

TBS-A4-123-017

$$\boxed{\textbf{T}urkana\textbf{B}asin\textbf{S}tromatolite} \text{ - } \boxed{Layer\textbf{A4}} \text{ - } \boxed{Area\textbf{123}} \text{ - } \boxed{Sample\textbf{017}}$$

4.2 Procedure

Following collection, stromatolites were taken to the National Museum of Kenya in Nairobi and halved using a rock saw along their (in-situ) top-down view. One half of the sample remained at the National Museum and the other half was sent to the Earth and Planetary Sciences Department of Rutgers University, Piscataway, New Jersey, USA. Upon arrival, stromatolites were sampled using a dental drill scraping perpendicular to the centerline of the cross section. Sample collection started 1 millimeter above the in-situ bottom of

the stromatolite and continued every millimeter toward the outer cortex at the (in-situ) top of the stromatolite. Each millimeter was given an identifier, but appended with the millimeter location from the bottom of the stromatolite (i.e. TBS-A4-123-017-005 is located 5mm from the base of the stromatolite). The discrete sample was collected on laboratory grade wax paper sheets and deposited into sample vials with conical cavities and septa tops to ease retrieval of contents with syringe needles by the MicoMass Multiprep unit (detailed below). While the dental-drill sampling method was used here was not the most precise and accurate, it was the most time and cost efficient method available.

4.3 Stable Isotope Measurements

Approximately 100 micrograms (μg) of powdered sample was loaded into a reaction vial for the automated stable isotope analysis using a Multiprep device attached to a Micromass Optima mass spectrometer. Samples were reacted for 800 seconds in phosphoric acid at 90°C and the evolved CO_2 was collected in a liquid nitrogen cold finger. Stable isotope values are reported relative to V-PDB through the analysis of an in-house laboratory reference material (RGF1). The 1-sigma standard deviation of RGF1 made during these analyses (typically 8 RGF1 analyses for every 24 samples) is 0.05 and 0.09‰ for δ^{18}O and δ^{13}C, respectively. RGF1 is routinely calibrated to NBS19 to insure consistency, using 1.95 and -2.20‰ for δ^{18}O and δ^{13}C, respectively as reported by Coplen (1994). The internal lab reference material differs from NBS-19 by +0.10 and +0.04‰ for δ^{18}O and δ^{13}C, respectively. The lab analyzes NBS-18 to monitor changes in source linearity for δ^{18}O values. The average δ^{18}O value of NBS-18 analyzed during the period in which these samples were analyzed is -23.07‰, similar to the value of -23.01‰ reported by Coplen (1994). Therefore, no correction for linearity was made.

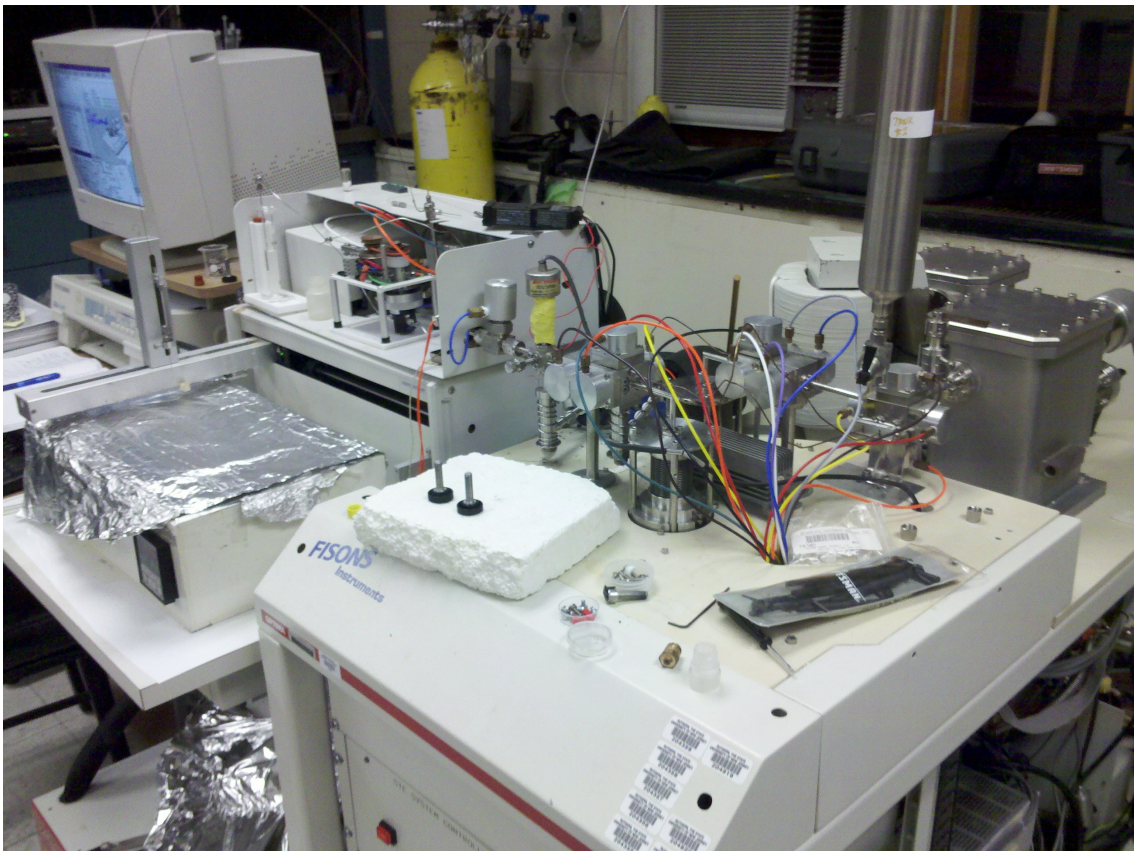

FIGURE 4.3: FISONS OPTIMA Mass Spectrometer equipped with a MicroMass Multiprep automatic sample processing system at the Stable Isotopes Laboratory of the Geological Sciences Department at Rutgers University, Piscataway, New Jersey.

Chapter 5

Results

To investigate the implications of the stable isotope values collected from the stromatolites sampled here, this study first evaluated the location of the stromatolite nucleus in cross section. At this point, the data obtained could be *folded over* itself. The section of data *in-situ* below the nucleus would be expected to have a slightly muted signal when compared to the section above due to differences in access to sunlight. Areas of laminae on the bottom of the stromatolite must have received refracted sunlight during growth as they do remain continuous throughout the lifetime of the stromatolite. Additionally, the nucleus at the center of the stromatolite serves as the starting point for reconstructing any environmental record (or change) that may have been recorded in the stable isotopes. Stable isotopte values from the stromatolites were then converted to temperatures using Equation 2.8.0.1

5.1 TBS-A4-107-006

TBS-A4-107-006 was collected from Area 107 on the Koobi Fora Ridge region of Koobi Fora. The cortex of the stromatolite is light brown to burnt orange with dark brown on its uppermost potion (see Figure 5.1). The upper and lower sections, as in TBS-A4-123-017, differ in fabric with the lower section dominated by regular, concentric laminae about the nucleus (at approximately 63 mm). Similarly to TBS-A4-123-017, the upper portion of this stromatolite (140 mm to 190 mm) has a much different texture than its lower section,

however the two differ in that this upper section is far less developed in TBS-A4-107-006. The upper section is dominated by a more irregular and angular fabric with open boreholes, and less common infilling of voids than TBS-A4-123-017.

The nucleus of TBS-A4-107-006 can be determined in cross section. Laminae grew outward from a central point approximately 63 mm above the bottom cortex. This (spheroidal) bottom section includes laminae to approximately 140 mm. The upper section of the stromatolite is approximately 50 mm of irregular laminae that cannot be traced visually. Only minute details are discerned under hand lens. Samples collected from 63 mm to 1 mm and 63 mm to 139 mm represent the same period of growth. The stable isotope data of both δ^{18}O and δ^{13}C are located in Appendix A.

5.2 TBS-A4-123-017

TBS-123-A4-017 was collected from Area 123 in the Bura Hasuma region of Koobi Fora. The cortex of the stromatolite is light brown to burnt orange with dark brown on its uppermost potion (see Figure 5.3). The stromatolite can be divided into two growth periods as defined by the shapes observed in cross section; the bottom spheroidal part is approximately 100 mm in diameter while the upper ellipsoidal part is approximately 70 mm. In addition to overall shape, these sections of the stromatolite also differ in fabric with the lower section dominated by regular, concentric laminae about the nucleus to the rounded cortex and the upper section dominated by a more irregular and angular fabric with frequent infilling of voids and predominantly flat-lying/bedded laminae. The nucleus of this stromatolite was likely a fossil clam shell judging from the shape of the inner most laminae of the bottom section. Laminae grew outward from this central point approximately 37 mm to the bottom cortex of the stromatolite and 67 mm to the top of the bottom section and another 70 mm to the top of the stromatolite. Some laminae can be traced around the entire section indicating that growth was contemporaneous and the central structure was not simply incorporated during a unidirectional growth cycle. Samples collected from 37mm to 1mm and 37mm to 100mm represent the same period of growth. The stable isotope data of both δ^{18}O and δ^{13}C are located in Appendix A.

FIGURE 5.1: TBS-A4-107-006 with millimeter scale

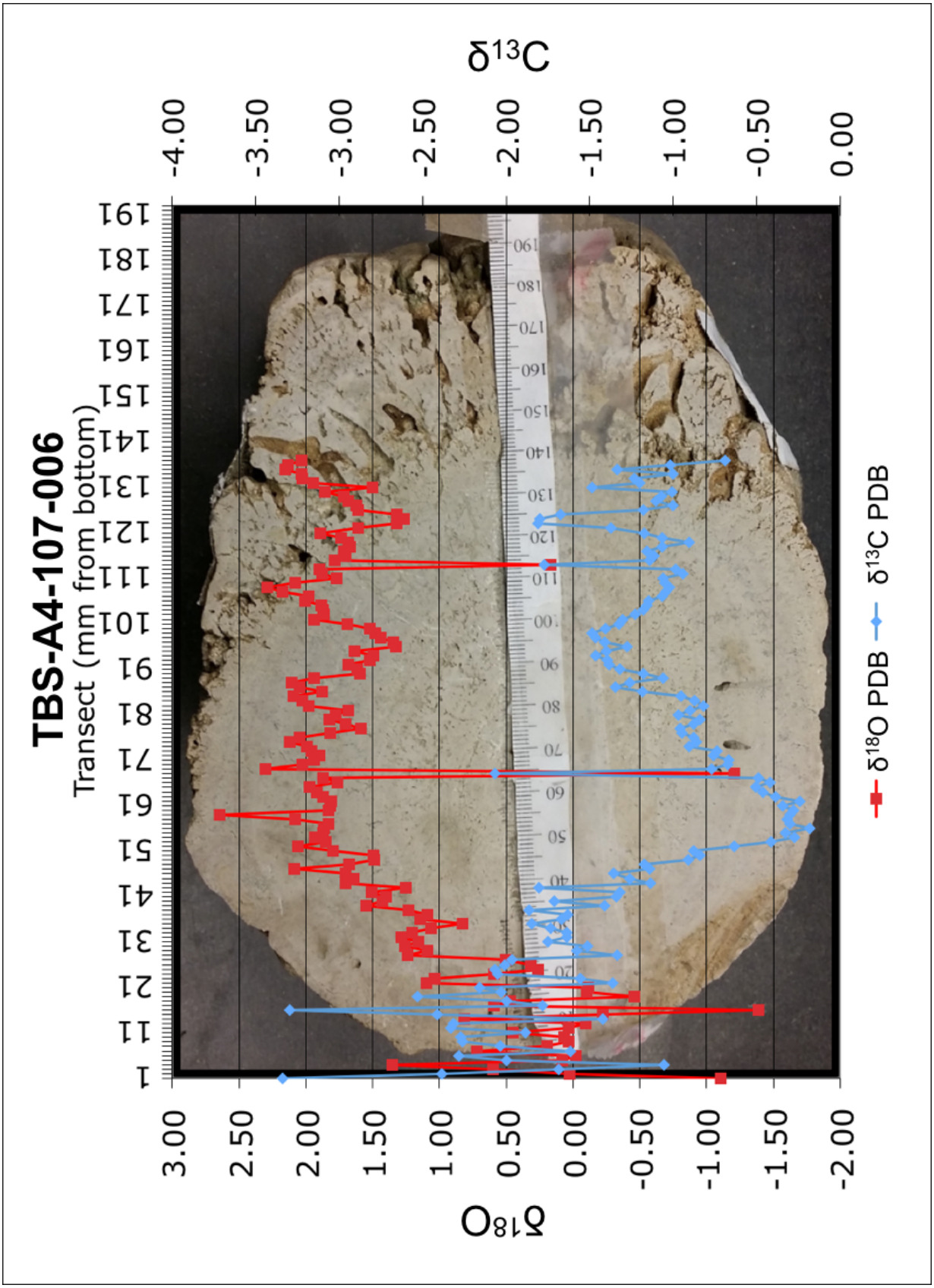

FIGURE 5.2: TBS-A4-107-006 data overlaying approximate sample locations. Data can be found in Table A.1

FIGURE 5.3: TBS-A4-123-017 with millimeter scale

5.3 Temperature Tests

Table 5.1 and Table 5.2 contain temperature statistics obtained by using the $\delta^{18}O_{water}$ for different environments as collected by others and compiled in Quinn (2015) and the values obtained by sampling stromatolites TBS-A4-107-006 and TBS-A4-123-017 respectively in Equation 2.8.0.1 to contextualize possible environments. For reference, $\delta^{18}O_{SMOW}$ data collected by Quinn, (2015) is included here as Table 2.1) and identified in Table 5.1 and Table 5.2. These results are discussed further in the following chapters.

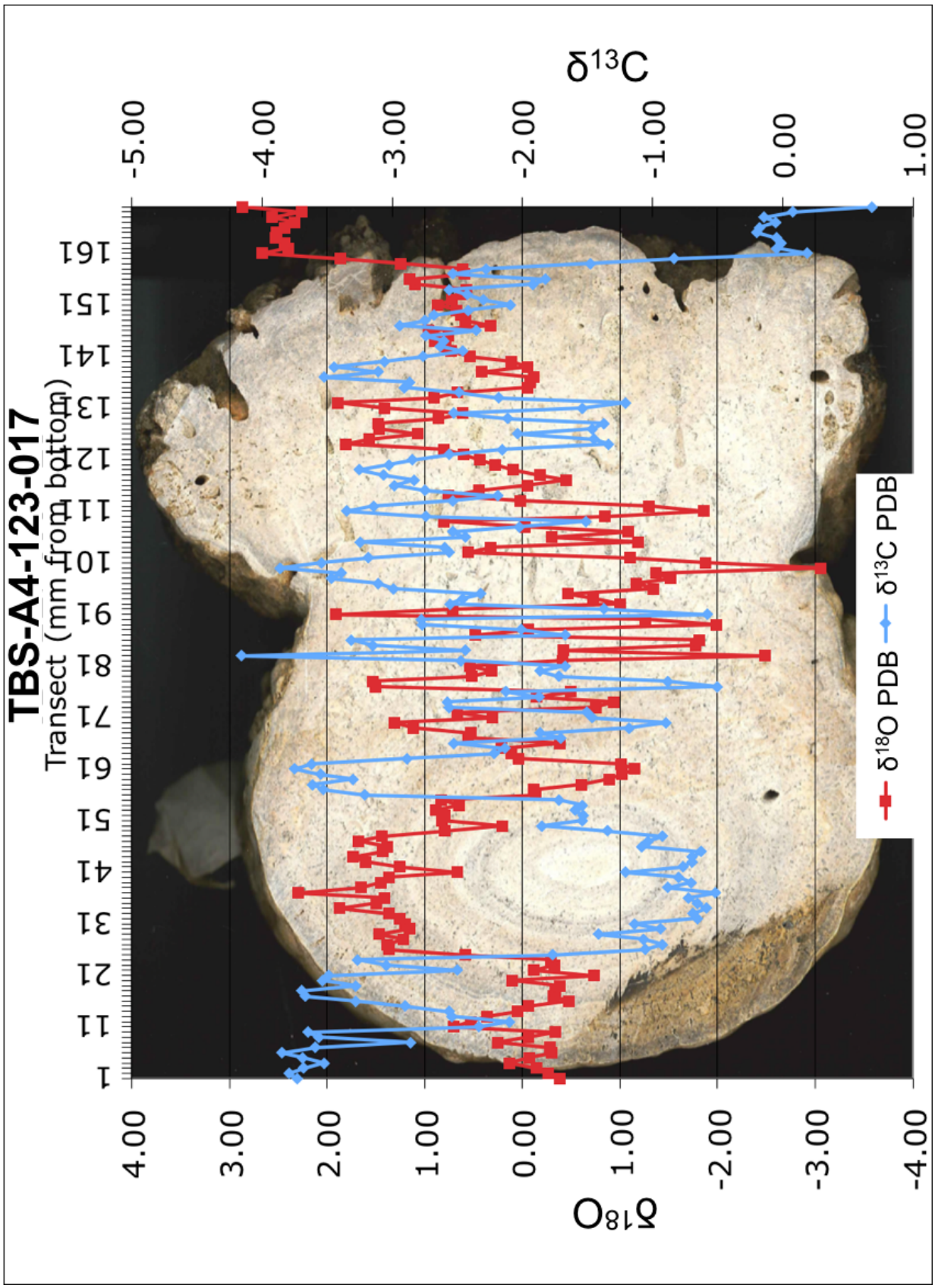

FIGURE 5.4: TBS-A4-123-017 data overlaying approximate sample locations. Data can be found in Table A.3

TABLE 5.1: Summary of Temperature Results for $\delta^{18}O_{water}$ in Equation 2.8.0.1 using $\delta^{18}O_{SMOW}$ from Quinn, 2015 for TBS-A4-107-006 Data

$\delta^{18}O_{SMOW}$	Omo River $-3.0‰$	Springs $-1.9‰$	Waterholes $-1.5‰$	Rivers $-1.4‰$	Rainwater $-0.3‰$	Streams $0.3‰$	Lake Turkana $6.00‰$
Maximum Temperature (C)	8.8°	13.2°	14.8°	15.2°	20°	22.8°	54.1°
Minimum Temperature (C)	-3.3°	-0.2°	1.1°	1.4°	5°	7.2°	32.5°
Mean Temperature (C)	0.2°	3.7°	5.1°	5.5°	9.5°	11.8°	39°

TABLE 5.2: Summary of Temperature Results for $\delta^{18}O_{water}$ in Equation 2.8.0.1 using $\delta^{18}O_{SMOW}$ from Quinn, 2015 for TBS-A4-123-017 Data

$\delta^{18}O_{SMOW}$	Omo River $-3.0‰$	Springs $-1.9‰$	Waterholes $-1.5‰$	Rivers $-1.4‰$	Rainwater $-0.3‰$	Streams $0.3‰$	Lake Turkana $6.00‰$
Maximum Temperature (C)°	16.7°	21.7°	23.5°	24°	29.4°	32.5°	66.9°
Minimum Temperature (C)°	-3.9°	-0.8°	0.4°	0.7°	4.3°	6.4°	31.4°
Mean Temperature (C)°	3.6°	7.5°	9°	9.3°	13.7°	16.2°	45.1°

TABLE 5.3: Summary of δ^{18}O treatment statistics

Stromatolite	Count	Sum	Mean	Variance
TBS-107-A4-006 δ^{18}O PDB	137	191.62	1.40	0.58
TBS-123-A4-017 δ^{18}O PDB	170	69.93	0.41	1.18

5.4 Statistics

The mean δ^{18}O of all stromatolite samples from Koobi Fora analyzed here yielded a mean of 0.85‰ and a standard deviation of 1.07. Table 5.3 on page 61 contains treatment statistics for δ^{18}O. The mean δ^{13}C of all stromatolite samples from Koobi Fora analyzed here yielded a mean of -1.78‰ and a standard deviation of 0.99. Table 5.5 on page 62 contains treatment statistics for δ^{13}C.

5.4.1 Results from Kruskal-Wallis

A one-way Analysis of Variance (ANOVA) between the stable isotope data sets of the stromatolites demonstrated that the data sets were likely not of Gaussian distribution and that the stomatolites were not from a single population (temporally, spatially, or both). A Kruskal-Wallis rank sum test on the data confirmed the same. While the one-way ANOVA uses the actual variability associated with the samples between data sets, the Kruskal-Wallis rank sum test only uses the rank of sample values within the population to analyze the distribution. The p-value for both analyses also highlights these differences.

P-values are a way of qualifying how likely two or more sample sets were collected from populations with identical distributions. In this study, the P-value is the probability that the stromatolites sampled here contain identical distributions of stable isotopes (with 95% confidence). Here, the P-value will determine whether the stromatolites originated from identical environmental conditions at the time of formation (i.e. they shared the same body of water). For both δ^{13}C and δ^{18}O, the p-values between the stromatolites are very low ($p < 0.001$) which implies that the samples did not come from stromatolites with the same distribution of stable isotopes and formed in different bodies of water.

TABLE 5.4: Results of ANOVA and Kruskal-Wallis rank sum test of $\delta^{18}O$

One-way Analysis of Variation (ANOVA)						
Variation Source	SS	df	MS	F	F crit	P-value
Between Groups	73.97	1	73.97	81.30	3.87	2.19628E-17
Within Groups	277.47	305	0.91			
Total	351.44	306				

	K-W Statistic	P-value	Critical Value
Kruskal-Wallis rank sum test	74.11	7.38E-18	3.84

TABLE 5.5: Summary of δ^{18}C treatment statistics

Stromatolite	Count	Sum	Mean	Variance
TBS-107-A4-006 δ^{18}C PDB	137	-176.79	-1.29	0.34
TBS-123-A4-017 δ^{18}C PDB	170	-2.17	0.41	1.16

TABLE 5.6: Results of ANOVA and Kruskal-Wallis rank sum test of δ^{13}C

One-way Analysis of Variation (ANOVA)						
Source of Variation	SS	df	MS	F	F crit	P-value
Between Groups	58.29	1	58.29	73.36	3.87	5.42456E-16
Within Groups	242.34	305	0.79			
Total	300.63	306				

	K-W Statistic	P-value	Critical Value
Kruskal-Wallis rank sum test	58.035	2.57E-14	3.84

5.5 Summary of Results

The majority of the data in Figure 5.4 and Figure 5.2 is well constrained and the $\delta^{18}O$ and δ^{13}C covariate well. The generally low amplitude of the $\delta^{18}O$ and δ^{13}C data during the formation of TBS-A4-107-006 suggests a more stable environment than TBS-A4-123-017. The higher amplitude, covariating $\delta^{18}O$ and δ^{13}C during the formation of TBS-A4-123-017 suggests a less stable environment. The data statistics presented here complicate hypotheses suggesting there was a single body of water for the entire A4 formative environment especially when placed in the context of temperatures conducive for stromatolite precipitation[1]. This makes a regional interpretation difficult, but the data does indicate that

[1]It is important to note that the statistics of temperatures calculated for TBS-A4-123-006 and TBS-A4-123-017 (Table 5.1 and Table 5.2 respetively) include a series of temperatures near the core of the stromatolites that are not conducive for stromatolite precipitation (and in fact encourage dissolution) in all of the environments identified here. With the exclusion of this core section, the minimum temperatures fall

although the stromatolites may not have been formed in the same body of water, the co-variation of the $\delta^{18}O$ and δ^{13}C data does imply that they formed in equilibrium with their environments if the kinetic effects associated with stromatolite lifecycles (as explained in Chapter 3 and discussed further in the following chapters).

around more reasonable temperatures for precipitation. Appendix A contains the calculated temperatures for reference.

Chapter 6

Discussion

The two stromatolites sampled in this study were collected from the A4 stratigaphic layer of the KBS Member at Koobi Fora in areas that can be interpreted as relatively shallow, slow moving water due to the sedimentology and basic requirements for stromatolite production (i.e. a balance of dissolved minerals and nutrients in the photic zone against pH, saturation, and temperature). While stable isotope ratios of the stromatolites in this study may fluctuate due to the variability of these requirements, the majority of these variables can be closely linked to the effect of the rainy seasons on regional hydrology.

6.1 Interpretation of Stable Isotopes in A4 Stromatolites

The palaeogeographic factors that limited the moisture regimes and depositional conditions of pedogenic carbonate formation are conducive for stromatolite development. While the pedogenic carbonate record essentially ends at the water's edge, the stromatolite community records successive $\delta^{13}C$ and $\delta^{18}O$ regimes at the nearshore and lake margin environments generated from atmospheric CO_2 and dissolved CO_2 from decaying plant matter. As discussed in Chapter 3 of this study, stromatolites could record depleted $\delta^{13}C$ values by forming under swamp conditions with a shift towards C_3 plants (Quinn et al. 2007) or due to formation in increasing water depth of an unmixed water column (Casanova and Hillare-Marcel, 1993). Additionally, stromatolite formation in waters of increasing depth

(within an unmixed, stratified water column) is indicated by $\delta^{18}O$ enrichment caused by the increased residence time of the bottom waters and is not evidenced in these samples (Casanova 1986; Hillaire-Marcel and Casanova, 1987). The data presented here though does not show exceptionally depleted $\delta^{13}C$ or an enriched $\delta^{18}O$ signal. The covariability between $\delta^{13}C$ and $\delta^{18}O$ stable isotope signals, as stated previously, demonstrates that the $CaCO_3$ formed in equilibrium with its environment and rules out an unmixed water column. This also confirms the interpretations by others that Turkana Basin stromatolites formed in a shallow water nearshore environment within the photic zone (Johnson, 1974; Abell et al., 1982; Casanova, 1986; Lepre et al., 2007). More information can be elucidated from the stable isotope analysis by contextualizing the data within the findings of Quinn et al., 2007 and Casanova, 1986.

When contextualized with the stable isotope values presented in Quinn et al. (2007) and Quinn (2015) as discussed in chapter 3, the stromatolites sampled here exhibit more fractionated $\delta^{13}C$ than the Koobi Fora Ridge pedogenic carbonates sampled by Quinn et al., (2007), and are indicative of an environment with a dominant C_4 (tropical grasses) component (Quinn et al., 2007). While Quinn et al., (2007) demonstrates that tropical grasses are evidence of subaerial floodplains in the paleo and modern environments, the data provided in this study cannot be directly correlated due to the unknown kinetic effects stromatolite growth has on isotope fractionation. Regardless, the C_4 signature suggested by the $\delta^{13}C$ is of an environment that is certainly conducive for stromatolite formation and correllates well with the A4 stromatolite morphology exhibited here. Although not directly referencing the A4 stromatolites, Casanova (1986) interprets the grading of centimeter scale, pinched-disc morphotypes to decimeter scale, spheroidal morphotypes as evidence of a developing floodplain environment with stromatolites growing along the maximum wetting surface. This gradation is observed in the A4 layers of Area 107 (6.2) and Area 123 (6.1). In fact, the A4 layer in Area 107 exhibits at least three cyclical packages of grading A4 stromatolites (figure 4.1), indicating an environment that is cyclically flooded and drained. Both stromatolites used in this study were collected from the top of the final cycle to capture the "end-of-life" period of the local stromatolite community.

FIGURE 6.1: Grading of stromatolites in Area 123 from centimeter scale, pinched disc morphotypes to decimeter scale, spheroidal morphotypes through the A4 layer.

FIGURE 6.2: Grading of stromatolites in Area 107 from centimeter scale, pinched disc morphotypes to decimeter scale, spheroidal morphotypes through the A4 layer.

6.1.1 Kinetic effects of stromatolite growth

The influence of kinetic isotope effects from stromatolite growth on the carbon and oxygen stable isotope ratios collected from precipitated $CaCO_3$ has not been studied in stromatolites as thoroughly as it has been in molluscs (McConnaughey, 1989; Dettman et al., 1999; Carre et al. 2006). In molluscs, high correlation between $\delta^{13}C$ and $\delta^{18}O$ has been used as an indicator for kinetic isotope effects and are attributed to rapid growth in molluscs (McConnaughey, 1989; Klein et al 1996; Dettman et al 1999). Potential drivers for kinetic effects in stromatolites may be linked to the aerobic (photic) and anaerobic (aphotic) system associated with the diurnal cycle of microbial communities. Additionally, since pH is a driver for precipitation and dissolution, and temperatures approaching and below 25°C have been observed to drive microbial modification of the pH in the microenvironment, prolonged exposure to temperature extremes outside of those favorable to microbial communities can lead to an internal recycling of carbonate by the EPS. This would lead to potentially overly-fractionated stable isotopes in the $CaCO_3$ preserved in the stromatolite.

Several studies have suggested that modern lake temperatures are similar to those of the the time period discussed here (e.g. Passey et al., 2010; Quinn et al., 2015) so, considering that average temperatures for modern Lake Turkana are between 24.5°C and 30°C (as discussed in Chapter 2) and that the ideal temperature for stromatolite growth is approximately 30°C (as discussed in Chapter 3), it is probable that A4 stromatolites precipitated near the warmer end of the modern day Lake Turkana average temperature (i.e. 30°C). Using this average/ideal temperature, an "Ideal" $\delta^{18}O_{water}$ can be derived for each stromatolite. Table 6.1 and Table 6.2 contain range and mean data for $\delta^{18}O_{water}$. Additionally, graphs in Figure 6.3 and Figure 6.4 demonstrates the the $\delta^{18}O_{water}$ to reach the ideal stromatolite producing temperature.

This negative shift in $\delta^{18}O_{water}$ when compared to the Lake Turkana $\delta^{18}O_{water}$ as recorded in Quinn (2015) may be indicative of a water regime near the Ancestral Omo Delta. At the time of the KBS Member, the delta shifted north from an initial approach from the east. The A4 stromatolite layer may be the result of this environmental shift. This interpretation compliments geogrpahic reconstructions of the basin in Figure 2.3 and as identified in Brown and Feibel (1991).

This shift in $\delta^{18}O_{water}$ does not, however, explain any kinetic isotope effects in the stromatolites. Those would be preserved as changes in the $\delta^{13}C$ and $\delta^{18}O$ ratios. As stated, a high rate of correlation in molluscs has been used to suggest the occurrence of the that kinetic isotope effects may have on the stable isotope data (McConnaughey, 1989; Klein et al 1996; Dettman et al 1999). To obtain the same ideal temperatures for stromatolite growth as is observed in shifting $\delta^{18}O_{water}$ of Lake Turkana with kinetic isotope effects would require a positive 1.75‰ shift of the ratios in TBS-A4-107-006 and a 2.75‰ shift in TBS-A4-123-017.

6.2 Revisiting hypotheses

Although the stable isotope curves for TBS-A4-107-006 and TBS-A4-123-017 (in Figure 6.3 and Figure 6.4 respectively) demonstrate two different environments during formation (i.e. relatively stable versus fairly dynamic), there is the common framework of a narrative shared between the two. Both stromatolites formed as ellipsoidal or pinched-disc morphotypes, which implies two things: the first is the simple availability of the substrate material (i.e. a shell bed preceded A4 and served as a $CaCO_3$ source) and the second is low energy water (i.e. morphologically these were not rolled around into oncolites and the microbial communities were able to establish themselves). These two pieces of evidence suggest that both of these stromatolites began formation in a floodplain which evolved into a lake-lateral river. This is further confirmed by the temperature evaluations conducted in Table 6.1 and Table 6.2.

Of particular note upon comparing the curves presented in Figure 6.3 and Figure 6.4 is how much more dynamic the precipitating environment of TBS-A4-123-017 was from that of TBS-A4-107-006. This data suggests that water level and temperature of the environment of TBS-A4-107-006 was much more hospitable than that of TBS-A4-123-017. The effects of infilling and drying also seem to be dampened somewhat. This could be due to Area 107 being closer to the heat-sink of the palaeo-lake or palaeo-Omo river body than Area 123. Furthermore, as discussed in Chapter 2, the KBS member thins as it approaches the Turkana basin margin. This thinning likely due to a lower lake level depth would imply a dynamic environment, more responsive to water level changes and more susceptible to

TABLE 6.1: Summary of Temperature Results for $\delta^{18}O_{water}$ from Quinn, 2015 in Equation 2.8.0.1 for TBS-A4-107-006 stable isotopes and a derived "ideal" $\delta^{18}O_{water}$ for the most favorable stromatolite producing temperatures.

$\delta^{18}O_{water}$	Omo River $-3.0‰$	Springs $-1.9‰$	Waterholes $-1.5‰$	Rivers $-1.4‰$	Rainwater $-0.3‰$	Streams $0.3‰$	Lake Turkana $6.00‰$	Ideal $4.31‰$
Maximum Temperature (C)	8.8°	13.2°	14.8°	15.2°	20°	22.8°	54.1°	43.9°
Minimum Temperature (C)	-3.3°	-0.2°	1.1°	1.4°	5°	7.2°	32.5°	24°
Mean Temperature (C)	0.2°	3.7°	5.1°	5.5°	9.5°	11.8°	39°	30°

TABLE 6.2: Summary of Temperature Results for $\delta^{18}O_{water}$ from Quinn, 2015 in Equation 2.8.0.1 for TBS-A4-123-017 stable isotopes and a derived "ideal" $\delta^{18}O_{water}$ for the most favorable stromatolite producing temperatures.

$\delta^{18}O_{water}$	Omo River $-3.0‰$	Springs $-1.9‰$	Waterholes $-1.5‰$	Rivers $-1.4‰$	Rainwater $-0.3‰$	Streams $0.3‰$	Lake Turkana $6.00‰$	Ideal $3.251‰$
Maximum Temperature (C)	16.7°	21.7°	23.5°	24°	29.4°	32.5°	66.9°	49.2°
Minimum Temperature (C)	-3.9°	-0.8°	0.4°	0.7°	4.3°	6.4°	31.4°	18.2°
Mean Temperature (C)	3.6°	7.5°	9°	9.3°	13.7°	16.2°	45.1°	30°

sequestration from the heat-sink near the basin's center. TBS-A4-107-006 is likely more indicative of the overall regional trend while TBS-A4-123-017 demonstrates local changes in water budget. Morphologically, infilling and temperature fluctuations near the point of "cauliflower" development compliment this assessment with TBS-A4-107-006 having a far less drastic morphological change than TBS-A4-123-017.

Interestingly, the lowest temperatures calculated from both data sets are predominantly found near the core of the stromatolites (i.e. around the nucleating surface, Appendix A contains the calculated temperatures for reference in Table A.2 and Table A.4). Most striking about the minimum temperatures identified in Table 6.1 and Table 6.2 is that the calculated environmental temperatures closest to the core of the stromatolite are near those temperatures that promote stromatolite dissolution and encourage EPS dissolution. This suggests that during the time that these layers were precipitated, the $\delta^{18}O_{water}$ was not the "ideal" identified here and closer to 5.5‰.

The temperature minima in the stromatolites - especially around the nucleating surface - are likely the result of a newly formed floodplain. These temperature lows are during lake highstands, when the large body of water to which the stromatolitic environment is connected acts as a heat sink and dampens temperature swings. During these earliest growth stages of the stromatolite (i.e. during the pinched disk morphology) the lake is connected to its floodplain. As these waters either recede or the semiannual sediment pulse sequester them from the larger lake body, drainage systems are formed with streams and rivers that respond more readily to the effects of rainwater and groundwater. All the while, the stromatolites continue to grow in size but with the added factor of sedimentation and infilling.

The morphology of these stromatolites is distinctive. Affectionately referred to as a "cauliflower" morphology, the upper portions of these stromatolites and their coinciding stable isotopes have previously identified as enigamatic and a mechanism for this morphological growth that rectifies the two has not previously been identified. Complicating matters, the covariance of the stable isotope values through the transition from the bottom portion to the top portion required that this morphology is evaluated as an indicator of an environmental change and not simply an anomaly of cyanobacteria communities. Figure 6.5

attempts to justify morphology and temperature with sediment infilling conditions. During the period of A4 formation, reduced (but still present) sediment accumulation noted by others (e.g. Carroll and Bohacs, 1999; Withjack et al., 2002; Quinn et al., 2007) permitted stromatolite formation.

Table 1.1 contained five hypotheses (plus one null-hypothesis) to explain the variation observed in the δ^{18}O and δ^{13}C values. Below, each hypothesis is addressed.

6.2.1 Hypothesis H_0

Hypothesis H_0 suggested "A4 stromatolites do not record δ^{18}O and δ^{13}C values that are in equilibrium with the environment and are not good indicators of palaeoenvironments." Based on the covariance of the δ^{18}O and δ^{13}C values, the correlation of δ^{18}O values with viable temperature ranges, the correlation of δ^{13}C values with viable paleogeographic distributions of C_3-C_4 pathways, and the correlation of stromatolite morphology with viable water energy levels from both stromatolites, the null hypothesis can be ruled out.

6.2.2 Hypothesis H_1

Hypothesis H_1 suggested "The δ^{18}O and δ^{13}C of the A4 stromatolites record contemporary environmental conditions at different locations of the basin lake (i.e. Lake Lorenyang)." Due to the distinct ranges stable isotope values for each stromatolite and the different $\delta^{18}O_{water}$ required to sustain stromatolite growth, it is clear that the stomatolites studied here record different environments and are not representative of the basin lake itself. Because Lake Turkana $\delta^{18}O_{water}$ values are likely significantly higher than those of Lake Lorenyang (Quinn 2015; Cerling 2003) and therefore unlikely to proxy well for the basin lake at the time of stromatolite formation (see Table 5.1 and Table 5.2), the variability and fluctuation of stable isotope values in the stromatolites studied here would require significant environmental changes throughout the stromatolite formation. While it is reasonable (and even likely) to assume that the basin lake would change through time, the scope of change for what is required to record the stable isotope values seen here is a bit excessive for a basin sized body of water. What can be stated is that stable isotope fluctuations

would be far more possible in a nearshore or lake proximal environment. A near shore sand bar or playa environment would allow such fluctuations, but would poorly rectify the morphological development of the stromatolites along the maximum wetting surface against (i.e. from perpendicular to water depth to parallel) against the generally increasing water temperature through time. Additionally, exploring this hypothesis has underscored the fact that the Lake Turkana $\delta^{18}O_{water}$ is a poor representation of the Lake Lorenyang environment. Using the $\delta^{18}O_{water}$ from the modern lake in Equation 2.8.0.1 with the stable isotopes collected from the the stromatolites studied here requires that the water temperatures drop far below those conducive for stromatolite formation and growth As discussed, temperatures below 25° run the risk of increasing pH above sustainable levels.

6.2.3 Hypothesis H_2

Hypothesis H_2 suggested "The 18O and $\delta^{13}C$ of the A4 stromatolites record environmental conditions associated with different time periods of the basin lake (i.e. Lake Lorenyang)." The data gathered during this research is not of high enough resolution to completely identify whether the A4 stratigraphic layers of Area 107 and Area 123 are contemporary. The timescale in Figure 2.5 suggests that the A4 stratigraphic layer was productive at some point between 1.616 and 1.599 Ma, leaving a large window for formation. Regardless of whether the stromatolites studied here are contemporary, the stable isotopes they record represent environments that began connected to the larger lake body and developed into disparate envonments. Morphologically the two areas had similar beginnings (i.e. floodplain environments), but clearly diverged.

6.2.4 Hypothesis H_3

Hypothesis H_3 suggested "The $\delta^{18}O$ and $\delta^{13}C$ of the A4 stromatolites record the environmental conditions of a near shore sand bar on Lake Lorenyang." As discussed in H_1, this is more plausible than the A4 stromatolites developing entirey in the major water body of the basin lake. This hypothesis does present its share of issues though. As mentioned, near shore sand bar or playa environments allow fluctuations of temperature and

energy, but are poor interpretations of the morphological development of the stromatolites. A slowly expanding floodplain does account for aspects of the stromatolite growth along the maximum wetting surface (i.e. from perpendicular to water depth to parallel) but poorly accounts for the increasing water temperature and stromatolite size (with relation to water depth) through time. The decreased sedimentation rates in the region during this period also complicate stromatolite growth as it reduces sediment trapping and binding inputs and complicates fossilization of the structure. And while placing the stromatolites in playa and sand bar environments, while not absolutely eliminating sediment input it does have consequences for energy inputs. Casanova (1986) demonstrated spheroidal oncolites represent higher energy (more agitated) hydrological conditions. While the stromatolites studied here started out as relatively flat pinched discs, the generally spheroidal shapes they developed suggest water that, at least periodically, moved around and between the community.

6.2.5 Hypothesis H_4

Hypothesis H_4 suggested "The $\delta^{18}O$ and $\delta^{13}C$ of the A4 stromatolites record the environmental conditions of a playa or solar pond environment which is primarily spring or rainwater-fed (i.e. groundwater, rainwater)." Energy levels of a playa or solar pond, as discussed above, are not conducive for the morphological development observed in the stromatolites. Likewise, fluctuating C_3-C_4 input would be a function of groundwater and rainwater run-off exclusively. Which could suggest a far less correlative relationship between $\delta^{18}O$ and $\delta^{13}C$ than what is observed here.

6.2.6 Hypothesis H_5

Hypothesis H_5 suggested "The $\delta^{18}O$ and $\delta^{13}C$ of the A4 stromatolites record the environmental conditions of an open river or stream system relatively dissociated from a lake or closed basin (i.e. rivers, streams)." Of all the hypotheses posited here, H_5 accounts for the stable isotope fluctuations, morphological development, energy and sedimentation requirements, and nutrient refreshing. Additionally, the temperature fluctuations throughout the

formation of the stromatolites do not necessarily require that the energy levels of the water to be eliminated, as in the more static water hypotheses. The greatest challenge to this hypothesis is the areal scale of the A4 stromatolite layer. Research by others (Feibel et al., 1989; Feibel et al., 1991; Brown and Feibel, 1991) found that just before A4 formation, channel and floodplain sediments are evidence of the prograding ancestral Omo channels. Although shallow lakes were frequent preceding A4 formation (1.8 to 1.7 Ma), they are limited during the A4 layer formation (1.7 to 1.4 Ma) and fluvial input is predominantly comprised of small distributary channels, such as those that could be conducive for stromatolites. Periods of lower water input are observed plainly in field observations of the stratigraphy local to the collection sites and can be identified by the prevalence of the pinched disc pioneer stromatolite populations attributed here to floodplain environments found several times through section (see Figure 2.4). Furthermore the correlation and covariance of δ^{18}O and δ^{13}C within both samples coupled with how distinct their stable isotope records are complements the notion of multiple distributary channels. Table 5.1 and Table 5.2 demonstrate the difficulty in assigning a static modern $\delta^{18}O_{water}$ as a proxy for Plio-Pleistocene $\delta^{18}O_{water}$ which would have gradually changed slightly over the lifetime of stromatolite formation as distributary channels and streams migrated upstream and seasonally between the rainy seasons due to water sourcing. This calls into question either the maximum temperatory or minimum temperature of each potential environment in those tables. However, Table 5.1 and Table 5.2 do highlight four environments where temperatures climb to or above 40°C (high enough to terminate stromatolite formation) and mantain a mean temperature near what is required for peak stromatolite formation. The minimum temperature of the range for both stromatolites can be identified as a period of time when the stromatolitic floodplain was connected to the larger lake body. As mentioned in Chapter 2, at temperatures less than 25°C, the mat increases in pH and oxygen penetration, which in combination lead to stromatolite dissolution (or more importantly for this study, no precipitation). A dissolved $CaCO_3$ record would be difficult to identify. Ultimately, after the pioneering stromatolite community is established and temperatures begin to rise, most likely environmental explanation with the most conducive mean temperatures are Springs, Waterholes, and Rivers. Evidence for the Omo River Delta and Turkana River outlet have been identified by others as being located near the collection

sites for both of the stromatolites for this study.

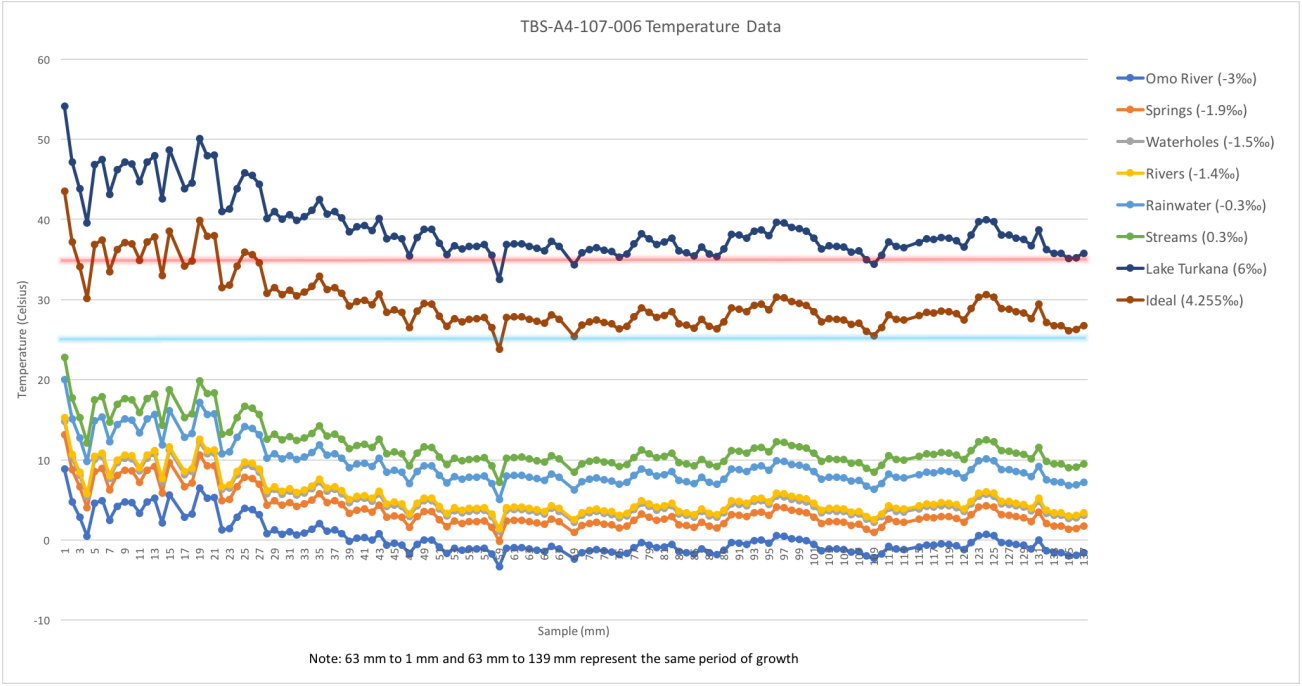

FIGURE 6.3: Graph depicting data from Table 6.1 for TBS-A4-107-006. The red and blue horizontal lines depict the upper and lower ends of temperature tolerance for stromatolite precipitation as discussed previously (35°C and 25°C respectively). Ideal $\delta^{18}O_{water}$ based on an average temperature of 30°C.

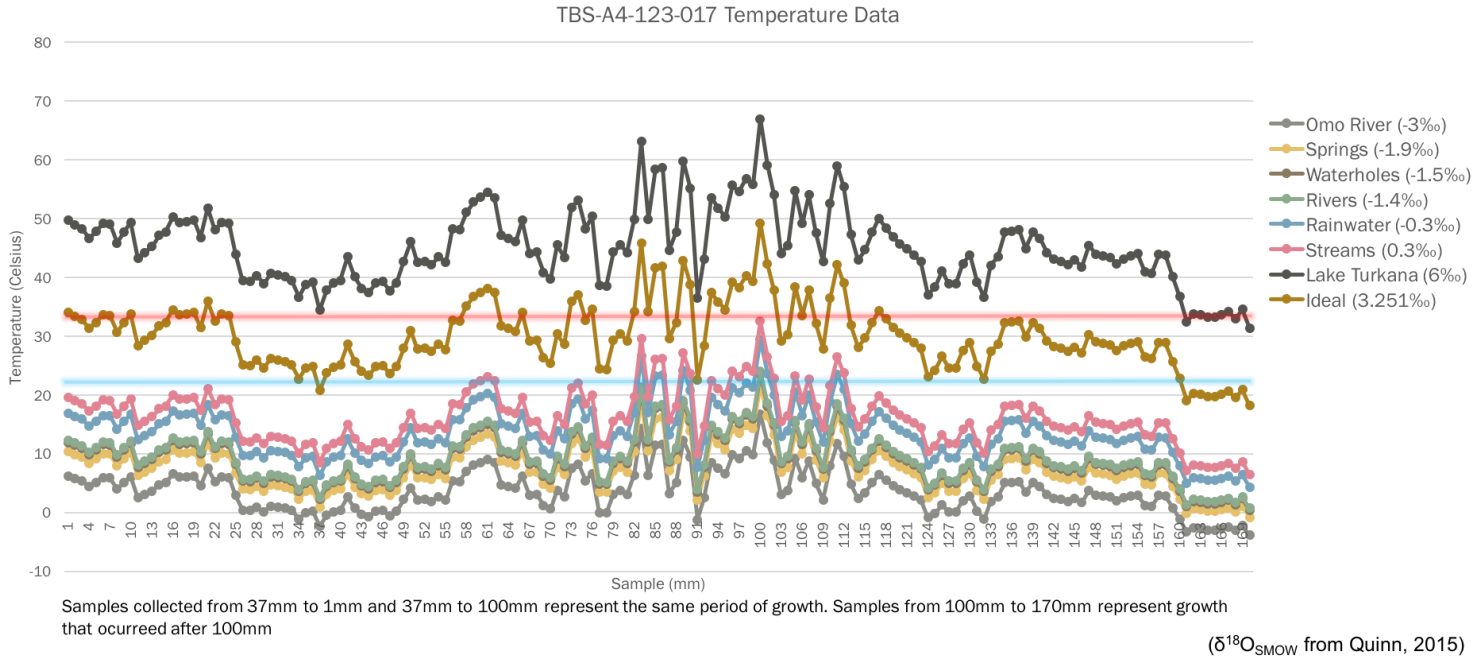

FIGURE 6.4: Graph depicting data from Table 6.2 for TBS-A4-123-017. The red and blue horizontal lines depict the upper and lower ends of temperature tolerance for stromatolite precipitation as discussed previously (35°C and 25°C respectively). Ideal $\delta^{18}O_{water}$ based on an average temperature of 30°C.

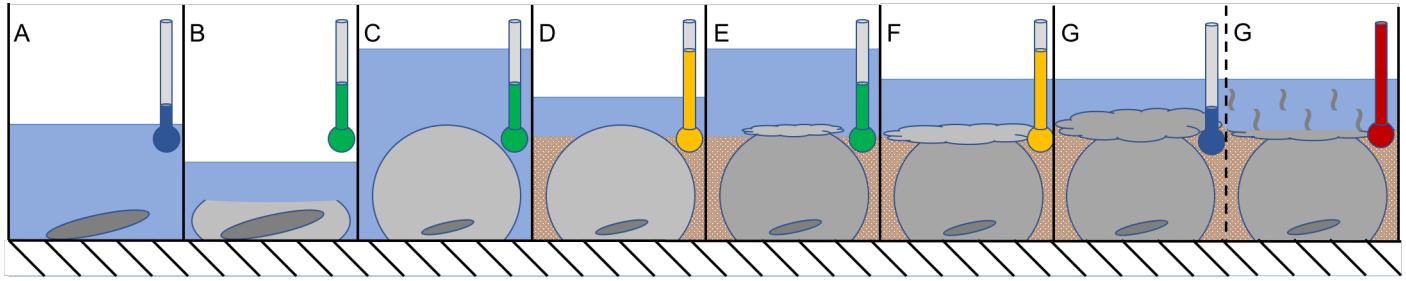

FIGURE 6.5: (A) While still connected to the larger body of water, a molluscan shell provides the nucleating surface for the stromatolite. (B) Water levels decrease while temperature gradually increases. Pinched disc stromatolites form on substrate material and grow along the maximum wetting surface, which at this point is perpendicular to depth. (C) Rising water levels of allow stromatolites to develop more spheroidal morphotypes. (D) Sediment infilling decreases water depth and causes partial burial. As this water body is not directly connected to the larger lake, the dampening effects of the larger body are not accessible. Increasing water temperatures lead to partial death of the microbial community and a stronger C_4 signal is observed in $\delta^{13}C$. (E) Water level and energy increase as waters are refreshed, exposing a nucleatng surface. Surviving microbes or pioneering communities develop another stromatolite and trigger growth along the maximum wetting surface. (F) Decreasing water depth from continued infilling, increases the temperature. A stronger C_4 signal is observed in $\delta^{13}C$. (G) Two scenarios are proposed here for the end-of-lfie stage of stromatote precipitation. If temperature decreases, the processes associated with respiration through the mat cross section notably increased and unmitigated inorganic $CaCO_3$ production occurs, overwhelming the photosynthetic cyanobacteria.With an increase in temperature pH decreases and dissolution processes begin.

Chapter 7

Conclusion

This study demonstrates that stromatolites from the A4 layer of the Koobi Fora Formation in Area 107 and Area 123 can be used for the palaeoenvironmental reconstruction and that although geographically and (potentially) chronologically separated, the Bura Hasuma (TBS-A4-123-017) stromatolite and the Koobi Fora Ridge (TBS-A4-107-006) stromatolite share a similar environmental interpretation. Morphological changes throughout the A4 stratigraphic layer point towards a gradual transgression and regression of a floodplain that periodically developes into distributary channels coupled with the occassional sediment infilling of the A4 layer. Stable isotope values collected from these specimen also indicate that these stromatolites thrived in an environment dominated by tropical grasses in lateral floodplain/nearshore environments. At the time of formation, water temperatures of stratigraphic layer A4 ranged from those that are favorable for stromatolite formation (30°C) to temperatures that stress cyanobacterial community survival (> 40°C).

Research presented here links previously conducted stable isotope studies of the region (Quinn et al., 2007; Quinn, 2015; etc.), environmental reconstructions (Lepre et al., 2007; Feibel et al., 2009; etc.), to the limited studies into stromatolite micro/macro-morphology (Casanova, 1986; Noffke and Awramik 2013; etc.) and stable isotope analyses of stromatolite (Abell et al., 1982; Abell and McClory, 1986; etc.). to confirm previous reconstructions of the palaeoenvironment stratigraphic and sedmendological interpretations (Feibel et al., 1989; Brown and Feibel, 1991; Feibel et al., 1991 etc.). This study demonstrates

that stromatolites from the Koobi Fora region need not be relegated to solely qualitative interpretations regarding environmental reconstructions, but can be used to confirm or complicate quantitative analyses.

Future research into stromatolitic stratagraphic layers in the Lake Turkana region would benefit from a greater sampling of stromatolites from across the region and through section. While several stromatolites were collected for this study throughout the Koobi Fora Formation and region, sampling each specimen was prohibitively time intensive and resource consuming. This research has shown that although more samples collected from a single stromatolite specimen can be useful, they may be unnecessary for tying two distinct areas together or teasing them a part. As was demonstrated by the statistical analyses conducted in Chapter 5, the range of stable isotope values is not so great as to force a researcher to arrive at sweepingly different conclusions with a smaller data set. Additionally, millimeter scale sampling may not be necessary, as there is little value added to the environmental interpretation with the larger datasets. Sampling restricted to key areas of stromatolite formation may provide the most value.

Laboratory analyses involved in this research focused on the microbially driven characteristics of stromatolites, that is the EPS ($CaCO_3$) formation. As discussed, microbial communities also utilize trapping and binding phases for laminae development. This may provide an interesting opportunity in the Lake Turkana region where present-day sediment pulses into the basin coincide with the rainy season at the headwaters. This seaonal pulsing may have been captured as trapped sediment in stromatolite laminae, which could provide a method of anchoring sections of the dataset to seasons, contextualizing stable isotope fluctuations. Furthermore, stable isotope analysis of the trapped sediment grains (e.g. strontium) could provide an indicator for water sourcing. Using an EMP for the analysis of mineral differences between laminae may also be useful for sourcing water input.

Utilizing stromatolites quantitatively, provides greater utility than relegating stromatolite layers to little more than marker beds. Interpretation of the A4 stromatolite layer increases the potential resolution of stratigraphic layer interpretations and demonstrates that in addition to predation and food scarcity, early hominids had to contend with a highly variable hydrological environment where water quality and availablility were often shifting.

Appendix A

Stable Isotope Data

The sample names in the following tables indicate the distance (in millimeters) a sample was collected from the *in-situ bottom of the stromatolite.* Laminae that are continuous around an entire stromatolite are represented by two sets of stable isotope values found on opposite sides of the nucleus of the stromatolite. As described earlier in this study, the semi-spheroidal oncolitic morphology of the stromatolites becomes less regular toward the stromatolite in situ "top" and the upper laminae of the stromatolite are less continuous around the stromatolite. That is, somewhere from the in-situ bottom up toward the in-situ top along the transect, stable isotope values for single laminations are no longer represented on both sides of the stromatolite nucleus.

A.1 TBS-107-A4-006

Table A.1: TBS-107-A4-006 Stable Isotope Data

Sample ID	δ^{13}**C PDB**	δ^{18}**O PDB**	**RU ID#**
006-001	−3.341	−1.103	20113764
006-002	−2.385	0.025	20113765
006-003	−1.684	0.595	20113766
006-004	−1.057	1.35	20113767

Continued on next page

Table A.1 – continued from previous page

Sample ID	δ^{13}C PDB	δ^{18}O PDB	RU ID#
006-005	−1.995	0.08	20113768
006-006	−2.285	−0.022	20113769
006-007	−1.614	0.716	20113770
006-008	−2.036	0.195	20113771
006-009	−2.262	0.033	20113772
006-010	−2.27	0.067	20113773
006-011	−1.883	0.448	20113774
006-012	−2.331	0.032	20113775
006-013	−2.313	−0.096	20113778
006-014	−1.422	0.814	20113779
006-015	−2.413	−0.221	20113780
006-016	−3.294	−1.39	20113781
006-017[1]	−1.781	0.589	20113782
006-018	−1.999	0.471	20113783
006-019	−2.53	−0.461	20113784
006-020	−2.028	−0.105	20113785
006-021	−2.158	−0.117	20113786
006-022	−1.362	1.093	20113787
006-023	−1.557	1.035	20113788
006-024	−2.051	0.589	20113789
006-025	−2.069	0.262	20113792
006-026[2]	−4.759	−5.602	20113793
006-027	−2.007	0.313	20113794
006-028	−1.963	0.504	20113795
006-029	−1.337	1.238	20113796
006-030	−1.579	1.092	20113797
006-031	−1.514	1.257	20140428
006-032	−1.751	1.16	20140429

Continued on next page

Table A.1 – continued from previous page

Sample ID	δ^{13}C PDB	δ^{18}O PDB	RU ID#
006-033	−1.636	1.287	20140430
006-034	−1.636	1.207	20140431
006-035	−1.732	1.064	20140432
006-036	−1.848	0.828	20140433
006-037	−1.671	1.146	20140434
006-038	−1.632	1.091	20140435
006-039	−1.865	1.233	20140436
006-040	−1.408	1.546	20140437
006-041	−1.715	1.429	20140438
006-042	−1.341	1.399	20140439
006-043	−1.321	1.506	20140442
006-044	−1.805	1.248	20140443
006-045	−1.134	1.702	20140444
006-046	−1.262	1.639	20140445
006-047	−1.357	1.703	20140446
006-048	−1.14	2.084	20140447
006-049	−1.172	1.675	20140448
006-050	−0.91	1.486	20140449
006-051	−0.837	1.491	20140450
006-052	−0.877	1.796	20140451
006-053	−0.636	2.056	20140465
006-054	−0.412	1.852	20140466
006-055	−0.272	1.933	20140467
006-056	−0.327	1.873	20140468
006-057	−0.184	1.865	20140469
006-058	−0.303	1.831	20140472
006-059	−0.315	2.082	20140473
006-060	−0.301	2.647	20140474

Continued on next page

Table A.1 – continued from previous page

Sample ID	δ^{13}C PDB	δ^{18}O PDB	RU ID#
006-061	−0.28	1.833	20140519
006-062	−0.341	1.816	20140520
006-063	−0.244	1.81	20140521
006-064	−0.385	1.87	20140522
006-065	−0.464	1.915	20140523
006-066	−0.506	1.973	20140524
006-067	−0.419	1.762	20140525
006-068	−0.488	1.872	20140526
006-069[3]	−2.066	−1.208	20140527
006-070	−0.769	2.301	20140528
006-071	−0.67	2.023	20140529
006-072	−0.668	1.938	20140530
006-073	−0.76	1.895	20140533
006-074	−0.736	1.961	20140534
006-075	−0.905	1.99	20140535
006-076	−0.862	2.117	20140536
006-077	−0.879	2.048	20140537
006-078	−0.945	1.815	20140538
006-079	−0.955	1.588	20140539
006-080	−0.877	1.701	20140540
006-081	−0.839	1.825	20140541
006-082	−0.971	1.774	20140542
006-083	−0.898	1.679	20140543
006-084	−0.82	1.98	20140544
006-085	−0.87	2.023	20140547
006-086	−0.952	2.095	20140548
006-087	−1.183	1.88	20140549
006-088	−1.346	2.043	20140550

Continued on next page

Table A.1 – continued from previous page

Sample ID	δ^{13}C PDB	δ^{18}O PDB	RU ID#
006-089	−1.259	2.108	20140551
006-090	−1.061	1.935	20140552
006-091	−1.178	1.593	20142978
006-092	−1.321	1.616	20142979
006-093	−1.385	1.679	20142980
006-094	−1.395	1.522	20142981
006-095	−1.465	1.497	20142982
006-096	−1.4	1.633	20142983
006-097	−1.275	1.324	20142984
006-098	−1.412	1.347	20142985
006-099	−1.462	1.438	20142986
006-100	−1.485	1.477	20142987
006-101	−1.405	1.522	20142988
006-102	−1.324	1.686	20142989
006-103	−1.302	1.936	20142992
006-104	−1.226	1.862	20142993
006-105	−1.178	1.873	20142994
006-106	−1.157	1.886	20142995
006-107	−1.147	2.006	20142996
006-108	−1.066	1.976	20142997
006-109	−1.045	2.172	20142998
006-110	−1.02	2.289	20142999
006-111	−1.052	2.077	20143000
006-112	−1.059	1.769	20143001
006-113	−0.943	1.876	20143002
006-114	−0.986	1.896	20143003
006-115[4]	−1.773	0.165	20143191
006-116	−1.143	1.781	20143192

Continued on next page

Table A.1 – continued from previous page

Sample ID	δ^{13}C PDB	δ^{18}O PDB	RU ID#
006-117	−1.117	1.704	20143193
006-118	−1.155	1.716	20143194
006-119	−1.064	1.667	20143195
006-120	−0.903	1.679	20143196
006-121	−1.064	1.737	20143197
006-122	−1.172	1.889	20143198
006-123	−1.373	1.607	20143199
006-124	−1.81	1.32	20143200
006-125	−1.801	1.266	20143201
006-126	−1.672	1.32	20143202
006-127	−1.176	1.608	20143205
006-128	−0.999	1.619	20143206
006-129	−1.102	1.681	20143207
006-130	−1.07	1.715	20143208
006-131	−1.008	1.857	20143209
006-132	−1.486	1.501	20143210
006-133	−1.198	1.946	20143211
006-134	−1.232	2.028	20143212
006-135	−1.004	2.035	20143213
006-136	−1.335	2.155	20143214
006-137	−1.017	2.13	20143215
006-138	−0.691	2.032	20143216

[4]data closely resemble laboratory standard and are excluded from analyses, figures, and interpretations

TABLE A.2: Temperatures derived from TBS-A4-107-006 stable isotope data using Equation 2.8.0.1 with $\delta^{18}O_{SMOW}$ of environments compiled by Quinn (2015) . All temperatures in degrees Celsius.

Sample ID	**Omo River**	**Springs**	**Water-holes**	**Rivers**	**Rain-water**	**Streams**	**Lake Turkana**
$\delta^{18}O_{water}$	-33.0‰	-31.9‰	-31.6‰	-31.5‰	-30.4‰	-29.8‰	-24.3‰
006-001	8.845	13.16	14.813	15.234	20.041	22.807	54.104
006-002	4.772	8.74	10.267	10.655	15.116	17.691	47.188
006-003	2.851	6.643	8.106	8.479	12.764	15.244	43.832
006-004	0.445	4.005	5.384	5.735	9.788	12.141	39.525
006-005	4.585	8.536	10.057	10.444	14.887	17.454	46.864
006-006	4.936	8.918	10.451	10.841	15.316	17.899	47.472
006-007	2.454	6.209	7.658	8.027	12.275	14.735	43.129
006-008	4.19	8.105	9.613	9.997	14.405	16.952	46.178
006-009	4.744	8.709	10.235	10.624	15.082	17.656	47.14
006-010	4.627	8.582	10.104	10.492	14.939	17.508	46.938
006-011	3.34	7.177	8.657	9.034	13.364	15.869	44.692
006-012	4.749	8.714	10.24	10.629	15.087	17.662	47.148
006-013	5.192	9.197	10.738	11.13	15.627	18.224	47.914
006-014	2.136	5.861	7.299	7.666	11.883	14.327	42.565
006-015	5.633	9.677	11.231	11.627	16.163	18.78	48.671
006-016	9.942	14.345	16.031	16.459	21.356	24.169	55.926
006-017	2.871	6.665	8.129	8.502	12.788	15.269	43.867
006-018	3.262	7.093	8.569	8.946	13.269	15.77	44.556
006-019	6.484	10.601	12.182	12.585	17.195	19.852	50.125
006-020	5.226	9.234	10.775	11.168	15.668	18.266	47.972
006-021	5.266	9.278	10.82	11.213	15.717	18.317	48.041
006-022	1.244	4.883	6.29	6.649	10.78	13.177	40.969
006-023	1.43	5.086	6.5	6.861	11.01	13.416	41.302
006-024	2.872	6.666	8.13	8.503	12.79	15.271	43.869

Continued on next page

Table A.2 – continued from previous page. All temperatures in °C.

Sample ID	Omo River	Springs	Water-holes	Rivers	Rain-water	Streams	Lake Turkana
	-3‰	-1.9‰	-1.5‰	-1.4‰	-0.3‰	0.3‰	6‰
006-025	3.964	7.859	9.359	9.741	14.129	16.665	45.785
006-027	3.791	7.67	9.165	9.546	13.917	16.445	45.483
006-028	3.153	6.973	8.446	8.821	13.134	15.63	44.363
006-029	0.792	4.386	5.777	6.131	10.218	12.59	40.152
006-030	1.249	4.888	6.295	6.654	10.786	13.182	40.977
006-031	0.73	4.319	5.707	6.062	10.142	12.511	40.042
006-032	1.035	4.654	6.053	6.41	10.521	12.906	40.593
006-033	0.64	4.219	5.604	5.958	10.029	12.393	39.877
006-034	0.888	4.492	5.886	6.242	10.339	12.716	40.327
006-035	1.336	4.983	6.394	6.753	10.894	13.295	41.134
006-036	2.09	5.811	7.248	7.614	11.827	14.268	42.483
006-037	1.078	4.701	6.102	6.459	10.574	12.962	40.67
006-038	1.252	4.892	6.299	6.658	10.79	13.187	40.984
006-039	0.807	4.402	5.794	6.149	10.237	12.61	40.179
006-040	-0.155	3.345	4.701	5.047	9.039	11.359	38.429
006-041	0.2	3.735	5.105	5.454	9.482	11.822	39.078
006-042	0.295	3.839	5.212	5.563	9.6	11.945	39.25
006-043	-0.034	3.477	4.838	5.185	9.19	11.517	38.65
006-044	0.76	4.352	5.741	6.096	10.18	12.55	40.096
006-045	-0.623	2.828	4.167	4.509	8.453	10.747	37.568
006-046	-0.435	3.035	4.381	4.725	8.688	10.993	37.914
006-047	-0.625	2.825	4.164	4.506	8.45	10.744	37.564
006-048	-1.743	1.591	2.887	3.218	7.045	9.274	35.486
006-049	-0.544	2.915	4.257	4.6	8.552	10.85	37.714
006-050	0.027	3.545	4.908	5.256	9.266	11.597	38.762
006-051	0.011	3.527	4.89	5.237	9.246	11.575	38.733

Continued on next page

Table A.2 – continued from previous page. All temperatures in °C.

Sample ID	Omo River	Springs	Water-holes	Rivers	Rain-water	Streams	Lake Turkana
	-3‰	-1.9‰	-1.5‰	-1.4‰	-0.3‰	0.3‰	6‰
006-052	-0.904	2.518	3.847	4.186	8.101	10.379	37.049
006-053	-1.663	1.68	2.979	3.311	7.146	9.38	35.636
006-054	-1.067	2.338	3.66	3.998	7.896	10.165	36.747
006-055	-1.305	2.075	3.389	3.724	7.597	9.852	36.304
006-056	-1.128	2.27	3.59	3.927	7.819	10.084	36.633
006-057	-1.107	2.294	3.615	3.952	7.846	10.112	36.673
006-058	-1.006	2.406	3.73	4.068	7.973	10.245	36.86
006-059	-1.738	1.596	2.892	3.223	7.05	9.28	35.494
006-060	-3.317	-0.156	1.077	1.392	5.045	7.181	32.494
006-061	-1.012	2.399	3.723	4.061	7.964	10.237	36.848
006-062	-0.96	2.456	3.782	4.121	8.03	10.305	36.944
006-063	-0.945	2.473	3.8	4.138	8.049	10.325	36.973
006-064	-1.121	2.279	3.599	3.936	7.828	10.094	36.647
006-065	-1.254	2.131	3.447	3.782	7.661	9.919	36.399
006-066	-1.42	1.948	3.256	3.59	7.451	9.7	36.089
006-067	-0.802	2.631	3.963	4.303	8.229	10.513	37.238
006-068	-1.127	2.272	3.592	3.929	7.82	10.086	36.635
006-069	9.243	13.591	15.256	15.679	20.519	23.302	54.767
006-070	-2.361	0.906	2.178	2.503	6.262	8.455	34.32
006-071	-1.566	1.786	3.089	3.422	7.267	9.508	35.817
006-072	-1.32	2.058	3.371	3.706	7.577	9.832	36.276
006-073	-1.193	2.199	3.517	3.853	7.738	9.999	36.513
006-074	-1.386	1.986	3.295	3.63	7.494	9.745	36.153
006-075	-1.471	1.891	3.198	3.531	7.387	9.632	35.994
006-076	-1.837	1.487	2.779	3.109	6.925	9.15	35.309
006-077	-1.639	1.706	3.006	3.338	7.176	9.412	35.681

Continued on next page

Table A.2 – continued from previous page. All temperatures in °C.

Sample ID	Omo River	Springs	Water-holes	Rivers	Rain-water	Streams	Lake Turkana
	-3‰	-1.9‰	-1.5‰	-1.4‰	-0.3‰	0.3‰	6‰
006-078	-0.958	2.458	3.785	4.123	8.033	10.308	36.949
006-079	-0.282	3.204	4.556	4.901	8.88	11.193	38.196
006-080	-0.621	2.83	4.169	4.511	8.455	10.75	37.572
006-081	-0.988	2.426	3.751	4.089	7.995	10.269	36.894
006-082	-0.838	2.591	3.921	4.261	8.183	10.465	37.17
006-083	-0.555	2.903	4.245	4.587	8.538	10.836	37.693
006-084	-1.443	1.923	3.23	3.564	7.423	9.67	36.047
006-085	-1.566	1.787	3.09	3.423	7.268	9.508	35.817
006-086	-1.775	1.555	2.85	3.181	7.003	9.231	35.425
006-087	-1.15	2.247	3.566	3.903	7.792	10.056	36.593
006-088	-1.625	1.721	3.022	3.354	7.193	9.43	35.706
006-089	-1.813	1.513	2.807	3.137	6.956	9.182	35.354
006-090	-1.31	2.069	3.382	3.718	7.59	9.845	36.294
006-091	-0.296	3.189	4.54	4.885	8.863	11.175	38.171
006-092	-0.367	3.11	4.459	4.803	8.773	11.082	38.039
006-093	-0.554	2.905	4.246	4.589	8.54	10.838	37.696
006-094	-0.081	3.426	4.785	5.132	9.131	11.456	38.564
006-095	-0.005	3.509	4.871	5.219	9.226	11.554	38.703
006-096	-0.416	3.056	4.403	4.746	8.712	11.017	37.949
006-097	0.523	4.091	5.472	5.824	9.885	12.242	39.666
006-098	0.452	4.012	5.391	5.743	9.796	12.149	39.536
006-099	0.175	3.708	5.076	5.425	9.451	11.789	39.032
006-100	0.055	3.575	4.939	5.288	9.301	11.633	38.813
006-101	-0.083	3.423	4.782	5.129	9.129	11.453	38.56
006-102	-0.575	2.881	4.222	4.564	8.513	10.81	37.657
006-103	-1.313	2.067	3.379	3.715	7.587	9.841	36.29

Continued on next page

Table A.2 – continued from previous page. All temperatures in °C.

Sample ID	Omo River	Springs	Water-holes	Rivers	Rain-water	Streams	Lake Turkana
	-3‰	-1.9‰	-1.5‰	-1.4‰	-0.3‰	0.3‰	6‰
006-104	-1.097	2.305	3.626	3.963	7.858	10.125	36.691
006-105	-1.129	2.27	3.589	3.926	7.818	10.083	36.631
006-106	-1.168	2.226	3.545	3.881	7.768	10.031	36.558
006-107	-1.516	1.841	3.146	3.479	7.33	9.573	35.909
006-108	-1.431	1.935	3.243	3.578	7.437	9.685	36.068
006-109	-1.996	1.31	2.597	2.925	6.724	8.939	35.01
006-110	-2.327	0.943	2.216	2.542	6.305	8.5	34.384
006-111	-1.721	1.615	2.912	3.243	7.072	9.303	35.526
006-112	-0.821	2.609	3.941	4.281	8.204	10.487	37.202
006-113	-1.137	2.261	3.58	3.917	7.808	10.073	36.617
006-114	-1.198	2.194	3.511	3.847	7.731	9.993	36.504
006-115	4.293	8.217	9.728	10.113	14.531	17.083	46.357
006-116	-0.857	2.57	3.9	4.24	8.159	10.44	37.136
006-117	-0.63	2.82	4.159	4.5	8.444	10.737	37.555
006-118	-0.665	2.782	4.12	4.461	8.401	10.692	37.491
006-119	-0.519	2.943	4.285	4.628	8.583	10.883	37.759
006-120	-0.555	2.903	4.244	4.587	8.538	10.836	37.693
006-121	-0.729	2.712	4.047	4.387	8.321	10.609	37.373
006-122	-1.177	2.216	3.534	3.871	7.757	10.019	36.541
006-123	-0.338	3.143	4.493	4.837	8.81	11.12	38.094
006-124	0.535	4.104	5.486	5.838	9.9	12.258	39.688
006-125	0.703	4.288	5.676	6.03	10.108	12.475	39.991
006-126	0.535	4.104	5.486	5.838	9.9	12.258	39.688
006-127	-0.342	3.138	4.488	4.832	8.805	11.115	38.086
006-128	-0.375	3.101	4.449	4.794	8.763	11.071	38.024
006-129	-0.562	2.896	4.237	4.58	8.53	10.827	37.682

Continued on next page

Table A.2 – continued from previous page. All temperatures in °C.

Sample ID	Omo River	Springs	Water-holes	Rivers	Rain-water	Streams	Lake Turkana
	-3‰	-1.9‰	-1.5‰	-1.4‰	-0.3‰	0.3‰	6‰
006-130	-0.661	2.787	4.124	4.466	8.406	10.698	37.499
006-131	-1.083	2.32	3.642	3.979	7.875	10.143	36.716
006-132	-0.019	3.494	4.855	5.203	9.208	11.536	38.677
006-133	-1.343	2.033	3.345	3.68	7.549	9.802	36.234
006-134	-1.581	1.77	3.072	3.405	7.248	9.488	35.788
006-135	-1.603	1.746	3.047	3.38	7.221	9.459	35.748
006-136	-1.947	1.364	2.653	2.982	6.786	9.004	35.101
006-137	-1.876	1.443	2.734	3.064	6.876	9.098	35.235
006-138	-1.593	1.756	3.058	3.391	7.233	9.472	35.766

A.2 TBS-123-A4-017

Table A.3: TBS-123-A4-017 Stable Isotope Data

Sample ID	δ^{13}C PDB	δ^{18}O PDB	RU ID#
017-001	−3.732	−0.388	20111240
017-002	−3.793	−0.26	20111241
017-003	−3.68	−0.149	20111242
017-004	−3.523	0.135	20111243
017-005	−3.685	−0.07	20111244
017-006	−3.844	−0.301	20111245
017-007	−3.588	−0.282	20111246
017-008	−2.859	0.253	20111247
017-009	−3.564	−0.065	20111248

Continued on next page

Table A.3 – continued from previous page

Sample ID	δ^{13}C PDB	δ^{18}O PDB	RU ID#
017-010	−3.647	−0.334	20111249
017-011	−2.336	0.705	20111250
017-012	−2.101	0.532	20111251
017-013	−2.543	0.358	20111254
017-014	−2.564	0.047	20111255
017-015	−2.903	−0.059	20111256
017-016	−3.279	−0.473	20111257
017-017	−3.665	−0.324	20111258
017-018	−3.695	−0.337	20111259
017-019	−3.279	−0.381	20111260
017-020	−3.535	0.102	20111261
017-021	−3.487	−0.731	20111262
017-022	−2.496	−0.121	20111263
017-023	−3.045	−0.331	20111264
017-024	−3.263	−0.295	20111265
017-025	−1.767	0.586	20111268
017-026	−1.059	1.37	20111269
017-027	−0.922	1.383	20111270
017-028	−1.072	1.215	20111271
017-029	−1.415	1.467	20111272
017-030	−0.939	1.156	20111273
017-031	−1.141	1.2	20111274
017-032	−0.656	1.252	20111275
017-033	−0.69	1.369	20111276
017-034	−0.588	1.877	20111283
017-035	−0.658	1.492	20111284
017-036	−0.721	1.415	20111285
017-037	−0.514	2.294	20111286

Continued on next page

Table A.3 – continued from previous page

Sample ID	δ^{13}C PDB	δ^{18}O PDB	RU ID#
017-038	−0.882	1.652	20111287
017-039	−0.706	1.448	20111288
017-040	−0.8	1.363	20111289
017-041	−1.208	0.665	20111290
017-042	−0.767	1.255	20111291
017-043	−0.7	1.602	20111292
017-044	−0.695	1.735	20111293
017-045	−0.629	1.434	20111294
017-046	−1.085	1.383	20111297
017-047	−1.037	1.679	20111298
017-048	−0.923	1.438	20111299
017-049	−1.346	0.791	20111300
017-050	−1.848	0.21	20111301
017-051	−1.539	0.823	20111302
017-052	−1.535	0.79	20111303
017-053	−1.594	0.891	20111304
017-054	−1.539	0.652	20111305
017-055	−1.72	0.831	20111306
017-056	−3.209	−0.14	20111307
017-057	−3.529	−0.114	20111308
017-058	−3.609	−0.604	20111311
017-059	−3.302	−0.89	20111312
017-060	−3.551	−1.015	20111313
017-061	−3.747	−1.15	20111314
017-062	−3.618	−1.006	20111315
017-063	−2.889	0.04	20111316
017-064	−2.217	0.118	20111317
017-065	−2.135	0.219	20111318

Continued on next page

Table A.3 – continued from previous page

Sample ID	δ^{13}C PDB	δ^{18}O PDB	RU ID#
017-066	−2.529	−0.387	20111319
017-067	−1.707	0.558	20111320
017-068	−1.863	0.525	20111321
017-069	−1.183	1.117	20111801
017-070	−0.895	1.313	20111766
017-071	−1.465	0.311	20111767
017-072	−1.504	0.668	20111768
017-073	−2.564	−0.752	20111769
017-074	−2.579	−0.935	20111770
017-075	−1.872	−0.146	20111771
017-076	−2.126	−0.498	20111772
017-077	−0.505	1.504	20111773
017-078	−0.886	1.532	20111774
017-079	−1.72	0.522	20111775
017-080	−1.867	0.316	20111776
017-081	−1.673	0.54	20111779
017-082	−2.472	−0.413	20111780
017-083	−4.157	−2.487	20111781
017-084	−2.435	−0.418	20111782
017-085	−3.152	−1.773	20111783
017-086	−3.314	−1.815	20111784
017-087	−1.668	0.477	20111785
017-088	−2.008	−0.059	20111786
017-089	−2.771	−1.985	20111787
017-090	−2.777	−1.26	20111788
017-091	−0.581	1.906	20111789
017-092	−1.377	0.716	20111790
017-093	−2.558	−1.005	20111793

Continued on next page

Table A.3 – continued from previous page

Sample ID	δ^{13}C PDB	δ^{18}O PDB	RU ID#
017-094	−2.458	−0.727	20111794
017-095	−2.319	−0.469	20111795
017-096	−2.987	−1.343	20111796
017-097	−3.108	−1.167	20111797
017-098	−3.464	−1.517	20111798
017-099	−3.391	−1.368	20111799
017-100	−3.858	−3.055	20111800
017-101	−3.539	−1.872	20111872
017-102	−3.184	−1.098	20111873
017-103	−2.563	0.552	20111874
017-104	−2.599	0.325	20111875
017-105	−3.249	−1.188	20111876
017-106	−2.44	−0.299	20111877
017-107	−2.537	−1.082	20111878
017-108	−2.02	−0.024	20111879
017-109	−1.513	0.807	20111880
017-110	−2.74	−0.842	20111881
017-111	−3.35	−1.856	20111882
017-112	−3.142	−1.297	20111883
017-113	−2.536	0.023	20111886
017-114	−2.188	0.755	20111887
017-115	−2.747	0.449	20111888
017-116	−2.982	−0.052	20111889
017-117	−2.832	−0.445	20111890
017-118	−3.065	−0.178	20111891
017-119	−3.256	0.091	20111892
017-120	−3.028	0.283	20111893
017-121	−2.843	0.435	20111894

Continued on next page

Table A.3 – continued from previous page

Sample ID	δ^{13}C PDB	δ^{18}O PDB	RU ID#
017-122	−2.561	0.602	20111895
017-123	−2.157	0.803	20111896
017-124	−1.338	1.806	20111897
017-125	−1.449	1.566	20111900
017-126	−2.036	1.073	20111901
017-127	−1.462	1.47	20111902
017-128	−1.373	1.472	20111903
017-129	−2.116	0.858	20111904
017-130	−2.528	0.607	20111905
017-131	−1.539	1.415	20111906
017-132	−1.21	1.887	20111907
017-133	−2.184	0.907	20111908
017-134	−2.487	0.666	20111909
017-135	−2.907	−0.05	20111910
017-136	−2.867	−0.08	20111911
017-137	−3.522	−0.119	20111912
017-138	−3.11	0.414	20112134
017-139	−3.446	−0.052	20112135
017-140	−3.056	0.117	20112136
017-141	−2.762	0.536	20112137
017-142	−2.458	0.733	20112138
017-143	−2.632	0.789	20112139
017-144	−2.605	0.899	20112140
017-145	−2.744	0.759	20112141
017-146	−2.355	0.961	20112142
017-147	−2.944	0.33	20112143
017-148	−2.747	0.584	20112144
017-149	−2.676	0.626	20112145

Continued on next page

Table A.3 – continued from previous page

Sample ID	δ^{13}C PDB	δ^{18}O PDB	RU ID#
017-150	−2.416	0.673	20112148
017-151	−2.089	0.866	20112149
017-152	−2.298	0.717	20112150
017-153	−2.423	0.633	20112151
017-154	−2.56	0.57	20112152
017-155	−1.916	1.101	20112153
017-156	−1.821	1.15	20112154
017-157	−2.537	0.592	20112155
017-158	−2.281	0.608	20112156
017-159	−1.478	1.245	20112157
017-160	−0.833	1.861	20112158
017-161	0.19	2.665	20112159
017-162	−0.046	2.398	20112162
017-163	−0.015	2.431	20112163
017-164	−0.044	2.524	20112164
017-165	−0.198	2.519	20112165
017-166	−0.179	2.435	20112166
017-167	−0.052	2.332	20112167
017-168	−0.143	2.566	20112168
017-169	0.08	2.26	20112169

TABLE A.4: Temperatures derived from TBS-A4-123-017 stable isotope data using Equation 2.8.0.1 with $\delta^{18}O_{SMOW}$ of environments compiled by Quinn, (2015) . All temperatures in degrees Celsius.

Sample ID	**Omo River** -3‰	**Springs** -1.9‰	**Water-holes** -1.5‰	**Rivers** -1.4‰	**Rain-water** -0.3‰	**Streams** 0.3‰	**Lake Turkana** 6‰
017-001	6.223	10.318	11.891	12.291	16.879	19.524	49.681
017-002	5.77	9.826	11.385	11.781	16.33	18.953	48.906
017-003	5.378	9.399	10.945	11.339	15.853	18.458	48.233
017-004	4.396	8.33	9.844	10.23	14.657	17.214	46.536
017-005	5.102	9.099	10.636	11.027	15.517	18.109	47.757
017-006	5.914	9.982	11.546	11.944	16.504	19.135	49.153
017-007	5.845	9.907	11.468	11.866	16.421	19.048	49.035
017-008	3.995	7.893	9.394	9.776	14.167	16.704	45.839
017-009	5.085	9.08	10.617	11.009	15.497	18.088	47.729
017-010	6.031	10.109	11.676	12.075	16.646	19.282	49.352
017-011	2.49	6.248	7.698	8.068	12.319	14.78	43.192
017-012	3.059	6.87	8.34	8.715	13.019	15.51	44.198
017-013	3.64	7.506	8.995	9.374	13.732	16.252	45.219
017-014	4.699	8.66	10.184	10.572	15.026	17.598	47.061
017-015	5.066	9.06	10.596	10.987	15.474	18.064	47.696
017-016	6.526	10.647	12.23	12.632	17.246	19.905	50.197
017-017	5.995	10.07	11.636	12.034	16.602	19.237	49.291
017-018	6.041	10.12	11.688	12.086	16.658	19.295	49.37
017-019	6.198	10.291	11.863	12.263	16.849	19.493	49.638
017-020	4.508	8.452	9.97	10.356	14.793	17.356	46.73
017-021	7.464	11.664	13.276	13.686	18.379	21.082	51.786
017-022	5.28	9.292	10.836	11.228	15.734	18.334	48.064
017-023	6.019	10.096	11.663	12.062	16.632	19.267	49.332
017-024	5.893	9.96	11.522	11.92	16.479	19.109	49.117

Continued on next page

Table A.4 – continued from previous page. All temperatures in °C.

Sample ID	Omo River -3‰	Springs -1.9‰	Water-holes -1.5‰	Rivers -1.4‰	Rain-water -0.3‰	Streams 0.3‰	Lake Turkana 6‰
017-025	2.882	6.677	8.141	8.514	12.802	15.283	43.886
017-026	0.382	3.936	5.312	5.663	9.709	12.059	39.41
017-027	0.342	3.891	5.266	5.616	9.658	12.006	39.336
017-028	0.862	4.464	5.857	6.212	10.306	12.682	40.28
017-029	0.085	3.608	4.973	5.322	9.338	11.671	38.867
017-030	1.048	4.667	6.067	6.424	10.536	12.922	40.615
017-031	0.909	4.515	5.91	6.266	10.365	12.743	40.365
017-032	0.747	4.337	5.726	6.08	10.163	12.533	40.072
017-033	0.384	3.938	5.314	5.665	9.711	12.061	39.413
017-034	-1.14	2.258	3.577	3.914	7.804	10.069	36.611
017-035	0.01	3.526	4.888	5.236	9.244	11.574	38.73
017-036	0.243	3.783	5.154	5.504	9.536	11.878	39.156
017-037	-2.342	0.927	2.2	2.525	6.286	8.481	34.356
017-038	-0.473	2.993	4.338	4.681	8.641	10.943	37.844
017-039	0.143	3.672	5.04	5.389	9.411	11.747	38.973
017-040	0.403	3.959	5.336	5.687	9.735	12.086	39.448
017-041	2.622	6.393	7.848	8.219	12.483	14.951	43.428
017-042	0.737	4.326	5.715	6.069	10.15	12.52	40.053
017-043	-0.322	3.16	4.51	4.855	8.83	11.141	38.122
017-044	-0.723	2.718	4.054	4.394	8.328	10.616	37.384
017-045	0.186	3.72	5.089	5.438	9.465	11.804	39.053
017-046	0.343	3.892	5.267	5.618	9.66	12.007	39.338

Continued on next page

Table A.4 – continued from previous page. All temperatures in °C.

Sample ID	Omo River -3‰	Springs -1.9‰	Water-holes -1.5‰	Rivers -1.4‰	Rain-water -0.3‰	Streams 0.3‰	Lake Turkana 6‰
017-047	-0.554	2.904	4.246	4.588	8.54	10.838	37.696
017-048	0.175	3.708	5.076	5.426	9.451	11.789	39.032
017-049	2.21	5.941	7.382	7.75	11.974	14.421	42.696
017-050	4.14	8.05	9.557	9.94	14.344	16.888	46.091
017-051	2.107	5.829	7.267	7.633	11.848	14.29	42.514
017-052	2.212	5.944	7.385	7.753	11.977	14.425	42.701
017-053	1.887	5.588	7.018	7.382	11.576	14.006	42.121
017-054	2.665	6.44	7.897	8.268	12.535	15.006	43.503
017-055	2.081	5.801	7.237	7.603	11.816	14.256	42.467
017-056	5.345	9.364	10.909	11.302	15.813	18.417	48.177
017-057	5.257	9.268	10.81	11.203	15.706	18.305	48.025
017-058	7	11.162	12.759	13.165	17.82	20.501	51.002
017-059	8.049	12.298	13.927	14.342	19.084	21.813	52.77
017-060	8.518	12.806	14.449	14.867	19.648	22.398	53.556
017-061	9.024	13.354	15.012	15.434	20.256	23.029	54.402
017-062	8.483	12.768	14.411	14.828	19.606	22.355	53.499
017-063	4.721	8.684	10.209	10.597	15.053	17.626	47.1
017-064	4.455	8.394	9.911	10.297	14.729	17.289	46.639
017-065	4.108	8.016	9.521	9.904	14.305	16.848	46.035
017-066	6.221	10.316	11.889	12.289	16.877	19.522	49.677
017-067	2.973	6.776	8.243	8.617	12.914	15.4	44.047
017-068	3.083	6.897	8.368	8.743	13.049	15.541	44.241
017-069	1.17	4.802	6.206	6.564	10.689	13.081	40.836
017-070	0.559	4.13	5.512	5.865	9.929	12.288	39.73
017-071	3.796	7.676	9.171	9.551	13.924	16.451	45.492

Continued on next page

Table A.4 – continued from previous page. All temperatures in °C.

Sample ID	Omo River -3‰	Springs -1.9‰	Water-holes -1.5‰	Rivers -1.4‰	Rain-water -0.3‰	Streams 0.3‰	Lake Turkana 6‰
017-072	2.612	6.382	7.836	8.207	12.47	14.937	43.409
017-073	7.542	11.749	13.363	13.773	18.473	21.179	51.917
017-074	8.216	12.48	14.114	14.53	19.286	22.023	53.052
017-075	5.368	9.388	10.934	11.327	15.841	18.445	48.215
017-076	6.616	10.745	12.33	12.733	17.355	20.018	50.35
017-077	-0.026	3.487	4.848	5.195	9.2	11.528	38.665
017-078	-0.112	3.392	4.75	5.097	9.093	11.416	38.508
017-079	3.091	6.906	8.377	8.752	13.059	15.552	44.256
017-080	3.781	7.659	9.153	9.534	13.904	16.431	45.464
017-081	3.033	6.842	8.312	8.686	12.988	15.477	44.153
017-082	6.312	10.414	11.99	12.391	16.986	19.635	49.831
017-083	14.332	19.073	20.882	21.341	26.575	29.573	63.08
017-084	6.33	10.434	12.011	12.412	17.009	19.659	49.863
017-085	11.433	15.955	17.683	18.122	23.136	26.014	58.38
017-086	11.602	16.136	17.869	18.309	23.336	26.221	58.656
017-087	3.24	7.069	8.545	8.921	13.242	15.742	44.518
017-088	5.066	9.059	10.596	10.987	15.473	18.063	47.695
017-089	12.281	16.868	18.62	19.065	24.145	27.059	59.765
017-090	9.441	13.805	15.476	15.9	20.757	23.548	55.096
017-091	-1.226	2.162	3.478	3.814	7.696	9.955	36.451
017-092	2.454	6.209	7.658	8.028	12.275	14.735	43.129
017-093	8.48	12.765	14.407	14.824	19.602	22.351	53.493
017-094	7.448	11.647	13.258	13.668	18.36	21.062	51.759

Continued on next page

Table A.4 – continued from previous page. All temperatures in °C.

Sample ID	Omo River -3‰	Springs -1.9‰	Water-holes -1.5‰	Rivers -1.4‰	Rain-water -0.3‰	Streams 0.3‰	Lake Turkana 6‰
017-095	6.512	10.632	12.214	12.616	17.229	19.887	50.173
017-096	9.761	14.15	15.83	16.257	21.139	23.945	55.626
017-097	9.09	13.425	15.085	15.507	20.335	23.111	54.512
017-098	10.43	14.873	16.573	17.004	21.94	24.775	56.733
017-099	9.855	14.251	15.934	16.362	21.251	24.061	55.782
017-100	16.736	21.652	23.524	23.999	29.408	32.501	66.914
017-101	11.828	16.38	18.119	18.561	23.606	26.5	59.025
017-102	8.827	13.141	14.794	15.214	20.02	22.784	54.074
017-103	2.992	6.798	8.265	8.639	12.937	15.425	44.081
017-104	3.751	7.626	9.119	9.499	13.868	16.393	45.412
017-105	9.168	13.509	15.172	15.595	20.429	23.208	54.642
017-106	5.909	9.976	11.54	11.937	16.498	19.128	49.144
017-107	8.768	13.077	14.728	15.147	19.949	22.711	53.975
017-108	4.942	8.925	10.457	10.847	15.323	17.907	47.482
017-109	2.159	5.886	7.325	7.692	11.912	14.356	42.605
017-110	7.871	12.106	13.73	14.143	18.87	21.592	52.472
017-111	11.765	16.313	18.05	18.491	23.531	26.423	58.923
017-112	9.581	13.956	15.631	16.057	20.924	23.722	55.329
017-113	4.781	8.749	10.276	10.665	15.126	17.702	47.203
017-114	2.328	6.071	7.516	7.885	12.12	14.574	42.906
017-115	3.333	7.17	8.65	9.026	13.356	15.861	44.681
017-116	5.039	9.03	10.565	10.956	15.44	18.029	47.649
017-117	6.426	10.539	12.118	12.52	17.125	19.78	50.027
017-118	5.481	9.511	11.061	11.455	15.979	18.588	48.41
017-119	4.547	8.495	10.014	10.401	14.841	17.406	46.798
017-120	3.892	7.78	9.278	9.66	14.041	16.573	45.659

Continued on next page

Table A.4 – continued from previous page. All temperatures in °C.

Sample ID	Omo River -3‰	Springs -1.9‰	Water-holes -1.5‰	Rivers -1.4‰	Rain-water -0.3‰	Streams 0.3‰	Lake Turkana 6‰
017-121	3.381	7.222	8.703	9.08	13.414	15.921	44.764
017-122	2.829	6.619	8.081	8.453	12.736	15.215	43.792
017-123	2.173	5.901	7.341	7.708	11.929	14.374	42.63
017-124	-0.932	2.487	3.815	4.153	8.065	10.342	36.997
017-125	-0.214	3.28	4.634	4.979	8.965	11.282	38.321
017-126	1.309	4.954	6.363	6.723	10.86	13.26	41.085
017-127	0.077	3.6	4.965	5.313	9.328	11.661	38.853
017-128	0.07	3.593	4.957	5.305	9.32	11.653	38.841
017-129	1.994	5.705	7.139	7.504	11.708	14.144	42.311
017-130	2.811	6.6	8.061	8.434	12.715	15.193	43.761
017-131	0.244	3.784	5.155	5.505	9.537	11.88	39.159
017-132	-1.171	2.223	3.541	3.878	7.765	10.027	36.553
017-133	1.837	5.533	6.961	7.325	11.514	13.942	42.032
017-134	2.617	6.387	7.842	8.213	12.476	14.944	43.418
017-135	5.034	9.025	10.56	10.951	15.435	18.023	47.641
017-136	5.137	9.137	10.676	11.067	15.56	18.154	47.818
017-137	5.273	9.285	10.828	11.22	15.725	18.325	48.052
017-138	3.453	7.301	8.784	9.162	13.502	16.013	44.89
017-139	5.04	9.032	10.567	10.958	15.442	18.031	47.652
017-140	4.458	8.397	9.914	10.3	14.732	17.293	46.644
017-141	3.047	6.857	8.327	8.701	13.005	15.495	44.177
017-142	2.399	6.148	7.596	7.965	12.207	14.664	43.032
017-143	2.217	5.949	7.39	7.758	11.983	14.43	42.708

Continued on next page

Table A.4 – continued from previous page. All temperatures in °C.

Sample ID	Omo River -3‰	Springs -1.9‰	Water-holes -1.5‰	Rivers -1.4‰	Rain-water -0.3‰	Streams 0.3‰	Lake Turkana 6‰
017-144	1.862	5.561	6.99	7.354	11.545	13.974	42.077
017-145	2.315	6.057	7.502	7.87	12.104	14.557	42.884
017-146	1.663	5.342	6.764	7.127	11.299	13.717	41.72
017-147	3.734	7.608	9.1	9.481	13.847	16.372	45.383
017-148	2.886	6.681	8.145	8.518	12.807	15.289	43.893
017-149	2.747	6.53	7.989	8.361	12.636	15.111	43.649
017-150	2.595	6.363	7.818	8.188	12.449	14.916	43.38
017-151	1.97	5.678	7.111	7.476	11.678	14.112	42.268
017-152	2.451	6.205	7.655	8.024	12.271	14.731	43.124
017-153	2.727	6.508	7.966	8.338	12.611	15.085	43.613
017-154	2.932	6.732	8.197	8.571	12.863	15.347	43.974
017-155	1.22	4.856	6.262	6.621	10.75	13.145	40.925
017-156	1.065	4.686	6.087	6.444	10.558	12.945	40.646
017-157	2.86	6.653	8.116	8.489	12.775	15.255	43.847
017-158	2.807	6.595	8.056	8.429	12.71	15.187	43.754
017-159	0.771	4.363	5.753	6.107	10.192	12.563	40.114
017-160	-1.095	2.307	3.629	3.966	7.861	10.128	36.695
017-161	-3.366	-0.211	1.02	1.335	4.982	7.115	32.399
017-162	-2.633	0.603	1.864	2.187	5.916	8.093	33.803
017-163	-2.725	0.501	1.759	2.08	5.799	7.971	33.628
017-164	-2.98	0.218	1.465	1.784	5.475	7.631	33.141

Continued on next page

Table A.4 – continued from previous page. All temperatures in °C.

Sample ID	Omo River -3‰	Springs -1.9‰	Water-holes -1.5‰	Rivers -1.4‰	Rain-water -0.3‰	Streams 0.3‰	Lake Turkana 6‰
017-165	-2.968	0.231	1.479	1.798	5.49	7.647	33.163
017-166	-2.735	0.491	1.748	2.069	5.787	7.958	33.609
017-167	-2.447	0.81	2.078	2.402	6.152	8.34	34.156
017-168	-3.095	0.09	1.332	1.65	5.328	7.477	32.919
017-169	-2.245	1.034	2.311	2.637	6.409	8.609	34.539
017-170	-3.903	-0.81	0.399	0.708	4.294	6.393	31.358

Bibliography

Bibliography

1 Abell, P. I. & McClory, J. P. Sedimentary carbonates as isotopic marker horizons at Lake Turkana, Kenya. *Geol. Soc. London, Spec. Publ.* 25, 153–158 (1986).

2 Abell, P. I. Palaeoclimates at Lake Turkana, Kenya, from oxygen isotope ratios of gastropod shells. *Nature* 297, 321–323 (1982).

3 Abell, P. I., Awramik, S. M., Osborne, R. H. & Tomellini, S. Plio-pleistocene lacustrine stromatolites from lake Turkana, Kenya: Morphology, stratigraphy and stable isotopes. *Sediment. Geol.* 32, 1–26 (1982).

4 Abell, P. I., Awramik, S. M., Osborne, R. H. & Tomellini, S. Plio-pleistocene lacustrine stromatolites from lake Turkana, Kenya: Morphology, stratigraphy and stable isotopes. *Sediment. Geol.* 32, 1–26 (1982).

5 Alin, S. R. & Cohen, A. S. Lake-level history of Lake Tanganyika, East Africa, for the past 2500 years based on ostracode-inferred water-depth reconstruction. *Palaeogeogr. Palaeoclimatol. Palaeoecol.* 199, 31–49 (2003).

6 Amundson, R. G. *Soil Formation*. *Treatise on Geochemistry* (Springer Science & Business Media, 2013). doi:10.1016/B0-08-043751-6/05073-8

7 Arnold, A. S., Wilson, J. S. & Boshier, M. G. A Simple Extended-Cavity Diode Laser. *Rev. Sci. Instrum.* 69, 1236–1239 (1998).

8 Arp, G. Photosynthesis-Induced Biofilm Calcification and Calcium Concentrations in Phanerozoic Oceans. *Science (80-.).* 292, 1701–1704 (2001).

9 Arp, G., Reimer, A. & Reitner, J. Microbialite Formation in Seawater of Increased Alkalinity, Satonda Crater Lake, Indonesia. *J. Sediment. Res.* 73, 105–127 (2003).

10 Arp, G., Reimer, A. & Reitner, J. Calcification in cyanobacterial biofilms of alkaline salt lakes. *Eur. J. Phycol.* 34, 393–403 (1999).

11 Arp, G., Reimer, A. & Reitner, J. Microbialite Formation in Seawater of Increased Alkalinity, Satonda Crater Lake, Indonesia. *J. Sediment. Res.* 73, 105–127 (2003).

12 Arp, G., Thiel, V., Reimer, A., Michaelis, W. & Reitner, J. Biofilm exopolymers control microbialite formation at thermal springs discharging into the alkaline Pyramid Lake, Nevada, USA. *Sediment. Geol.* 126, 159–176 (1999).

13 Grines, F. *Evolutionary History of the Australopithecines*. (Transaction Publishers, 1988). at <https://books.google.com/books?hl=en&lr=&id=AmQ46CDN6DsC&pgis=1>

14 Bainbridge, R. Stratigraphy of the Lower Member, Koobi Fora Formation, northern Karari Escarpment, East Turkana Basin, Kenya. (1976). at <https://scholar.google.com/scholar?q=Bainbridge+1976+Turkana&btnG=&hl=en&as_sdt=0%2C31#0>

15 Baumgartner, L. K. *et al.* Sulfate reducing bacteria in microbial mats: changing paradigms, new discoveries. *Sediment. Geol.* 185, 131–145 (2006).

16 Baumgartner, L. K. *et al.* Microbial diversity in modern marine stromatolites, Highborne Cay, Bahamas. *Environ. Microbiol.* 11, 2710–2719 (2009).

17 Behrensmeyer, A. New Hominid Remains and Early Artefacts from Northern Kenya: Preliminary Geological Interpretation of a New Hominid Site in the Lake Rudolf Basin. (1970). at <http://www.nature.com/nature/journal/v226/n5242/abs/226225a0.html>

18 Behrensmeyer, A. K. *et al.* The structure and rate of late Miocene expansion of C4 plants: Evidence from lateral variation in stable isotopes in paleosols of the Siwalik Group, northern Pakistan. *Bull. Geol. Soc. Am.* 119, 1486–1505 (2007).

19 Birkeland, P. W. & others. *Soils and geomorphology*. (1984). at <http://www.cabdirect.org/abstracts/19841989866.html>

20 Bissett, A. *et al.* Microbial mediation of stromatolite formation in karst-water creeks. *Limonology Oceanogr.* 53, 1159–1168 (2008).

21 Black, M. VI. The Algal Sediments ofAndros Island, Bahamas. (1933). at <http://rstb.royalsocietypublishing.org/content/222/483-493/165.full-text.pdf+html>

22 Boer, P. Mechanical effects of micro-organisms on intertidal bedform migration*. *Sedimentology* (1981). at

<http://onlinelibrary.wiley.com/doi/10.1111/j.1365-3091.1981.tb01670.x/abstract>

23 Bowen, B. The geology of the Upper Cenozoic sediments in the East Rudolf embayment of the Lake Rudolf basin, Kenya. (1974). at <http://lib.dr.iastate.edu/cgi/viewcontent.cgi?article=7022&context=rtd>

24 Brown, F. H., Haileab, B. & McDougall, I. Sequence of tuffs between the KBS Tuff and the Chari Tuff in the Turkana Basin, Kenya and Ethiopia. *J. Geol. Soc. London.* 163, 185–204 (2006).

25 Brown, F. H. & Feibel, C. S. Revision of lithostratigraphic nomenclature in the Koobi Fora region, Kenya. *J. Geol. Soc. London.* 143, 297–310 (1986).

26 Brown, F. H. & Feibel, C. S. Stratigraphy, depositional environments, and palaeogeography of the Koobi Fora Formation. *Koobi Fora Res. Proj. Vol. 3 Foss. ungulates Geol. Foss. artiodactyls, palaeoenvironments* 1–30 (1991). at <https://scholar.google.com/scholar?q=feibel+et+al.%2C+1991&btnG=&hl=en&as_sdt=0%2C31#1>

27 Brown, F. H. Development of Pliocene and Pleistocene chronology of the Turkana basin, East Africa, and its relation to other sites. *Integr. paths to past* 285–312 (1994). at <https://scholar.google.com/scholar?q=Brown,+F.H.,+1994.+Development+of+Pliocene+and+Pleistocene+chronology+of+the++Turkana+Basin,+East+Africa,+and+its+relation+to+other+sites.+In:+Corruccini,+R.S.,++Ciochon,+R.L.+(Eds.),+Integrative+Paths+to+the+Past.+Pre>

28 Brown, F. H. Development of Pliocene and Pleistocene chronology of the Turkana basin, East Africa, and its relation to other sites. *Integr. paths to past* 285–312 (1994). at <https://scholar.google.com/scholar?q=Brown+and+Feibel%2C+1991&btnG=&hl=en&as_sdt=0%2C31#4>

29 Brubaker, K. L., Entekhabi, D. & Eagleson, P. S. Estimation of continental precipitation recycling. *J. Clim.* 6, 1077–1089 (1993).

30 Buick, R. Carbonaceous filaments from North Pole, Western Australia: Are they fossil bacteria in Archaean stromatolites? *Precambrian Res.* 24, 157–172 (1984).

31 Burggraf, D., White, H., Frank, H. & Vondra, C. Hominid habitats in the Rift

Valley, part 2. *Hominid Sites* (1981). at <https://scholar.google.com/scholar?q=Hominid+habitats++in+the+rift+valley%3A+part+1.&btnG=&hl=en&as_sdt=0%2C31#1>

32 Burns, B. P., Goh, F., Allen, M. & Neilan, B. a. Microbial diversity of extant stromatolites in the hypersaline marine environment of Shark Bay, Australia. *Environ. Microbiol.* 6, 1096–101 (2004).

33 Carré, M., I. Bentaleb, O. Bruguier, E. Ordinola, N.T. Barrett, M. Fontugne (2006). Calcification rate influence on trace element concentrations in aragonitic bivalve shells: Evidences and mechanisms. *Geochimica et Cosmochimica Acta* 70: 4906-4920.

34 Casanova, J. East African rift stromatolites. *Geol. Soc. London, Spec. Publ.* 25, 201–210 (1986).

35 Casanova, J. East African rift stromatolites. *Geol. Soc. London, Spec.* (1986). at <http://sp.lyellcollection.org/content/25/1/201.short>

36 Casanova, J. & Hillare-Marcel, C. Carbon and oxygen isotopes in African lacustrine stromatolites: palaeohydrological interpretation. *Geophys. Monogr. Ser.* 78, (1993).

37 Casanova, J. & Tiercelin, J. J. Construction stromatolitiques en milieu carbonaté sodique: les oncolites des plaines inondables du lac Magadi (Kenya). *CR Acad. Sci. Paris* 295, 1139 – 1144 (1982).

38 Casanova, J. in *Phaneroz. Stromatolites II* 193–226 (Springer Netherlands, 1994). doi:10.1007/978-94-011-1124-9_8

39 Casanova, J. East African Rift stromatolites. *Geol. Soc. London, Spec. Publ.* 25, 201–210 (1986).

40 Cerling, T. E., Quade, J., Wang, Y. & Bowman, J. R. Carbon isotopes in soils and palaeosols as ecology and palaeoecology indicators. *Nature* 341, 138–139 (1989).

41 Cerling, T. Paleochemistry of Plio-Pleistocene Lake Turkana, Kenya. *Palaeogeogr. Palaeoclimatol. Palaeoecol.* (1979). at <http://www.sciencedirect.com/science/article/pii/0031018279901056>

42 Cerling, T. Stable carbon isotopes in palaeosol carbonates. *Palaeoweathering, palaeosurfaces Relat. …* 27, 43–60 (1999).

43 Cerling, T. The stable isotopic composition of modern soil carbonate and its relationship to climate. *Earth Planet. Sci. Lett.* (1984). at <http://www.sciencedirect.com/science/article/pii/0012821X8490089X>

44 Cerling, T. & Quade, J. Stable carbon and oxygen isotopes in soil carbonates. *Clim. Chang. Cont. Isot.* … (1993). at <http://onlinelibrary.wiley.com/doi/10.1029/GM078p0217/pdf>

45 Cerling, T., Wang, Y. & Quade, J. Expansion of C4 ecosystems as an indicator of global ecological change in the late Miocene. *Nature* (1993). at <http://www.nature.com/nature/journal/v361/n6410/abs/361344a0.html>

46 Cerling, T. E., Harris, J. M. & Passey, B. H. Diets of East African Bovidae Based on Stable Isotope Analysis. *J. Mammal.* 84, 456–470 (2003).

47 Chafetz, H. S. & Folk, R. L. Travertines: Depositional Morphology and the Bacterially Constructed Constituents. *J. Sediment. Res.* 54, (1984).

48 Chafetz, H. Differences in the 18O and 13C signatures of seasonal laminae comprising travertine stromatolites. *J. Sediment.* … 61, 1015–1028 (1991).

49 Cohen, A. S., Talbot, M. R., Awramik, S. M., Dettman, D. L. & Abell, P. Lake level and paleoenvironmental history of Lake Tanganyika, Africa, as inferred from late Holocene and modern stromatolites. *Bull. Geol. Soc. Am.* 109, 444–460 (1997).

50 Cohen, A. *et al.* Understanding paleoclimate and human evolution through the hominin sites and paleolakes drilling project. *Sci. Drill.* 60–65 (2009). doi:10.2204/iodp.sd.8.10.2009

51 Coplen, T. B. Reporting of stable hydrogen, carbon, and oxygen isotopic abundances (Technical Report). *Pure Appl. Chem.* 66, 273–276 (1994).

52 Corsetti, F. A. & Storrie-Lombardi, M. C. Lossless compression of stromatolite images: a biogenicity index? *Astrobiology* 3, 649–655 (2003).

53 Costerton, J. W. Overview of microbial biofilms. *J. Ind. Microbiol.* 15, 137–140 (1995).

54 Costerton, J. W., Lewandowski, D. R., Caldwell, D. E., Korber, D. R. & Lappin-Scott, H. M. Microbial biofilms. *Annu. Rev. Microbiol.* 49, 711–745

(1995).

55 Craig, H. The measurement of oxygen isotope paleotemperatures. *Stable Isot. Oceanogr. Stud.* … (1965). at <https://scholar.google.com/scholar?q=craig+h+1965&btnG=&hl=en&as_sdt=0%2C31#1>

56 Craig, H. Isotopic standards for carbon and oxygen and correction factors for mass-spectrometric analysis of carbon dioxide. *Geochim. Cosmochim. Acta* 12, 133–149 (1957).

57 Dade, W. B. *et al.* Effects of bacterial exopolymer adhesion on the entrainment of sand. *Geomicrobiol. J.* 8, 1–16 (1990).

58 Decho, A. W., Visscher, P. T. & Reid, R. P. Production and cylcing of natural mcirobial exopolymers (EPS) within a marine stromatolite. *Palaeogeogr. Palaeoclimatol. Palaeoecol.* 219, 71–86 (2005).

59 Decho, A. W. & Decho, A. W. Microbial bio"lms in intertidal systems: an overview. *Cont. Shelf Res.* 20, 1257–1273 (2000).

60 Decho, A. Exopolymer microdomains as a structuring agent for heterogeneity within microbial biofilms. *Microb. Sediments* (2000). at <http://link.springer.com/chapter/10.1007/978-3-662-04036-2_2>

61 Défarge, C. & Trichet, J. From biominerals to ‘organominerals’ : the example of the modern Lacustrine Calcareous Stromatolites from Polynesian Atolls. *Bull. Inst. Océanogr. Monaco* 14, 265–272 (1995).

62 Degens, E. T. in *Org. Geochem.* 304–329 (Springer Berlin Heidelberg, 1969). doi:10.1007/978-3-642-87734-6_14

63 Deines, P. & Gold, D. . The isotopic composition of carbonatite and kimberlite carbonates and their bearing on the isotopic composition of deep-seated carbon. *Geochim. Cosmochim. Acta* 37, 1709–1733 (1973).

64 Dettman, D. L., Reische, A. K. & Lohmann, K. C. Controls on the stable isotope composition of seasonal growth bands in aragonitic fresh-water bivalves (unionidae). *Geochim. Cosmochim. Acta* 63, 1049–1057 (1999).

65 Dunham, R. J. Classification of carbonate rocks according to deposition texture. *Am. Assoc. Pet. Geol.* 1, 108–121 (1962).

66 Dupraz, C. & Visscher, P. T. Interactions in the Geo-Biosphere: Processes of Carbonate Precipitation in Microbial Mats. *Am. Geophys. Union* (2009). at <http://adsabs.harvard.edu/abs/2009AGUFM.B21A0313D>

67 Dupraz, C. & Visscher, P. Microbial lithification in marine stromatolites and hypersaline mats. *Trends Microbiol.* (2005). at <http://www.sciencedirect.com/science/article/pii/S0966842X05001976>

68 Dupraz, C., Pattisina, R. & Verrecchia, E. P. Translation of energy into morphology: Simulation of stromatolite morphospace using a stochastic model. *Sediment. Geol.* 185, 185–203 (2006).

69 Dupraz, C., Visscher, P. T., Baumgartner, L. K. & Reid, R. P. Microbe-mineral interactions: early carbonate precipitation in a hypersaline lake (Eleuthera Island, Bahamas). *Sedimentology* 51, 745–765 (2004).

70 Dupraz, C. *et al.* Processes of carbonate precipitation in modern microbial mats. *Earth-Science Rev.* 96, 141–162 (2009).

71 Ebinger, C. J. *et al.* Rift deflection, migration, and propagation: Linkage of the Ethiopian and Eastern rifts, Africa. *Geol. Soc. Am. Bull.* 112, 163–176 (2000).

72 Eckman, J. E. *et al.* Wave and sediment dynamics along a shallow subtidal sandy beach inhabited by modern stromatolites. *Geobiology* 6, 21–32 (2008).

73 Ehleringer, J. Carbon isotope ratios and physiological processes in aridland plants. *Stable Isot. Ecol. Res.* (1989). at <http://link.springer.com/chapter/10.1007/978-1-4612-3498-2_3>

74 Eltahir, E. & Gong, C. Dynamics of wet and dry years in West Africa. *J. Clim.* (1996). at <http://journals.ametsoc.org/doi/abs/10.1175/1520-0442(1996)009%3C1030:DOWADY%3E2.0.CO%3B2>

75 Epstein, S., Buchsbaum, R., Lowenstam, H. A. & Urey, H. C. Revised carbonate-water isotopic temperature scale. … *Soc. Am.* … (1953). at <http://gsabulletin.gsapubs.org/content/64/11/1315.short>

76 Epstein, S. & Mayeda, T. Variation of O18 content of waters from natural sources. *Geochim. Cosmochim. Acta* 4, 213–224 (1953).

77 Eugster, H. P. Chapter 15 Lake Magadi, Kenya, and Its Precursors. *Dev. Sedimentol.* 28, 195–232 (1980).

78 Fairbanks, R. G. The origin of continental shelf and slope water in the New York Bight and Gulf of Maine: Evidence from H2 18O/H2 16O ratio measurements. *J. Geophys. Res.* 87, 5796 (1982).

79 Feibel, C. S., Brown, F. H. & McDougall, I. Stratigraphic context of fossil hominids from the Omo group deposits: northern Turkana Basin, Kenya and Ethiopia. *Am. J. Phys. Anthropol.* 78, 595–622 (1989).

80 Feibel, C. S. Freshwater stingrays from the Plio-Pleistocene of the Turkana Basin, Kenya and Ethiopia. *Lethaia* 359–366 (1994).

81 Feibel, C. S. Quaternary Lake Margins of the Levant Rift Valley. *Hum. Paleoecol. Levantine Corridor* 21–36 (2004).

82 Feibel, C. S., Lepre, C. J. & Quinn, R. L. Stratigraphy, correlation, and age estimates for fossils from Area 123, Koobi Fora. *J. Hum. Evol.* 57, 112–22 (2009).

83 Feibel, C. S. Tephrostratigraphy and geological context in paleoanthropology. *Evol. Anthropol. Issues, News, Rev.* 8, 87–100 (1999).

84 Feibel, C. S., Lepre, C. J. & Quinn, R. L. *Stratigraphy, correlation, and age estimates for fossils from Area 123, Koobi Fora*. *J. Hum. Evol.* 57, (2009).

85 Feibel, C. S., Lepre, C. J. & Quinn, R. L. Stratigraphy, correlation, and age estimates for fossils from Area 123, Koobi Fora. *J. Hum. Evol.* 57, 112–122 (2009).

86 Feibel, C. S. & Brown, F. H. Paleoenvironments of the Koobi Fora Formation, Turkana Basin, northern Kenya. *Dep. Geol. Geophys.* PhD, 330 (1988).

87 Feibel, C. S. & Brown, F. H. Paleoenvironments of the Koobi Fora Formation, Turkana Basin, northern Kenya. *Dep. Geol. Geophys.* PhD, (1988).

88 Feibel, C. Stratigraphy and paleoenvironments of the Koobi Fora Formation along the western Koobi Fora Ridge, East Turkana, Kenya. (1983). at <https://scholar.google.com/scholar?q=feibel%2C+1983+stratigraphy+and+paleoenvironments+of+the+koobi+fora+formation+along+the+western+koobi+fora+ridge&btnG=&hl=en&as_sdt=0%2C31#0>

89 Feibel, C. Fossil fish nests from the Koobi Fora Formation (Plio-Pleistocene) of northern Kenya. *J. Paleontol.* (1987). at <http://journals.cambridge.org/abstract_S0022336000028274>

90 Feibel, C. A terrestrial auxiliary stratotype point and section for the Plio-Pleistocene boundary in the Turkana Basin, East Africa. *Quat. Int.* (1997). at <http://www.sciencedirect.com/science/article/pii/S1040618296000638>

91 Feibel, C., Harris, J. & Brown, F. Palaeoenvironmental context for the late Neogene of the Turkana Basin. *Koobi Fora Res.* … (1991). at <https://scholar.google.com/scholar?q=feibel+et+al.%2C+1991&btnG=&hl=en&as_sdt=0%2C31#2>

92 Feibel, C., Harris, J. & Brown, F. Palaeoenvironmental context for the late Neogene of the Turkana Basin. *Koobi Fora Res.* … (1991). at <https://scholar.google.com/scholar?q=Brown+and+Feibel%2C+1991&btnG=&hl=en&as_sdt=0%2C31#1>

93 Feibel, C., Lepre, C. & Quinn, R. Stratigraphy, correlation, and age estimates for fossils from Area 123, Koobi Fora. *J. Hum. Evol.* (2009). at <http://www.sciencedirect.com/science/article/pii/S0047248409000852>

94 Felton, A. a. *et al.* Paleolimnological evidence for the onset and termination of glacial aridity from Lake Tanganyika, Tropical East Africa. *Palaeogeogr. Palaeoclimatol. Palaeoecol.* 252, 405–423 (2007).

95 Ferguson, A. & Harbott, B. Geographical, physical and chemical aspects of Lake Turkana. … *Turkana A Rep. Find. Lake Turkana* … (1972). at <https://scholar.google.com/scholar?q=Ferguson%2C+A.+J.+D.+%26+B.+J.+Harbott%2C+1982.+Geographical%2C+physical+and+chemical+aspects+of+Lake++Turkana.+In+A.+J.+Hopson+%28ed.%29%2C+Lake+Turkana&btnG=&hl=en&as_sdt=0%2C31#0>

96 Fontes, J. C. & Gasse, F. PALHYDAF (Palaeohydrology in Africa) program: objectives, methods, major results. *Palaeogeogr. Palaeoclimatol. Palaeoecol.* 84, 191–215 (1991).

97 Ford, T. D. & Pedley, H. M. A review of tufa and travertine deposits of the world. *Earth-Science Rev.* 41, 117–175 (1996).

98 Frostick, L. E. *African Basins*. *Sediment. Basins World* 3, (Elsevier, 1997).

99 Gamachu, D. Aspects of climate and water budget in Ethiopia. *Asp. Clim. water Budg. Ethiop.* (1977). at <http://www.cabdirect.org/abstracts/19796729625.html>

100 Gasse, F. & Rognon, P. Le Quaternaire des bassins lacustres de l'Afar. *Rev. Geogr. phys. Geol. dyn.* XV, 414 (1973).

101 Gat, J. Oxygen and hydrogen isotopes in the hydrologic cycle. *Annu. Rev. Earth Planet. Sci.* (1996). at <http://www.annualreviews.org/doi/abs/10.1146/annurev.earth.24.1.225>

102 Gat, J., Bowser, C. & Kendall, C. The contribution of evaporation from the Great Lakes to the continental atmosphere: estimate based on stable isotope data. *Geophys. Res. Lett.* (1994). at <http://onlinelibrary.wiley.com/doi/10.1029/94GL00069/full>

103 Gathogo, P. & Brown, F. Revised stratigraphy of Area 123, Koobi Fora, Kenya, and new age estimates of its fossil mammals, including hominins. *J. Hum. Evol.* (2006). at <http://www.sciencedirect.com/science/article/pii/S0047248406001035>

104 Ghinassi, M. *et al.* Shoreline fluctuations of Lake Hayk (northern Ethiopia) during the last 3500years: Geomorphological, sedimentary, and isotope records. *Palaeogeogr. Palaeoclimatol. Palaeoecol.* 365-366, 209–226 (2012).

105 Ghosh, P. *et al.* 13C–18O bonds in carbonate minerals: A new kind of paleothermometer. *Geochim. Cosmochim. Acta* 70, 1439–1456 (2006).

106 Glaessner, M. F., Preiss, W. V & Walter, M. R. Precambrian Columnar Stromatolites in Australia : Morphological and Stratigraphic Analysis Published by : American Association for the Advancement of Science Stable URL : http://www.jstor.org/stable/1726191 Precambrian Columnar Stromatolites in Australia . 164, 1056–1058 (2009).

107 Golubic, S. & Browne, K. M. Schizothrix gebeleinii sp. nova builds subtidal stromatolites, Lee Stocking Island, Bahamas. *Arch. für Hydrobiol. Suppl. Algol. Stud.* 117, 273–290

108 Gonfiantini, R., Roche, M. & Olivry, J. The altitude effect on the isotopic composition of tropical rains. *Chem.* … (2001). at <http://www.sciencedirect.com/science/article/pii/S0009254101002790>

109 Gong, C. & Eltahir, E. Sources of moisture for rainfall in West Africa. *Water Resour. Res.* (1996). at <http://onlinelibrary.wiley.com/doi/10.1029/96WR01940/full>

110 Gow, C. Unusual occurrence of biogenic (cyanobacterial) carbonate sediments from a sink-hole lake in Western Transvaal, South Africa. *S. Afr. J. Sci.* 77, 564 – 565 (1981).

111 Grant, J. & Gust, G. Prediction of coastal sediment stability from photopigment content of mats of purple sulphur bacteria. *Nature* (1987). at <http://adsabs.harvard.edu/abs/1987Natur.330..244G>

112 Grassineau, N. V *et al.* Antiquity of the biological sulphur cycle: evidence from sulphur and carbon isotopes in 2700 million-year-old rocks of the Belingwe Belt, Zimbabwe. *Proc. Biol. Sci.* 268, 113–9 (2001).

113 Griffiths, J. Climate of Africa. World Survey of Climatology, vol. 10. (1972). at <https://scholar.google.com/scholar?q=griffiths+1972+climate&btnG=&hl=en&as_sdt=0%2C31#0>

114 Harris, J. Koobi Fora Research Project, Vol. 2. The fossil ungulates: Proboscidea, Perissodactyla, and Suidae. Clarendon. (1983). at <https://scholar.google.com/scholar?q=Harris%2C+J.M.+%28ed.%29+%281983%29.+Koobi+Fora+Research+Pmject%2C+Volume+2.+The++Fossil+Ungulates%3A+Proboscidea%2C+Perissodactyla+and+Suidae.+Clat-+endon+Press%2C+Oxford%2C+321+pp.&btnG=&hl=en&as_sdt=0%2C31#1>

115 Harris, J. M., Leakey, M. G. & Brown, F. H. A Brief History of Research at Koobi Fora, Northern Kenya. *Ethnohistory* 53, 35–69 (2006).

116 Herezeg, A. L. & Fairbanks, R. G. Anomalous carbon isotope fractionation between atmospheric CO2 and dissolved inorganic cargon induced by intense photosynthesis,. *Geoclim. Cosmochim, Acta* 51, 859–899 (1987).

117 Hillaire-Marcel, C. & Casanova, J. Isotopic hydrology and paleohydrology of the Madagi (Kenya)-Natron (Tanzania) basin during the late Quaternary. *Palaeogeogr. Palaeoclimatol.* (1987). at <http://www.sciencedirect.com/science/article/pii/0031018287900587>

118 Hillaire-Marcel, C., Carro, O. & Casanova, J. 14C and dating of Pleistocene and Holocene stromatolites from East African paleolakes. *Quat. Res.* 25, 312–

329 (1986).

119 Hillaire-Marcel, C., Carro, O. & Casanova, J. 14C and dating of Pleistocene and Holocene stromatolites from East African paleolakes. *Quat. Res.* 25, 312–329 (1986).

120 Hillaire-Marcel, C., Carro, O., Causse, C., Goy, J.-L. & Zazo, C. Th/U dating of Strombus bubonius-bearing marine terraces in southeastern Spain. *Geology* 14, 613 (1986).

121 Jean-Denis Taupin, Anne Coudrain-Ribs, Robert Gallaire, Gian Maria Zuppi, A. F. Rainfall characteristics (delta18O, delta2H, DeltaT and DeltaHr) in Western Africa: regional scale and influence of irrigated areas. *J. Geophys.* … (2000). at <http://hal.ird.fr/ird-01230541/>

122 Jenny, H. Soil genesis with ecological perspectives. *Ecol. Stud* (1980). at <https://scholar.google.com/scholar?q=jenny+h+1980&btnG=&hl=en&as_sdt=0%2C31#0>

123 Jenny, H. Factors of soil formation—-A sytem of quantitative pedology. (1941). at <http://www.sidalc.net/cgi-bin/wxis.exe/?IsisScript=UACHBC.xis&method=post&formato=2&cantidad=1&expresion=mfn=022061>

124 Johnson, G. Cainozoic lacustrine stromatolites from hominid-bearing sediments east of Lake Rudolf, Kenya. *Nature* (1974). at <http://adsabs.harvard.edu/abs/1974Natur.247..520J>

125 Johnson, T. & Malala, J. Lake Turkana and its link to the Nile. *Nile* (2009). at <http://link.springer.com/chapter/10.1007/978-1-4020-9726-3_15>

126 Joordens, J. & Vonhof, H. An astronomically-tuned climate framework for hominins in the Turkana Basin. *Earth Planet.* … (2011). at <http://www.sciencedirect.com/science/article/pii/S0012821X11002767>

127 Kalkowsky, E. Oolith und Stromatolith im norddeutschen Buntsandstein. *Zeitschrift der Dtsch. Geol. Gesellschaft* (1908). at <https://www.schweizerbart.de/papers/zdgg_alt/detail/60/66518/Oolith_und_Stromatolith_im_norddeutschen_Buntsandstein>

128 Kempe, S. & Kazmierczak, J. Calcium carbonate supersaturation and the formation of in situ calcified stromatolites. *Facet.* … (1990). at <https://scholar.google.com/scholar?q=lyons+et+al+1984+stromatolite&bt

nG=&hl=en&as_sdt=0%2C31#5>

129 Kempe, S. Alkalinity: The link between anaerobic basins and shallow water carbonates? *Naturwissenschaften* 77, 426–427 (1990).

130 Klein, R. G. The Human Career: Human Biological and Cultural Evolution. (University of Chicago Press, 2009). at https://books.google.com/books?id=D3KeGWcev1AC&pgis=1

131 Klein, R.T., K. C. Lohmann, C.W. Thayer (1996). Sr/Ca and 13C/12C ratios in skeletal calcite of *Mytilus trossulus*: Covariation with metabolic rate, salinity, and carbon isotopic composition of seawater. *Geochimica et Cosmochimica Acta* 60: 4207- 4221.

132 Krumbein, W. E., Paterson, D. M. & Stal, L. J. Biostabilization of sediments. ix, 526p. (1994). at <https://scholar.google.com/scholar?q=Biostabilzation+BIS&btnG=&hl=en&as_sdt=0%2C31#0>

133 Krumbein, W. Stromatolites—the challenge of a term in space and time. *Dev. Precambrian Geol.* (1983). at <http://www.sciencedirect.com/science/article/pii/S0166263508702573>

134 Kruskal, W. H. & Wallis, W. A. Use of Ranks in One-Criterion Variance Analysis. *J. Am. Stat. Assoc.* (2012).

135 Kruskal, W. H. & Wallis, W. A. Use of Ranks in One-Criterion Variance Analysis. *J. Am. Stat. Assoc.* 47, 583–621 (1952).

136 Lachniet, M. & Patterson, W. Stable isotope values of Costa Rican surface waters. *J. Hydrol.* (2002). at <http://www.sciencedirect.com/science/article/pii/S0022169401006035>

137 Leakey, M. D., Hay, R. L., Curtis, G. H., Drake, R. E. & Jackes, M. K. Fossil hominids from the Laetoli Beds. *Nature* 262, 460–466 (1976).

138 Leakey, M. G. *et al.* New hominin genus from eastern Africa shows diverse middle Pliocene lineages. *Nature* 410, 433–40 (2001).

139 Lee, C., McKenzie, J. A. & Sturm, M. Carbon isotope fractionation and changes in the flux and composition of particulate matter resulting from biological activity during a sediment trap experiment in Lake Greifen, Switzerland.

Limnol. Oceanogr. 32, 83–96 (1987).

140 Leng, M. J., Lamb, A. L., Lamb, H. F. & Telford, R. J. Palaeoclimatic implications of isotopic data from modern and early Holocene shells of the freshwater snail Melanoides tuberculata, from lakes in the Ethiopian Rift Valley. *J. Paleolimnol.* 21, 97–106 (1999).

141 Lepre, C. J., Quinn, R. L., Joordens, J. C. A., Swisher, C. C. & Feibel, C. S. Plio-Pleistocene facies environments from the KBS Member, Koobi Fora Formation: implications for climate controls on the development of lake-margin hominin habitats in the northeast Turkana Basin (northwest Kenya). *J. Hum. Evol.* 53, 504–14 (2007).

142 Lepre, C. & Kent, D. New magnetostratigraphy for the Olduvai Subchron in the Koobi Fora Formation, northwest Kenya, with implications for early Homo. *Earth Planet. Sci. Lett.* (2010). at <http://www.sciencedirect.com/science/article/pii/S0012821X09007559>

143 Levin, N. E., Brown, F. H., Behrensmeyer, A. K., Bobe, R. & Cerling, T. E. Paleosol carbonates from the Omo Group: Isotopic records of local and regional environmental change in East Africa. *Palaeogeogr. Palaeoclimatol. Palaeoecol.* 307, 75–89 (2011).

144 Levin, N. E., Brown, F. H., Behrensmeyer, A. K., Bobe, R. & Cerling, T. E. Paleosol carbonates from the Omo Group: Isotopic records of local and regional environmental change in East Africa. *Palaeogeogr. Palaeoclimatol. Palaeoecol.* 307, 75–89 (2011).

145 Levin, N., Zipser, E. & Cerling, T. Isotopic composition of waters from Ethiopia and Kenya: insights into moisture sources for eastern Africa. *J. Geophys.* … (2009). at <http://onlinelibrary.wiley.com/doi/10.1029/2009JD012166/full>

146 Lisker, S., Vaks, A., Bar-Matthews, M., Porat, R. & Frumkin, A. Stromatolites in caves of the Dead Sea Fault Escarpment: implications to latest Pleistocene lake levels and tectonic subsidence. *Quat. Sci. Rev.* 28, 80–92 (2009).

147 Litvinova, T. V. New data on the structure and composition of stromatolite buildups (Northern Anabar Region). *Lithol. Miner. Resour.* 44, 389–398 (2009).

148 Logan, B. W., Rezak, R. & Ginsburg, R. N. Classification and Environmental Significance of Algal Stromatolites. *J. Geol.* 72, 68–83 (1964).

149 Lourens, L.J., Hilgen, F.J., Shackleton, N.J., Laskar, J., Wilson, D. in *A Geol. Time Scale* (Gradstein, F.M., Ogg, J.G., Smith, A. G.) 409–440 (Cambridge University Press, 2004).

150 Ludwig, R., Al-Horani, F. a., de Beer, D. & Jonkers, H. M. Photosynthesis-controlled calcification in a hypersaline microbial mat. *Limnol. Oceanogr.* 50, 1836–1843 (2005).

151 Lyons, W. B., Long, D. T., Hines, M. E., Gaudette, H. E. & Armstrong, P. B. Calcification of cyanobacterial mats in Solar Lake, Sinai. *Geology* 12, 623–626 (1984).

152 Lyons, W., Hines, M. & Gaudette, H. Major and minor element pore water geochemistry of modern marine sabkhas: the influence of cyanobacterial mats. *Microb. Mats Stromatolites. Alan R. Liss, New …* (1984). at <https://scholar.google.com/scholar?q=lyons+et+al+1984+stromatolite&btnG=&hl=en&as_sdt=0%2C31#7>

153 Macintyre, I. G., Prufert-Bebout, L. & Reid, R. P. The role of endolithic cyanobacteria in the formation of lithified laminae in Bahamian stromatolites. *Sedimentology* 47, 915–921 (2000).

154 McDougall, I. & Brown, F. Precise 40Ar/39Ar geochronology for the upper Koobi Fora Formation, Turkana Basin, northern Kenya. *J. Geol. Soc. London.* (2006). at <http://jgs.lyellcollection.org/content/163/1/205.short>

155 McDougall, I., Brown, F. H., Cerling, T. E. & Hillhouse, J. W. A reappraisal of the geomagnetic polarity time scale to 4 MA using data from the Turkana Basin, East Africa. *Geophys. Res. Lett.* 19, 2349–2352 (1992).

156 McLoughlin, N., Wilson, L. & Brasier, M. Growth of synthetic stromatolites and wrinkle structures in the absence of microbes–implications for the early fossil record. *Geobiology* (2008). at <http://onlinelibrary.wiley.com/doi/10.1111/j.1472-4669.2007.00141.x/full>

157 Merz, M. U. E. The biology of carbonate precipitation by cyanobacteria. *Facies* 26, 81–101 (1992).

158 Miller, M. & Bassler, B. Quorum sensing in bacteria. *Annu. Rev. Microbiol.* (2001). at <http://www.annualreviews.org/doi/abs/10.1146/annurev.micro.55.1.165>

159 Neu, T. & Boer, C. De. Biofilm development in time on a silicone voice prosthesis—A case study. *Microb. Ecol.* … (1994). at <http://www.tandfonline.com/doi/abs/10.3109/08910609409141571>

160 Neumann, A. The composition, structure and erodability of subtidal mats, Abaco, Bahamas. *J. Sediment.* … (1970). at <http://archives.datapages.com/data/sepm/journals/v38-41/data/040/040001/0274.htm>

161 Nicholson, R., Gillham, R. & Reardon, E. Pyrite oxidation in carbonate-buffered solution: 1. Experimental kinetics. *Geochim. Cosmochim.* … (1988). at <http://www.sciencedirect.com/science/article/pii/0016703788902621>

162 Noback, M. L. MSc in Biogeology Dissertation Seasonality at Plio-Pleistocene Lake Turkana , Kenya : What can freshwater bivalves tell us ? (2009).

163 Noffke, N. Multidirected ripple marks rising from biological and sedimentological processes in modern lower supratidal deposits (Mellum Island, southern North Sea). *Geology* (1998). at <http://geology.gsapubs.org/content/26/10/879.short>

164 Noffke, N. Extensive microbial mats and their influences on the erosional and depositional dynamics of a siliciclastic cold water environment (Lower Arenigian, Montagne Noire,. *Sediment. Geol.* (2000). at <http://www.sciencedirect.com/science/article/pii/S0037073800000981>

165 Noffke, N. Erosional remnants and pockets evolving from biotic–physical interactions in a Recent lower supratidal environment. *Sediment. Geol.* (1999). at <http://www.sciencedirect.com/science/article/pii/S0037073898001353>

166 Noffke, N. Mikrobiell induzierte Sedimentstrukturen (M.I.S.S.) in siliziklastischen Wattablagerungen, PhD thesis. (1997).

167 Noffke, N. & Gerdes, G. Microbially Induced Sedimentary Structures--A New Category within the Classification of Primary Sedimentary Structures: PERSPECTIVES. … *Sediment.* … (2001). at <http://archives.datapages.com/data/doi/10.1306/D4268D60-2B26-11D7-8648000102C1865D>

168 Noffke, N. & Gerdes, G. Microbially Induced Sedimentary Structures--A New Category Within the Classification of Primary Sedimentary Structures--

Reply. … *Sediment.* … (2002). at <http://archives.datapages.com/data/sepm/journals/v72/data/072/072004/0589.htm>

169 Noffke, N., Gerdes, G., Klenke, T. & Krumbein, W. A microscopic sedimentary succession of graded sand and microbial mats in modern siliciclastic tidal flats. *Sediment. Geol.* (1997). at <http://www.sciencedirect.com/science/article/pii/S0037073897000390>

170 Noffke, N., Gerdes, G., Klenke, T. & Krumbein, W. Microbially induced sedimentary structures indicating climatological, hydrological and depositional conditions within Recent and Pleistocene coastal facies zones (. *Facies* (2001). at <http://link.springer.com/article/10.1007/BF02668164>

171 Owen, R. B., Renaut, R. W., Scott, J. J., Potts, R. & Behrensmeyer, A. K. Wetland sedimentation and associated diatoms in the Pleistocene Olorgesailie Basin, southern Kenya Rift Valley. *Sediment. Geol.* 222, 124–137 (2009).

172 Owen, R. B., Renaut, R. W., Hover, V. C., Ashley, G. M. & Muasya, a. M. Swamps, springs and diatoms: wetlands of the semi-arid Bogoria-Baringo Rift, Kenya. *Hydrobiologia* 518, 59–78 (2004).

173 Owen, R. & Renaut, R. Sedimentology, stratigraphy and palaeoenvironments of the Holocene Galana Boi Formation, NE Lake Turkana, Kenya. *Geol. Soc. London, Spec.* … (1986). at <http://sp.lyellcollection.org/content/25/1/311.short>

174 Paerl, H. W., Steppe, T. F. & Reid, R. P. Bacterially mediated precipitation in marine stromatolites. *Environ. Microbiol.* 3, 123–30 (2001).

175 Palacios-Fest, M. R., Cohen, A. S., Lezzar, K., Nahimana, L. & Tanner, B. M. Paleolimnological investigations of anthropogenic environmental change in Lake Tanganyika: III. Physical stratigraphy and charcoal analysis. *J. Paleolimnol.* 34, 31–49 (2005).

176 Paterson, D. Biological mediation of sediment erodibility: ecology and physical dynamics. *Cohesive sediments* (1997). at <https://scholar.google.com/scholar?q=paterson+1997+mat&btnG=&hl=en&as_sdt=0%2C31#0>

177 Paterson, D. & Daborn, G. Sediment stabilisation by biological action: significance for coastal engineering. *Dev.* … (1991). at

<https://scholar.google.com/scholar?q=Paterson%2C+D.M.%2C+Daborn%2C+G.R.%2C+1991.+Sediment+stabilization+by++biological+actions%3A+significance+for+coastal+engineering.+In%3A+Pere-+grine%2C+D.H.%2C+Loveless%2C+J.H.+%28Eds.%29.+Developments+in+Coastal++Engi>

178 Patterson, B., Behrensmeyer, A. & Sill, W. Geology and fauna of a new Pliocene locality in north-western Kenya. *Nature* (1970). at <http://europepmc.org/abstract/med/16057594>

179 Perry, C. Grain susceptibility to the effects of microboring: implications for the preservation of skeletal carbonates. *Sedimentology* (1998). at <http://onlinelibrary.wiley.com/doi/10.1046/j.1365-3091.1998.00134.x/full>

180 Petersen, F., Tao, L. & Scheie, A. DNA binding-uptake system: a link between cell-to-cell communication and biofilm formation. *J. Bacteriol.* (2005). at <http://jb.asm.org/content/187/13/4392.short>

181 Petrisor, A. & Decho, A. Using geographical information techniques to quantify the spatial structure of endolithic boring processes within sediment grains of marine stromatolites. *J. Microbiol. Methods* (2004). at <http://www.sciencedirect.com/science/article/pii/S0167701203002951>

182 Philippis, R. De & Sili, C. Exopolysaccharide-producing cyanobacteria and their possible exploitation: a review. *J. Appl.* … (2001). at <http://link.springer.com/article/10.1023/A:1017590425924>

183 Philippis, R. De & Vincenzini, M. Exocellular polysaccharides from cyanobacteria and their possible applications. *FEMS Microbiol.* … (1998). at <http://femsre.oxfordjournals.org/content/22/3/151.abstract>

184 Pickford, M. & Morales, J. Biostratigraphy and palaeobiogeography of East Africa and the Iberian Peninsula. *Palaeogeogr. Palaeoclimatol.* … (1994). at <http://www.sciencedirect.com/science/article/pii/0031018294900787>

185 Planavsky, N., Reid, R. P., Lyons, T. W., Myshrall, K. L. & Visscher, P. T. Formation and diagenesis of modern marine calcified cyanobacteria. *Geobiology* 7, 566–76 (2009).

186 Quade, J., Levin, N., Semaw, S., Stout, D., Renne, P., Rogers, M.J., et al. Paleoenvironments of the earliest stone toolmakers, Gona, Ethiopia. *Geological Society of America Bulletin.* 116, 1529 (2004).

187 Quinn, Rhonda. Influence of Plio-Pleistocene basin hydrology on the Turkana hominin enamel carbonate δ(18)O values. *Journal of human evolution.* 86. (2015). 10.1016/j.jhevol.2015.06.004.

188 Quinn, R. L., Lepre, C. J., Wright, J. D. & Feibel, C. S. Paleogeographic variations of pedogenic carbonate delta13C values from Koobi Fora, Kenya: implications for floral compositions of Plio-Pleistocene hominin environments. *J. Hum. Evol.* 53, 560–73 (2007).

189 Quinn, R., Lepre, C. & Feibel, C. Pedogenic carbonate stable isotopic evidence for wooded habitat preference of early Pleistocene tool makers in the Turkana Basin. *J. Hum.* … (2013). at <http://www.sciencedirect.com/science/article/pii/S0047248413000997>

190 Rau, G. Carbon-13 depletion in a subalpine lake: carbon flow implications. *Science* 201, 901–2 (1978).

191 Reid, P., Dupraz, C., Visscher, P. & Sumner, D. Microbial processes forming marine stromatolites. *Foss. Recent Biofilms* (2003). at <http://link.springer.com/chapter/10.1007/978-94-017-0193-8_6>

192 Reid, R., James, N. & Macintyre, I. Shark Bay stromatolites: microfabrics and reinterpretation of origins. *Facies* (2003). at <http://link.springer.com/article/10.1007/s10347-003-0036-8>

193 Renaut, R. W. Late Quaternary Geology of the Lake Bogoria Fault-Trough, Kenya Rift Valley. (1982).

194 Richert, L., Golubic, S. & Guédès, R. Le. Characterization of exopolysaccharides produced by cyanobacteria isolated from Polynesian microbial mats. *Curr.* … (2005). at <http://link.springer.com/article/10.1007/s00284-005-0069-z>

195 Riding, R. Abiogenic, microbial and hybrid authigenic carbonate crusts: components of Precambrian stromatolites. *Geol. Croat.* (2008). at <http://hrcak.srce.hr/30642>

196 Riding, R. Microbial carbonates: The geological record of calcified bacterial-algal mats and biofilms. *Sedimentology* 47, 179–214 (2000).

197 Satyanarayana, T., Raghukumar, C. & Shivaji, S. Extremophilic microbes: Diversity and perspectives. *Curr. Sci.* 89, 78–90 (2005).

198 Sharp, Z. *Stable isotope geochemistry*. *Earth-Science Rev.* 9, (2009).

199 Spiro, B. *et al.* Climate variability in the Upper Jordan Valley around 0.78 Ma, inferences from time-series stable isotopes of Viviparidae, supported by mollusc and plant palaeoecology. *Palaeogeogr. Palaeoclimatol. Palaeoecol.* 282, 32–44 (2009).

200 Srivastava, P. Paleoclimatic implications of pedogenic carbonates in Holocene soils of the Gangetic Plains, India. *Palaeogeogr. Palaeoclimatol. Palaeoecol.* (2001). at <http://www.sciencedirect.com/science/article/pii/S0031018201002760>

201 Stal, L. Microphytobenthos, their extracellular polymeric substances, and the morphogenesis of intertidal sediments. *Geomicrobiol. J.* (2003). at <http://www.tandfonline.com/doi/abs/10.1080/713851126>

202 Stal, L. J. *Cyanobacterial mats and stromatolites*. *Ecol. Cyanobacteria II Their Divers. Sp. Time* 9789400738, (2012).

203 Sutherland, I. The biofilm matrix–an immobilized but dynamic microbial environment. *Trends Microbiol.* (2001). at <http://www.sciencedirect.com/science/article/pii/S0966842X01020121>

204 Sutherland, I. Biofilm exopolysaccharides: a strong and sticky framework. *Microbiology* (2001). at <http://mic.microbiologyresearch.org/content/journal/micro/10.1099/00221287-147-1-3>

205 Sutherland, I. Exopolysaccharides in biofilms, flocs and related structures. *Water Sci. Technol.* (2001). at <http://wst.iwaponline.com/content/43/6/77.abstract>

206 Sutherland, I. Microbial polysaccharides from Gram-negative bacteria. *Int. Dairy J.* (2001). at <http://www.sciencedirect.com/science/article/pii/S0958694601001121>

207 Talbot, M. R. A review of the palaeohydrological interpretation of carbon and oxygen isotopic ratios in primary lacustrine carbonates. *Chem. Geol. Isot. Geosci. Sect.* 80, 261–279 (1990).

208 Taupin, J.-D., Coudrain-Ribs, A., Gallaire, R., Zuppi, G. M. & Filly, A. Rainfall

characteristics (δ18O, δ2H, ΔT and ΔHr) in western Africa : Regional scale and influence of irrigated areas. *J. Geophys. Res.* 105, 11911–11924 (2000).

209 Tebbut, G. L., Conley, C. D. & Boyd, D. W. Lithogenesis of a distinctive carbonate rock fabric. *Contr.Geol.* 4, 1–13 (1965).

210 Tiercelin, J.-J. Rifts continentaux: tectonique, climats, sédiments: exemples: la sédimentation dans le nord du Rift Gregory (Kenya) et dans le Rift de l'Afar (Ethiopie) depuis le Miocène. (1981).

211 Tindall, K. Stratigraphy and sedimentology of the Koobi Fora Formation, eastern Koobi Fora Ridge, East Turkana, Kenya. (1985). at <https://scholar.google.com/scholar?q=tindall+1985+Kenya&btnG=&hl=en&as_sdt=0%2C31#0>

212 Trenberth, K. E. Atmospheric moisture recycling: Role of advection and local evaporation. *J. Clim.* 12, 1368–1381 (1999).

213 Trichet, J. & Defarge, C. Non-biologically supported organomineralization. *7th Int. Symp. Biominer.* 14, 203–236. (1995).

214 Troelsen, H. & Jørgensen, B. B. Seasonal dynamics of elemental sulfur in two coastal sediments. *Estuar. Coast. Shelf Sci.* 15, 255–266 (1982).

215 Visscher, P. T. *et al.* Formation of lithified micritic laminae in modem marine stromatolites (Bahamas): The role of sulfur cycling. *Am. Mineral.* 83, 1482–1493 (1998).

216 Visscher, P., Reid, R. & Bebout, B. Microscale observations of sulfate reduction: correlation of microbial activity with lithified micritic laminae in modern marine stromatolites. *Geology* (2000). at <http://geology.gsapubs.org/content/28/10/919.short>

217 Visscher, P., Reid, R., McKenzie, J. & Vasconcelos, C. Geomicrobial mechanisms of carbonate precipitation: Novel insights from laminated structures. in *Geochim. Cosmochim. Acta* A808–A808 (PERGAMON-ELSEVIER SCIENCE LTD, OXFORD OX5 1GB, ENGLAND, 2002).

218 Vizy, E. K. Connections between the summer east African and Indian rainfall regimes. *J. Geophys. Res.* 108, 1–19 (2003).

219 Vlassov, V. V., Laktionov, P. P. & Rykova, E. Y. Extracellular nucleic acids. *BioEssays* 29, 654–667 (2007).

220 Vondra, C.F., Johnson, G.D., Bowen, B.E., & Behrensmeyer, A. K. Preliminary stratigraphical studies of the East Rudolf Basin, Kenya. *Nature* 231, 245–248 (1971).

221 W-Gabriel, G. & Aronson, J. L. Chow Bahir rift: A 'failed' rift in southern Ethiopia. *Geology* 15, 430–433 (1987).

222 Walsh, M. M., Oren, A. & Chela-flores, J. *Microbial Mats. Biofilms* 14, (Springer Netherlands, 2010).

223 Walter, M. Preservation of Biological Information in Thermal Spring Deposits: Developing a Strategy for the Search for Fossil Life on Mars. *Icarus* 101, 129–143 (1993).

224 Walter, M. R., Veevers, J. J., Calver, C. R. & Grey, K. Neoproterozoic stratigraphy of the Centralian Superbasin, Australia. *Precambrian Res.* 73, 173–195 (1995).

225 Whitchurch, C. & Tolker-Nielsen, T. Extracellular DNA required for bacterial biofilm formation. *Science 295, 1487* (2002). at <http://science.sciencemag.org/content/295/5559/1487.short>

226 White, H., Jr, D. B., Jr, R. B. & Vondra, C. Hominid habitats in the Rift Valley: part 1. *Hominid sites their Geol. …* (1981). at <https://scholar.google.com/scholar?q=Hominid+habitats++in+the+rift+valley%3A+part+1.&btnG=&hl=en&as_sdt=0%2C31#0>

227 White, T. D., Suwa, G., Hart, W. K., Walter, R. C., WoldeGabriel, G., de Heinzelin, J., Clark, J.D., Asfaw, B., Vrba, E. New discoveries of Australopithecus at Maka in Ethiopia. *Nature* 366, 261–265 (1993).

228 Wieland, Andrea Karin Eschemann, and Michael Kühl. "Oxygen and sulfide cycling in sediments from Orkney Islands." Proceedings of the Matbiopol Meeting, Marseille 22-25 February, 2001. University of Pau, 2001.

229 Wieman, C. E. & Hollberg, L. Using Diode Lasers for Atomic Physics. *Rev. Sci. Instrum.* 62, 1–20 (1991).

230 Williamson, P. G. Palaeontological documentation of speciation in Cenozoic molluscs from Turkana Basin. *Nature* 293, 437–443 (1981).

231 Williamson, P. G. Molluscan biostratigraphy of the Koobi Fora hominid-bearing deposits. *Nature* 295, 140–142 (1982).

232 Williamson, P. Evidence for an early Plio-Pleistocene rainforest expansion in East Africa. *Nature* 315, 487–498 (1985).

233 WoldeGabriel, G., Hart, W. K., Katoh, S., Beyene, Y. & Suwa, G. Correlation of Plio–Pleistocene Tephra in Ethiopian and Kenyan rift basins: Temporal calibration of geological features and hominid fossil records. *J. Volcanol. Geotherm. Res.* 147, 81–108 (2005).

234 Wynn, J. Paleosols, stable carbon isotopes, and paleoenvironmental interpretation of Kanapoi, Northern Kenya. *J. Hum. Evol.* (2000). at <http://www.sciencedirect.com/science/article/pii/S0047248400904317>

235 Wynn, J. Paleosols, stable carbon isotopes, and paleoenvironments of hominid evolution in the Neogene Turkana Basin, northern Kenya. (2001). at <https://scholar.google.com/scholar?q=wynn+2001+turkana&btnG=&hl=en&as_sdt=0%2C31#0>

236 Wynn, J. Influence of Plio-Pleistocene aridification on human evolution: Evidence from paleosols of the Turkana Basin, Kenya. *Am. J. Phys. Anthropol.* (2004).